International Scientific-Technical and Production Journal

The Paton WELDING JOURNAL

July 2003 # 7

English translation of the monthly «Avtomaticheskaya Svarka» (Automatic Welding) journal published in Russian since 1948

Founders: *The E.O. Paton Electric Welding Institute of the NAS of Ukraine* *International Association «Welding»*

Publisher: *International Association «Welding»*

Address:
E.O. Paton Electric Welding Institute,
International Association «Welding»,
11, Bozhenko str., 03680, Kyiv, Ukraine
Tel.: (38044) 227 67 57
Fax: (38044) 268 04 86
E-mail: journal@paton.kiev.ua
http://www.nas.gov.ua/pwj

State Registration Certificate
KV 4790 of 09.01.2001

Subscriptions:
$460, 12 issues per year,
postage and packaging included.
Back issues available.

CONTENTS

AUTOMATED THERMAL STRAIGHTENING OF WELDED THIN-SHEET STRUCTURES

B.E. PATON, L.M. LOBANOV, G.A. TSYBULKIN, O.V. MAKHNENKO and **Yu.N. PEREVERZEV**
E.O. Paton Electric Welding Institute, NASU, Kyiv, Ukraine

Automated thermal straightening of welded thin-sheet structures with buckling deformations has been developed. An automated system has been designed for thermal straightening of welded sheet structures, based on application of mathematical simulation, manipulation robot, deformation measurement system and microplasma heat source. Automated thermal straightening allows elimination of skilled manual labour, provides a high quality of the surface of a welded structure sheet, improves process efficiency and ecological characteristics.

Keywords: *welded thin-sheet structures, welding deformations, thermal straightening, automation of process, mathematical modeling*

Experience in manufacture of welded thin-sheet structures shows that the type of local deformations, often observed in sheet metal, i.e. buckling, is formed due to loss in stability because of compression stresses caused by a longitudinal shrinkage of welds in welding-on of stiffeners. If these deformations exceed the allowable level, then the thermal straightening is usually used, resulting in occurrence of plastic deformations of shortening in sheet metal, allowing removal of the «excessive» metal.

Thermal straightening of welded thin-sheet structures can be considered as non-efficient expenses. Thus, in shipbuilding yards its volumes, as to the expenses for the qualified manpower, are 10–15 % of total expenses for assembly and welding of hull structures, and can reach 40–45 % and more in some cases of straightening of thin-walled structures [1–3]. In manufacture of railway car bodies the buckling deformations are approximately 50 % of all types of welding deformations of shape changes, and the expenses for thermal straightening can reach 20 % of the cost of manufacture of the car body [4]. Moreover, there are no until now data about development and application of the automated thermal straightening of welded thin-walled structures.

Value of residual plastic deformations in thermal straightening depends on maximum value and distribution of temperature of heating, power of supply source, quantity and arrangement of heat spots, residual stresses and rigidity of structure, rigidity of external fastening, etc. Thus, the effectiveness of thermal straightening depends on a large number of parameters that is a major problem in automation of this technological operation. One of the ways for the solution of this problem is the selection of optimum parameters of heating, quantity and arrangement of heat spots using the mathematical modeling of the process of thermal straightening for each definite structure. The modern level of the computer engineering and calculation methods for prediction of stress-strain state in thin-sheet structures allows us to make this modeling and to determine the optimum parameters of the thermal straightening process quickly in a real time.

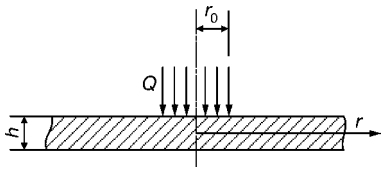

Figure 1. Scheme of heating round spot in metal sheet: h — sheet thickness; r_0 — heat spot radius; Q — heat source power

The proper selection of heat source is important in automation of the process of thermal straightening of thin-sheet welded structures. Traditionally, the heating with a gas flame is used, however, this heat source has some drawbacks from the point of view of the process automation. It is rational to study the feasibility of use of alternative sources of heating, for example, by electrical resistance, induction, plasma and other sources. To automate the control of the welded structure shape and positioning of a heating device, it is necessary to use either industrial robot or a special manipulator.

Mathematical modeling. It can help solving two problems: firstly, to determine optimum parameters of heating, at which the maximum residual plastic shrinkage deformations can be produced without a local loss in stability of the metal sheet and, secondly, to determine the required quantity of local heats and their arrangement to eliminate or decrease the distortion of structure within admissible limits. Mathematical modeling of the process of thermal straightening should be fulfilled quickly, in a real time, i.e. mathematical model should be maximum simplified. For this purpose the shape of heat spot was selected round (Figure 1). This made it possible to develop a unidimensional model of heating a round spot in metal sheet of infinite sizes. The following assumptions were taken: plane stressed state and absence of off-plane displacements; symmetry in sheet plane; unlimited sizes of sheet that corresponds to real conditions of heating with a concentrated source at some distance from the sheet edge. Here, the methods of solution of problems thermoplasticity were used [5]. As a result of continuous observation of formation and propagation and plastic shrinkage deformations during heat-

ing and cooling the residual plastic shrinkage from this heating in metal sheet were determined. Model was also added by the feasibility of allowance for the process of a local buckling. By continuous clarifying the optimum parameters of heating at which the maximum residual plastic shrinkage deformations were possible to produce without a local buckling of metal sheet were determined.

As an example, the calculated data of distributions of temperature, plastic deformations and stresses in steel (St.3) sheet of 2 mm thickness are given in Figures 2 and 3 at different moments of time from heating beginning. Radius of heat spot is 10 mm, effective capacity of heat source is 245 J/s, time of heating is 30 s. Figure 4 gives data from [6] concerning the recommended diameters of heating up to 600 °C, and also the obtained calculated data concerning the maximum diameters of spot, at which a local buckling has not yet occurred at different time of heating up to 600 °C. The smaller time of heating, the larger radius of heat spot. To obtain these data a developed approach was used in which buckling is occurred in a sufficiently large area where the temperature compression stresses are occurred. To evaluate the critical state at which buckling is occurred the method of Bubnov–Galerkin for a rigid round plate, hinge-supported around the contour and free in a radial direction, was used [7].

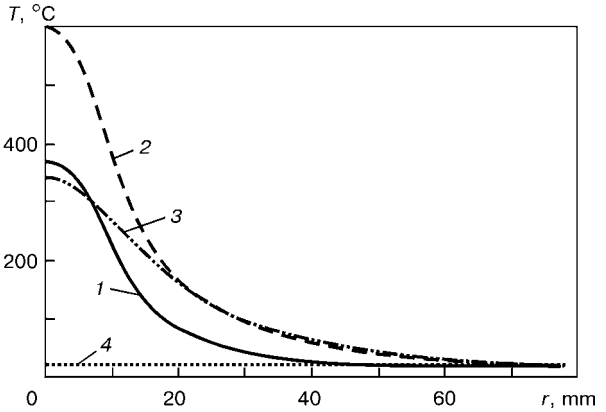

Figure 2. Calculated distributions of temperature in steel sheet at different moment of time from heating beginning: *1* — t = 10; *2* — 30; *3* — 35; *4* — 300 s

After calculation of optimum parameters of round heat spot for the given material and thickness of metal sheet, it is necessary to determine the quantity of these spots and their arrangement for the given structure with allowance for width and length of buckling zone, quantity of waves of buckling and their maximum deflections (Figure 5). To evaluate the «exces-

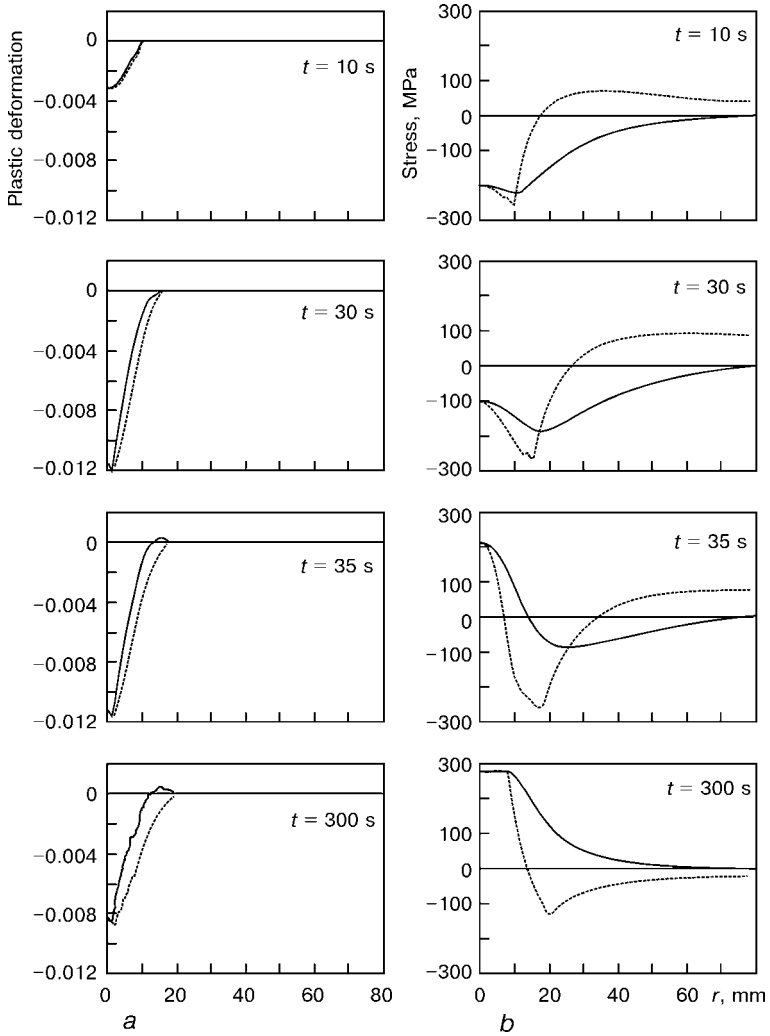

Figure 3. Calculated distributions of plastic deformations (*a*) and stresses (*b*) in steel sheet at the different moments of time from the heating beginning (solid curve — radial deformations; spot curve — tangent deformations)

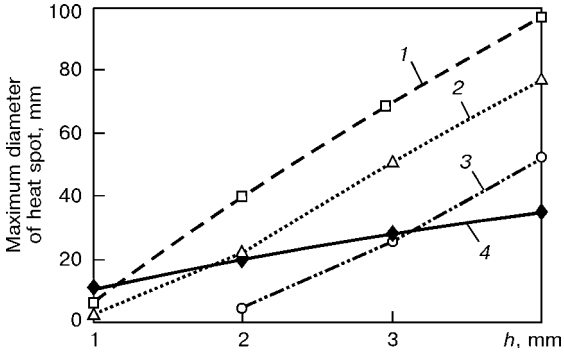

Figure 4. Dependence of maximum diameter of heat spot on sheet thickness: *1* — t = 10; *2* — 30; *3* — 60 s; *4* — calculated data of Kuzminov

sive» area F of sheet, which is necessary to remove in thermal straightening in the zone of buckling $0 < x < a$, $0 < y < b$, the following formula is used in a general form:

$$F = \frac{1}{2}\int_0^a\int_0^b\left[\left(\frac{dU_z}{dx}\right)^2 + \left(\frac{dU_z}{dy}\right)^2\right]dxdy, \qquad (1)$$

where U_z is the displacement of sheet points in a direction normal to surface.

Value F can be also determined approximately, if only the value of maximum deflection f_0 in the center of buckling $0 < x < a$, $0 < y < b$ is known:

$$F = \frac{f_0^2\pi^2}{8}\left(\frac{a}{b} + \frac{b}{a}\right). \qquad (2)$$

As a result of heating round spot in metal sheet the residual plastic shrinkage deformations $\varepsilon^p_{rr}(r)$, $\varepsilon^p_{\beta\beta}(r)$ (where r — current radius) are formed, which lead to the decrease in area of metal sheet:

$$F_1 = 2\pi\int_0^\infty r\,(\varepsilon^p_{rr} + \varepsilon^p_{\beta\beta})\,dr. \qquad (3)$$

Thus, if the values of «excessive» area of metal sheet F and decrease in area of metal sheet from one heat spot F_1 are determined, then the required quantity of heat spots is approximately equal to

$$N = \frac{F}{F_1}. \qquad (4)$$

In determination of optimum arrangement of heat spots at the area of metal sheet with buckling the following main rules are used [6, 8]:

- heat spots cannot be located near the welded stiffeners closer than by 75–100 mm, otherwise the plastic shrinkage deformations, caused by heating, will increase the buckling deflection similar to the action of shrinkage from welds;
- heat spots are, first of all, arranged along the welded stiffeners in the zone of residual compression stresses that promotes, to some degree, the formation and propagation of plastic shrinkage deformations;
- distance between neighboring heat spots is determined so that the temperature fields from heat spots could not influence each other, that makes it possible to perform thermal straightening without breaks for cooling metal sheet;
- if it is impossible in fulfillment of above rules to arrange all required quantity of heat spots on the sheet area, then the process of thermal straightening should be divided in two, three or more series of heating which are fulfilled after metal sheet cooling.

Figure 6 gives an example of arrangement of round heat spots (heat spot radius is 10 mm, heat source capacity is 245 J/s, heating time is 30 s) on the area of 1000×650×2 mm size sheet for different maximum buckling deflections (5, 10 and 13 mm). Parameters of heat spot were found as optimum from point of view of maximum residual plastic shrinkage deformations for metal sheet made from 2 mm thick steel St.3 at 600 °C maximum temperature of heating, 30 s time of heating and absence of a local buckling of sheet during heating.

Selection of heat source. As has been already noted, heating with a gas flame is used traditionally for the thermal straightening. However, this heat source has a number of drawbacks from the point of view of process automation and providing stable heat characteristics. An addition, the flame heating has low ecological characteristics.

Tests of electrical resistance heat source revealed such an essential drawback as increased requirements to roughness of metal sheet surface, and also damages of sheet surface that is inadmissible in thermal straightening.

Source of induction heating by high-frequency currents using a generator of 15 kW capacity and a specially-developed induction heating device (Figure 7) showed its efficiency for the metal sheet thickness from 6 mm and larger. For the smaller thickness the induction heat source did not provide small sizes of heat spot that led to buckling of the metal sheet.

Small sizes of zone of concentrated heating could be provided by a microplasma heat source MPI-4 of 2 kW capacity using a non-transferred arc plasmatron

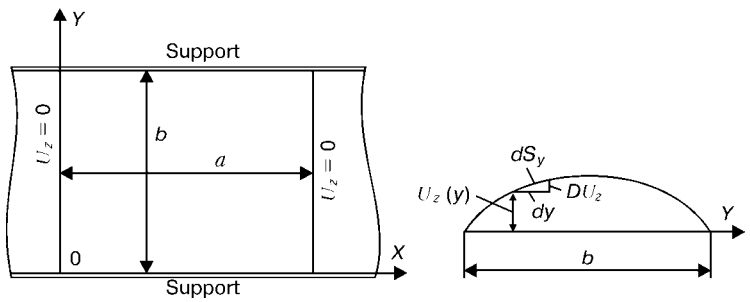

Figure 5. Layout of area of welded structure of $a \times b$ size with a buckling deformation

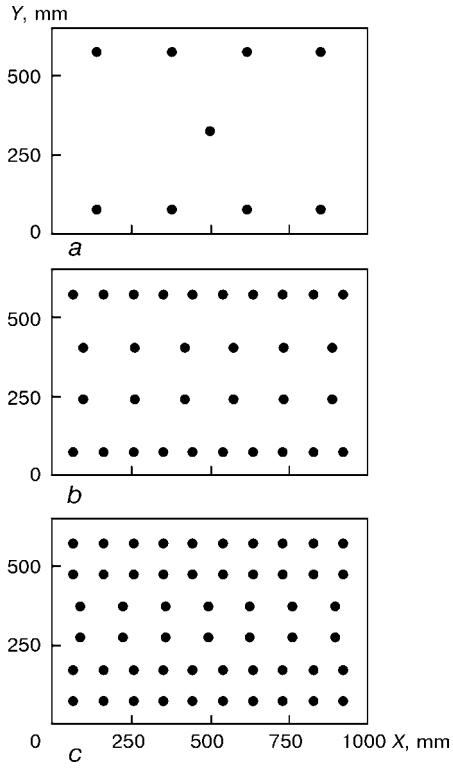

Figure 6. Arrangement of heat spots for different maximum deflections of buckling: 5 (*a*), 10 (*b*) and 13 (*c*) mm

(Figure 8). Here, the microplasma heating does not depend on the surface roughness, does not damage the metal sheet at a proper selected condition, it is easily controlled and has a low consumption of energy and high ecological characteristics. The drawbacks include the difficulty in providing stable characteristics at long-time conditions of operation. Taking into account the availability of heat source MPI-4 and feasibility of manufacture of a transferred-arc torch, the microplasma heat source was selected.

The laser heat source with a defocused beam satisfies almost all requirements specified to heat source for thermal straightening of thin-sheet structures, namely highly-concentrated heating, simplicity in adjustment and control, stability of characteristics, ecology. The main drawback is the high cost. However, taking into account the modern tendency to a

Figure 7. Induction heating HF source with a heating device

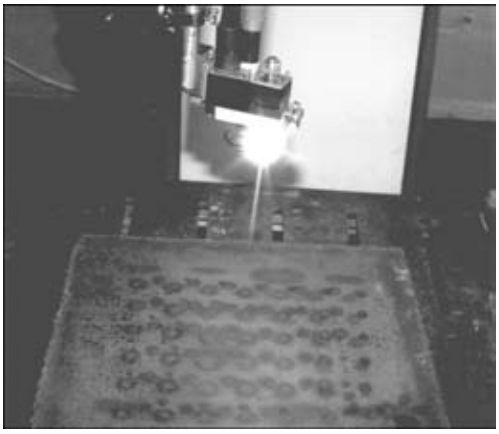

Figure 8. Microplasma heat source MPI-4 with an arc-transferred torch

an abrupt reduction in cost for laser sources, then they can be referred to most challenging heat sources for automation of the thermal straightening process.

System of control of structure deformation. Automation of the process of thermal straightening of thin-sheet structures required the creation of system of evaluation of a deformation value. The developed system provides the measurement of deformations in programmed preset points, uniformly arranged at a definite pitch over the entire area of the structure sheet. Here, using the developed algorithm [9] a localizing of points of maximum deformations is realized, coordinates of these points and values of deformations proper are measured and recorded in the robot memory. On the basis of this information the controlling program defines the quantity and arrangement of heat spots necessary for thermal straightening of buckling, or interrupts the process, if the structure deformation is admissable. As a measuring element in control system, a potentiometer gauge of linear displacements, possessing satisfactory accuracy (± 0.2 mm) and simplicity of signal processing, is used.

Automated complex. An automated complex for thermal straightening of thin-sheet welded structures has been developed on the base of developed mathematical models (Figure 9). It includes a manipulation

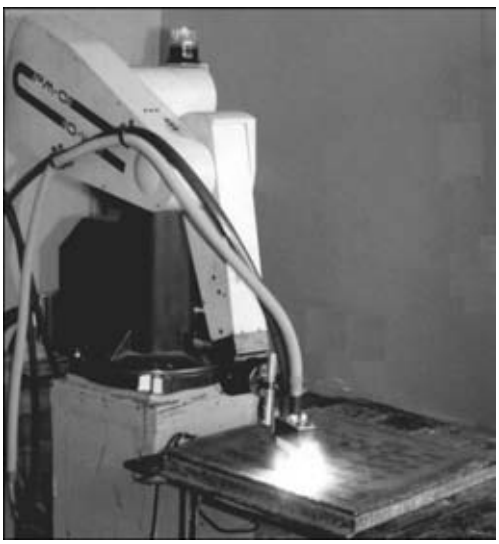

Figure 9. Automated complex for thermal straightening of thin-sheet welded structures

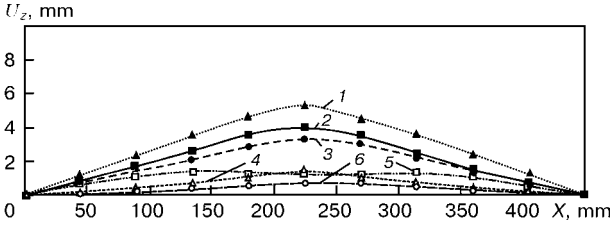

Figure 10. Results of measurement of deflections U_z of welded specimens in a central transverse section before (*1–3*) and after (*4–6*) automated thermal straightening (*1–6* — numbers of specimens)

robot RM-01 (PUMA 560), equipped with systems of control of deformations and control of process of straightening, and a microplasma heat source. Gauge of deformations and plasmatron, fulfilling the role of a heating device, are arranged on the robot operating head so that the transition from operation of measurement to the operation of heating and, vice versa, took place by a simple turn of the head, accomplished by the robot command. The controlling program can locate in a control block in the robot or in the computer which is directly connected to the robot control system.

The process of the automated straightening occurs as follows. Operator introduces data to the computer about material and metal sheet thickness, power parameters of heat source and sizes of heat spot. Computer defines the optimum heat duration (when necessary, the optimum power heating and spot radius can be calculated). Then the operator in the condition «teaching» records the coordinates of three angular points of sheet surface in the robot memory to preset the limits of buckling area and the so-called zero plane, relative to which the deformation will be measured. Further, the straightening process is performed completely in the automatic condition: firstly, the sheet deformation is measured, then the data of measurement are processed, then the heating of required spots in places, preset by the program, is occurred. During some preset time the robot waits for structure cooling and then repeats the deformation measurement. The data of measurements are processed and process of straightening is completed (if the deformations in structure are admissible), or repeated taking into account the recent measurements.

Test results. Using the created complex, experiments of automated thermal straightening of thin-sheet structures were made under the laboratory conditions on small specimens of 450×450 mm size. Specimen was produced by welding a sheet (St.3) of 2 mm thickness to a frame of 50×50 mm angle. Value of buckling deformations was controlled by a linear heat input or welds length. Figure 10 shows results of measurements of deflections of three welded specimens of 450×450×2 mm size in a central section before and after the automated thermal straightening. Figure 11 shows a welded specimen No.1 with a buckling deformation before and after straightening. Value of deflection was decreased from 4 to 1.4 mm. Taking into account the small total sizes of the specimen, this is a good result. Series of experiments confirmed the principal feasibility of use of the automated thermal straightening of the thin-sheet structures. Advantages

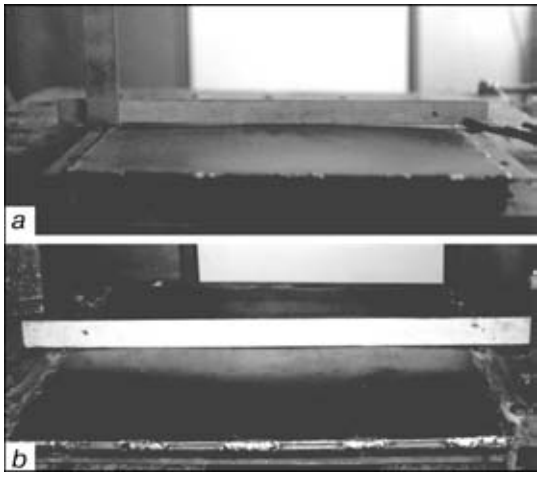

Figure 11. Welded specimen No.1 (450×450×2 mm) before (*a*) and after (*b*) automated thermal straightening

of the automated straightening are evident, as the process is impact-free, eliminates the skilled manual labour, provides high quality of welded structure surface, improves the efficiency as a result of process optimizing and feasibility of control of several complexes by one operator and improves the ecological characteristics.

CONCLUSIONS

1. The feasibility of creation of the technology of the automated thermal straightening of thin-sheet structures with buckling deformation is shown for the first time.

2. Automated complex has been developed for thermal straightening of welded thin-sheet structures using a mathematical modeling, manipulation robot, systems of measurement of deformations and microplasma heat source.

3. Process of the automated thermal straightening allows elimination of the skilled manual labour, provides high quality of welded structure sheet surface, increases the process efficiency, improves the ecological characteristics.

4. Automated thermal straightening of welded thin-sheet structures can find application in branches of industry, which manufacture different hull welded structures, such as ship and railway car building, tank construction, etc.

1. (1993) *Welded building structures*. Refer. Book. Ed. by L.M. Lobanov. Vol.1. Principles of design of structures. Kyiv: Naukova Dumka.
2. Lopatin, N.I. (1998) Calculation of general and local welding deformations in welding of thin-sheet structures from aluminium alloys. *Voprosy Materialovedeniya*, **4**, 47–52.
3. Zaikin, V.M. (1984) Calculation of conditions of thermal nonimpact straightening of welded structures from aluminium-magnesium alloys. *Avtomatich. Svarka*, **6**, 62–66.
4. Matsui, S. (1982) Prevention of welding deformations in thin-skin welded structures. *J. Light Metal Welding and Construction*, **1**, 3–11.
5. Makhnenko, V.I. (1976) *Calculation methods of study of welded stress and strain kinetics*. Kyiv: Naukova Dumka.
6. Kuzminov, S.A. (1974) *Welding deformations of hull structures*. Leningrad: Sudostroenie.
7. Volmir, A.S. (1967) *Stability of deformable systems*. Moscow: Nauka.
8. Mikhajlov, V.S. (1972) *Straightening of hull welded structures*. Leningrad: Sudostroenie.
9. Tsybulkin, G.A. (1999) Algorithm of search of sheet structure maximum deformations using robotic manipulator. *Avtomatich. Svarka*, **6**, 55–57.

IMPROVEMENT OF FATIGUE RESISTANCE OF TEE WELDED JOINTS IN SHEET ALUMINIUM ALLOY AMg6

V.A. SHONIN, V.S. MASHIN, O.V. VOJTENKO and **V.V. NOVOZHILOV**
E.O. Paton Electric Welding Institute, NASU, Kyiv, Ukraine

It is shown that smoothing of the metal surface on the boundaries of sheet tee joints of aluminium and elimination of angular deformation by high-frequency peening provide a lowering of the values of stress concentration factor 1.6 times. Joint peening increases the ultimate fatigue strength by 40 % at zero-to-compression and by 10 % at repeated stress cycles.

Keywords: *aluminium alloys, welded tee joints, joint profile, angular residual deformation, stress concentration, high-frequency peening, fatigue resistance*

One-sided electric-arc welding on of stiffeners to the skin of a shell structure (tee welded joints) of aluminium alloys induces a considerable residual angular deformation. It results from non-uniform shrinkage of weld metal and leads to non-flatness of the base metal surface on the face side of the structure, in the zone of stiffener welding [1–3]. Under the impact of transverse forces in operation, the angular residual deformation causes an additional bending moment in the base metal on weld boundaries, which leads to increase of the level of stress concentration [4], and, hence, to lowering of fatigue resistance of welded joints [5, 6].

Various methods of thermal and cold straightening of the entire structure and its individual components [2, 3, 5, 7] are known for correction of postweld angular deformation. They are based on application of a non-uniform linear or volume plastic deformation of the metal in the bending plane. Straightening induces residual stresses of different sign and level, which are non-uniformly distributed across the thickness of a structural element.

Impact of the known methods [2] of concentrated heating, used for straightening thick-walled structural elements by plastic shortening of the surface layer of the metal from the convex side, is similar to non-uniform heating in welding. It leads to formation of tensile residual stresses on the surface and compressive stresses in the central layers of the metal. Such a processing promotes a significant lowering of fatigue resistance of welded joints.

Cold straightening methods are due to plastic elongation of the metal layer on the concave surface of the structural element with formation of compressive residual stresses [5]. This is hammer peening and roller treatment of the weld, application of a force along or across the joint and applying mechanical vibration to the structural element [7]. Shot blasting can be also included into cold straightening. The main drawback of the above methods of cold straightening is development of high tensile residual stresses in the central layers of the metal at increase of treatment intensity. In addition, cold straightening does not always improve the profile geometry in the zone of transition from the weld to base metal [2, 5].

In aircraft construction one-sided treatment of the surface with steel shot is widely used for straightening of dents in thin-walled elements of aluminium alloys [8, 9]. The work-hardened surface layer of the metal in the treatment zone acts on practically undeformed metal layers, located below this layer, as an off-center tensile force, and causes elastic reverse deformation (bending out). A system of residual stresses balanced across the thickness develops: compressive stresses in the active work-hardened layer, tensile stresses in the lower lying and central metal layers, as well as compressive stresses on the element surface on its reverse side. Shot blasting of a low intensity creates low levels of tensile residual stresses in the central layers of the metal and promotes a significant improvement of fatigue resistance of the element in the zone of dent correction.

High-frequency mechanical peening of a thin surface layer of the metal in the concentrator zone along weld boundary does not have these drawbacks. It is performed with a single-row group of needle-like strikers [10]. Peening increases the radius of transition from the weld surface to the base metal, induces high compressive residual stresses in the work-hardened layer and provides a significant increase of fatigue resistance of welded joints at transverse action of alternating stresses. In case of a one-sided high-frequency peening of welded joints improvement of the transition on the weld boundary may be accompanied by manifestation of the effect of bending out in the welded element plane, similar to that achieved in shot-blasting treatment of base metal. This may promote elimination of residual angular deformation in sheet welded joints.

The purpose of this work is to establish the possibility of elimination of residual angular bending deformation and improvement of the fatigue resistance of a tee joint in sheet aluminium alloy AMg6 (Al–6.2 Mg), welded with consumable electrode in inert gases, by application of local high-frequency peening of the surface layer of the metal on weld

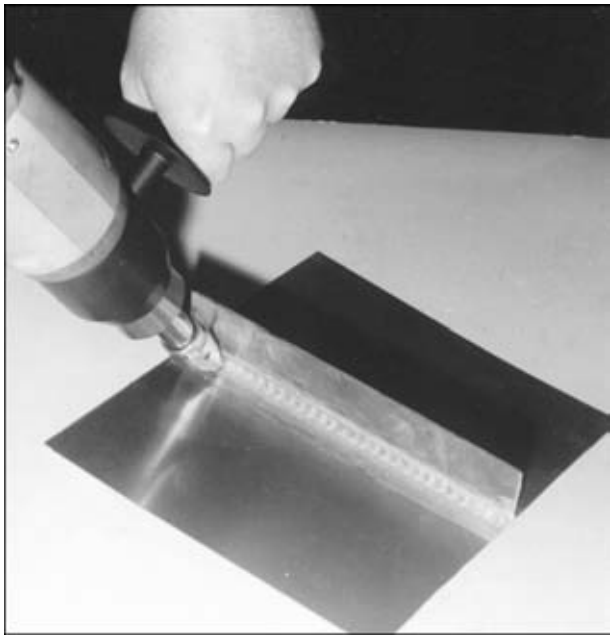

Figure 1. High-frequency peening of a fragment of the welded joint, performed with a manual tool

boundaries, improving the geometry of transition of the surfaces of the weld and base metal.

Investigations were performed on plates of 250×500×1.85 mm size of AMg6 alloy, in the central part of which a stiffener (500×40×1.85 mm) of the same alloy was welded on with two fillet welds. Pulsed-arc welding of a joint was performed with Sv-AMg6 consumable electrode of 1.6 mm diameter in a helium-argon mixture of gases in the following mode: welding current I_w = 80–85 A; arc voltage U_a = 18.0–18.5 V; welding speed v_w = 43–45 m/h; wire feed rates v_f = 5.9–6.0 m/min. Basic current value I_b and value of pulse repetition rate F_p were defined as

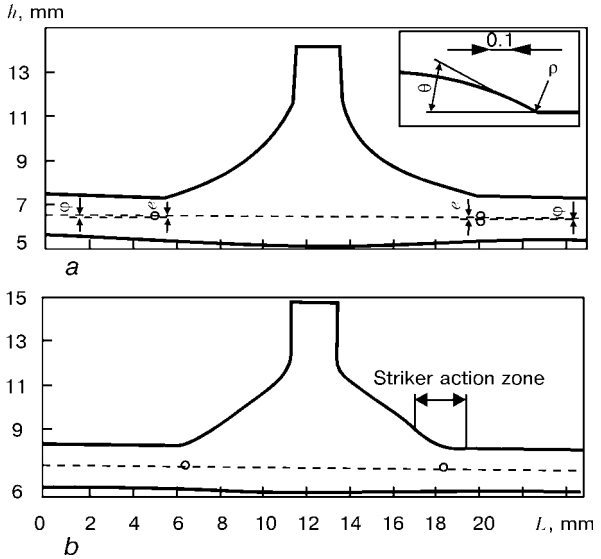

Figure 2. Profiles of welded joints in the initial condition (*a*) and after high-frequency peening of the surface layer of the metal on weld boundaries (*b*) (*h*, *L* — coordinates of measurements; points — projections of the axis, relative to which angular deformation proceeds)

$$I_b = I_w/(1.5–2.0), \quad F_p = KI_b,$$

where K = 0.9–1.1. Helium content in the mixture was 55 vol.%. Welding of tee joint blanks was performed in the condition of rigid restraint.

High-frequency peening with a single-row group of strikers of the metal surface on weld boundaries in welded blanks (Figure 1) was performed with an ultrasonic converter of «Ultramet» type of 300 W power [10]. Dependence of bending out angle on the mode and conditions of peening was studied on small (50×50 mm) plates of the base metal. Influence of different factors on the angle of bending out relative to the line of one-sided peening in the plate middle along its entire length was determined. Strikers of 2, 3 and 5 mm diameter were used. Average speed of tool displacement was varied in the range of 1–5 mm/s.

Geometry of joint profile in welded blanks after welding and high-frequency peening of the surface on weld boundaries, as well as the angle of bending out φ′ in small-sized plates of the base metal after peening, were determined by the method of profilemetry in toolmakers' microscope BMI-1. Residual angular (post-welding) deformation φ, eccentricity e were determined for base distance 5 mm from the fusion zone, as well as angle θ and radius of transition ρ from weld surface to base metal (Figures 2 and 3).

Influence of high-frequency peening on fatigue resistance of welded joints was evaluated on specimens of 50×230 mm size with working zone width of 25 mm, which were cut out of a welded blank in as-welded condition and after high-frequency peening. Values of stress concentration factor in welds were determined, using the known calculation procedures [4], proceeding from the data of measurement of the joint profile parameters. Fatigue testing of welded joints was conducted under axial cyclic load at stress cycle asymmetry factors R_σ = 0 and 0.4 and frequency of 4–5 Hz with application of electrohydraulic machine UE-10. In testing the fatigue life was limited by value $N = 1 \cdot 10^6$ loading cycles.

Measurement of residual angular deformation on the reverse side of the initial joints showed that the maximum (up to 3°) angle of residual deformation is observed directly under the weld in the zone of the greatest thickness of the deposited metal. On the boundaries of welds with the base metal the residual angular deformation φ (Figure 2, *a*) exceeded 2°. Beyond the welded joint the angular deformation is negligible.

In the case of MIG welding with weld location in the central zone of the cross-section of large-sized blanks of a tee joint, the minimum longitudinal residual bending of the base metal under the stiffener was ensured. In the zones of action of compressive residual welding stresses on the edges of the main plate the deflection was equal to 11–15 mm on a 500 mm length as a result of the loss of stability.

Results of studying the influence of the modes of one-sided high-frequency peening on the change of the residual angular deformation by bending out of the base metal plates relative to the axis of peening zone demonstrated that bending out angle φ' essentially depends on the average speed of displacement of the tool in peening and thickness of metal being treated (Figure 3). Maximum (up to 5°) angle of bending out at plate thickness of 1.85 mm is formed at a minimum (1 mm/s) peening speed and with increase of the latter the bending out angle becomes smaller. Striker diameter did no have any significant influence on the dependence of the angle of plate bending out on the average peening speed (Figure 3, *a*).

As is seen from Figure 3, *b* the above data indicate that the maximum bending out angle is provided at thickness of the processed metal of 1.0–1.2 mm. Increase of plate thickness up to 2.5 mm and more leads to decrease of this angle. In plates less than 1.0 mm thick, a negative bending out angle forms, which is indicative of irrationality of applying the used peening modes to correct the angular deformation in joints of such a thickness. This is due to the fact that the area of metal surface, where plastic elongation occurs on the side opposite to peening, turns out to be greater than that directly in the zone of striker impact.

In welded blanks the transverse residual angular deformation was eliminated only in the zone of peening on weld boundaries (see Figure 2, *b*). Peening was performed with strikers of 2 mm diameter at average speed of tool displacement of 4–5 mm/s. Additional peening of the entire weld surface and of areas of its maximum thickness did not lead to any noticeable change of the angular residual deformation of the surface on the reverse side of the joint.

Under the impact of high-frequency peening of the surface layer of the metal on weld boundaries the deflection along the edges of the main plate decreased by not more than 25 %. It is probable that the residual longitudinal deformation of the welded blank changes only slightly as a result of high-frequency peening, and does not ensure a full relieving of the longitudinal tensile residual stresses caused by the welding process. In this case in the peened joints ρ value increased 2.6 times, angle of transition θ from the weld surface to the base metal decreased 2.3 times, and residual angular deformation also decreased significantly, which

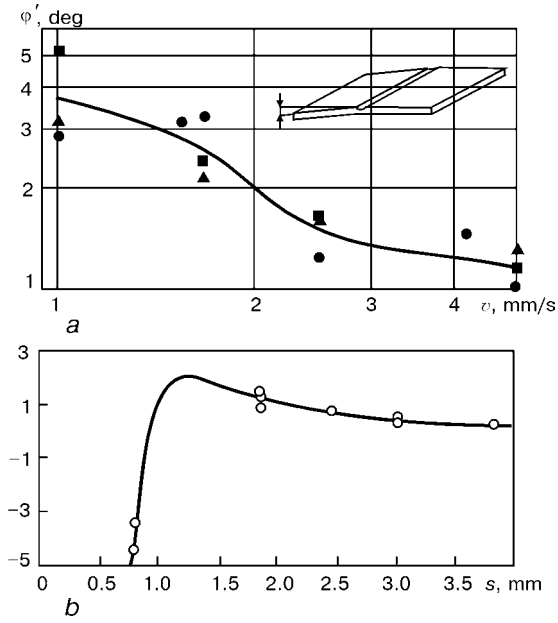

Figure 3. Dependence of bending out angle φ' of 1.85 mm thick plate on speed v of the manual tool movement at one-sided high-frequency peening with strikers of a diameter of 2 (●), 3 (▲) and 5 (■) mm (a) and on plate thickness s in treatment with strikers of 2 mm diameter at peening speed of 5 mm/s (*b*)

provided a 1.6 times decrease of the values of stress concentration factor (Table).

Testing for single static tension of specimens of the initial joints and those with peened weld boundaries showed that peening only slightly changes the fracture mode. Specimens failed in the base metal beyond the welds. They had practically the same values of ultimate tensile strength σ_t = 335–342 MPa. However, use of peening led to an earlier development of plastic deformations in the joints, which resulted in the lowering of conditional elastic limit $\sigma_{0.01}$ by 29 % (from 129.1 to 92.5 MPa), and proof stress $\sigma_{0.2}$ by 11 % (174.4–155.1 MPa), compared to the respective characteristics of the initial specimens.

At cyclic testing the fatigue crack in the initial welded specimens initiated in the surface layer of the metal on weld boundary and propagated at an angle of 90° in the direction towards the applied load. The same nature of fatigue fracture was observed also in the specimens with the peened surface. The fatigue crack initiated in them under a work-hardened layer of the metal in the stress concentration zone.

One-sided high-frequency mechanical peening of metal surface on weld boundaries significantly im-

Changes of parameters of profile geometry and stress concentration in a welded tee joint of AMg6 alloy, induced by one-sided high-frequency peening of the surface layer of the metal on weld boundaries

Condition of the joint	θ, *deg*		ρ, *mm*		σ_α		*e*, *mm*		K_e		$\alpha_\sigma K_e$	
	$\bar{\theta}$	S_θ	$\bar{\rho}$	S_ρ	$\bar{\alpha}_\sigma$	S_α	$\bar{e}$	S_e	$\bar{K}_e$	S_K	$\bar{\alpha}_\sigma\bar{K}_e$	$S_{\alpha K}$
Initial	17.8	8.3	0.75	0.6	1.39	0.36	0.078	0.048	1.25	0.16	1.75	0.52
After peening	7.9	2.4	1.97	0.6	1.07	0.02	–	–	–	–	–	–

Note. S – standard deviations of the considered parameters; α_σ – coefficient of stress concentration, due to the shape of the transition surface from the weld to base metal; K_e – stress concentration factor, due to eccentricity e; dash above the symbol is the average statistical value of the parameter.

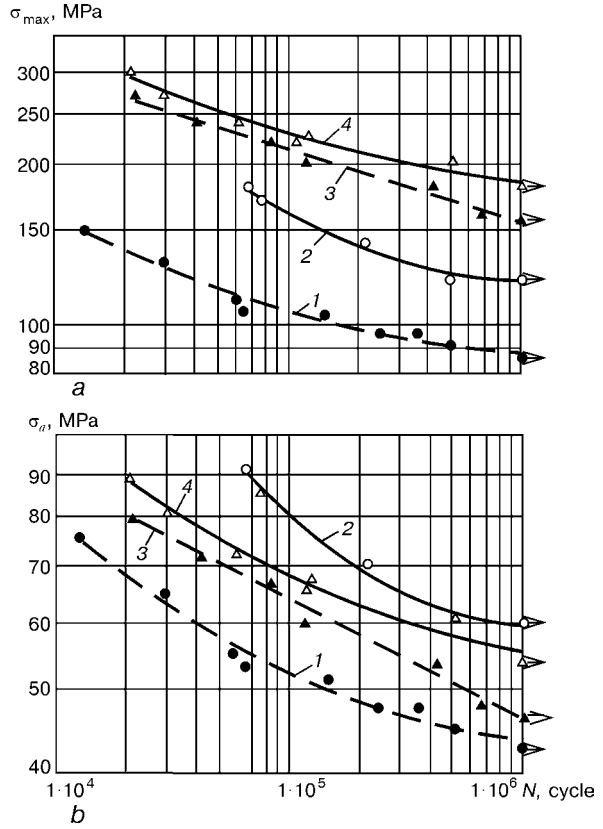

Figure 4. Results of fatigue testing of specimens of tee joint of AMg6 alloy 1.85 mm thick, produced at nominal maximum σ_{max} (*a*) and amplitude σ_a (*b*) stresses: *1, 3* — after welding; *2, 4* — after welding and high-frequency peening; *1, 2* — $R_\sigma = 0$; *3, 4* — $R_\sigma = 0.4$ (points are experimental data; points with arrows — no specimen fracture occurred)

proved the characteristics of fatigue resistance of the tee joint of AMg6 alloy (Figure 4, *a*). It is established that the effectiveness of peening as a measure to improve the fatigue resistance of the joints depends on asymmetry of external stress. The greatest increase of fatigue resistance σ_{max} of welded tee joints is observed at zero-to-compression stress cycle $R_\sigma = 0$. As a result of peening the fatigue life of the joints rises more than 10 times, and the ultimate fatigue strength at $N = 1 \cdot 10^6$ stress cycles rises by 30 %. At coefficient of stress cycle asymmetry $R_\sigma = 0.4$ a lower (by almost 1.5 times) increase of the fatigue life and increase of ultimate fatigue strength by approximately 9 % are observed.

Smaller difference between the fatigue life of the joints in the initial condition and of those with peened weld boundaries at $R_\sigma = 0.4$ is related to manifestation of plastic deformations, as the level of acting maximum stresses in the joints exceeded the proof stress $\sigma_{max} > \sigma_{0.2}$. This is probably, what causes in the peened joints relaxation of tensile stresses, which balance the compressive residual stresses of the surface work-hardened metal layer. As a result, the magnitudes of compressive residual stresses, induced by peening, decreased, which is exactly what caused a lowering of the specimen fatigue life. Now in the initial joints plastic deformation lead to a decrease of the angular residual deformation and lowering of stress concentration on weld metal boundaries, which promoted longer fatigue life of the specimens.

Comparison of S–N curves, represented by stress amplitudes (Figure 4, *b*) shows that at $R_\sigma = 0.4$ a higher fatigue life of the initial specimens and a lower fatigue life of the peened specimens is found than in the case of $R_\sigma = 0$. Limits of ultimate fatigue strength σ_a at $R_\sigma = 0.4$ drop to values of σ_a at $R_\sigma = 0$ only in the case of increase of the basic fatigue life. Peened joints have lower fatigue resistance at $R_\sigma = 0.4$ than at $R_\sigma = 0$. At decrease of the basic fatigue life values of σ_a at $R_\sigma = 0.4$ become essentially smaller than at $R_\sigma = 0$.

Obtained results indicate that at overloading ($\sigma_{max} > \sigma_{0.2}$) of specimens of tee welded joints with a residual angular deformation at cyclic stresses higher than the metal yield point, a smaller increase of specimen fatigue life is provided than in the case of application of a one-sided high-frequency peening under the same conditions of cyclic stresses.

CONCLUSIONS

1. To improve the joint profile on weld boundaries and eliminate the residual angular deformation of tee welded joints of aluminium alloys, it is rational to apply one-sided high-frequency peening at base metal thickness of 1.5–3.0 mm.

2. The established modes of one-sided high-frequency peening of tee joints of AMg6 alloy 1.85 mm thick, made by MIG welding, provide a lowering of the stress concentration factor 1.6 times and improvement of the ultimate fatigue strength by 40 % at zero-to-compression stress cycle.

3. A positive effect of high-frequency peening of the joints is lowered under the impact of external load, under the conditions of which the nominal maximum stresses in the welded joint exceed the proof stress.

1. Kiselyov, S.N. (1972) *Gas electric welding of aluminium alloys*. Moscow: Mashinostroenie.
2. Trochun, I.P. (1964) *Internal forces and strains in welding*. Moscow: Mashgiz.
3. Kuzminov, S.A. (1974) *Welding distortions of ship hull structures*. Leningrad: Sudostroenie.
4. Makhnenko, V.I., Mosenkis, R.Yu. (1985) Calculations of stress concentration factors in welded joints with butt and fillet welds. *Avtomatich. Svarka*, **8**, 7–19.
5. Stepanov, V.G., Klestov, M.I. (1977) *Surface strengthening of hull structures*. Leningrad: Sudostroenie.
6. Sanders, W.W., Day, R.H. (1983) Fatigue of aluminium alloy weldments. *WRC Bull.*, August, 21.
7. Sagalevich, V.M. (1974) *Methods of elimination of welding strains and stresses*. Moscow: Mashinostroenie.
8. Stepnov, M.N., Giatsintov, E.V. (1973) *Fatigue of light structural alloys*. Moscow: Mashinostroenie.
9. Hertel, H. (1969) *Ermüdungsfestigkeit der Konstruktion*. Berlin: Springer.
10. Trufyakov, V.I., Shonin, V.A., Mashin, V.S. et al. (2001) Application of high-frequency peening to improve the fatigue resistance of butt welded joints in aluminium alloys. *The Paton Welding J.*, **7**, 6–10.

DECREASE IN STRUCTURAL HETEROGENEITY OF INCOMPLETE REFINING REGION OF THE HAZ OF WELDED JOINTS IN PEARLITIC STEELS

V.V. DMITRIK and **A.N. PASHCHENKO**
Ukrainian Engineering Academy, Kharkiv, Ukraine

Intensity of initiation and development of damage at creep of welded joints in heat-resistant steels is shown to depend upon the kind of initial metal structure in incomplete refining region. Control of temperature conditions of the latter can provide improvement of operational reliability of welded joints.

Keywords: *automatic welding, pearlitic steels, welded joints, microdamage, initial structure, structural heterogeneity, steam pipelines*

Heat-resistant pearlitic steels 15Kh1M1F and 12Kh1MF are used to make steam pipelines for power plants, for example steam power plant. Extension of service life of steam pipelines to over 200,000 h is a very topical issue in terms of cost effectiveness. Fracture of welded joints in steam pipelines operating under conditions of low-temperature creep at $T_{op} < 0.5\ T_{melt}$ (life > 150,000 h) occurs mostly in an incomplete refining region of the HAZ [1–4]. Statistics of fracture rate in this region includes a substantial spread in time, i.e. from 5000 to 250,000 h of operation [3, 5–9]. Investigation of fracture of welded joints shows that the use of regulatory documents, e.g. «Appendix to TU 14-3-460–75. Scale of Microstructures of Metal of Boiler Pipes of Steels 12Kh1MF, 15Kh1M1F and 12Kh2MFSR», which specify the acceptance structure, unfortunately does not lead to prevention of fracture of welded joints in the above region.

The purpose of this study was to decrease the initial structural heterogeneity of metal of the incomplete refining region in order to increase its resistance to microdamages under service creep conditions.

Resistance of welded joints to microdamages under conditions of operating stresses and temperatures depends upon their initial structure, including structural heterogeneity, physical service conditions and other factors [1, 2, 5, 6, 9–16].

Metal of the incomplete refining region undergoes heating during welding in a temperature range of A_{c_1}–A_{c_3}. Values of microhardness of metal of this region may be much lower than those of the base metal (which is not subjected to a corresponding heating during welding) [4, 11, 17], although this is not always the case [4, 5, 10, 18, 19].

Experimental procedure. Experimental program included calculation-experimental modelling of temperature conditions [8, 20, 21], which allowed a smooth approximation of isotherms characterising temperature fields of the incomplete refining region and cooling rates. Coordinates of fragments of the region studied, where the mutually differing structures are formed, were determined on the basis of the determined temperature values. It was found that formation of these structures and sizes of the fragments depend upon the heat input into the base metal and geometry of the welded joints, and are controlled by the cooling rate after welding heating. Corresponding parameters of automatic metal-electrode welding in a mixture of shielding gases (80–85 % CO_2 + 15–20 % Ar) for samples of steels 15Kh1M1F and 12Kh1MF were selected on the basis of data characterising certain temperature conditions. This made it possible to optimise the initial structure of the incomplete refining region, i.e. produce structure which differed to a minimum possible degree from that of the base metal (for example, here new products of decomposition of austenite should be bainite or sorbite). The base metal structure consisted of 30 % ferrite and bainite making the balance.

Samples of the same melt, having identical chemical composition and subjected to identical heat treatment, were used for the experiments. Welding parameters used for these experiments are given in the Table. Preheating was 300 °C in all the cases.

Microstructural analysis, electron microscopy, X-ray microanalysis («Nephot 2», «EVM-1200A» and «Camebax») and radiography were employed for examinations. Creep was evaluated on standard specimens (Figure 1) using machines of the AIMA-5-2 and IP-4M types, as well as on specimens cut from welded joints that fractured during operation.

Pores were studied by transmission electron microscopy using carbon replicas and by the light metallography methods. Amount and composition of carbide phases were determined by analysis of the resulting precipitates by the photometry methods. Precipitation of carbides M_3C and $M_{23}C_6$ was provided

Welding parameters	*Welding speed, m/h*	*Welding current, A*	*Arc voltage, V*
Standard	30–50	400	34–36
Suggested	20–25	330–370	32

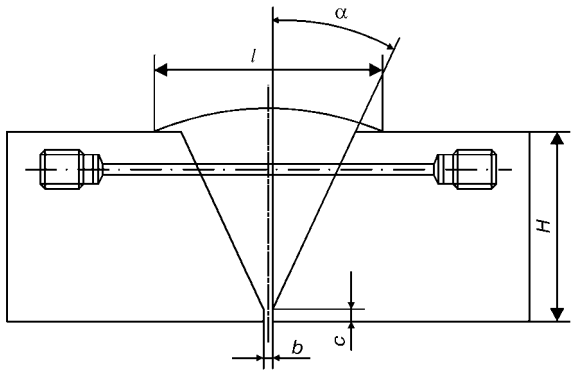

Figure 1. Schematic of cutting of specimens for creep tests: H = = 50 mm; $c = b = 2$ mm; $l = 65$ mm; $\alpha = (27\pm3)^{\circ}$

by anodic dissolution in salt solutions, and that of carbides VC and Mo_2C — in acid solutions. Structure of carbides was identified from X-ray patterns made by using diffractometer «Dron-3M». Types of carbides were identified also from the photos of replicas of corresponding steels made at a certain magnification, i.e. by comparing them with photos of carbides studied [22]. Microhardness (instrument PMT-3) was measured across the section of welded joints.

Experimental results. It was found that welding heating of the base metal determined not only width of the incomplete refining regions of the HAZ, but also its local increase (Figures 2 and 3), while the time of heating the metal to a temperature range of A_{c_1}–A_{c_3} and the cooling rate determined also the region structure. As shown by the examinations, sizes of grains of structure of the region considered (welded joints in steels 15Kh1M1F and 12Kh1MF) changed insignificantly during welding heating, compared with structure of the base metal, and amounted to index 6–9 (GOST 5639–82). Bainite in the incomplete refining region after welding heating retained its orientation corresponding to bainite of the base metal.

Size and structure of local dark-etched edges in structure of this region (Figure 4) depend upon the time of its heating in a temperature range of A_{c_1}–A_{c_3} and upon the cooling rate. Such edges are new products of decomposition of austenite and consist of coarse-laminar or spheroidised pearlite, which agrees

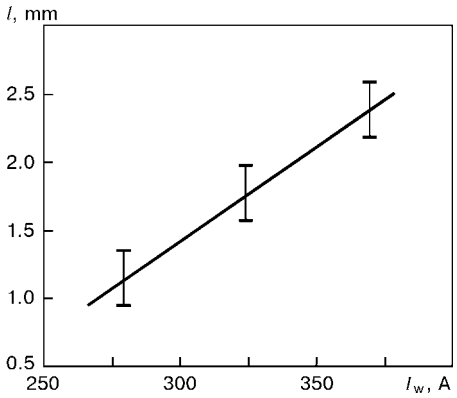

Figure 2. Dependence of width l of the incomplete refining region upon welding current I_w: automatic welding; $v_w = 20$ m/h; specimens of steel 15Kh1M1F (see Figure 1)

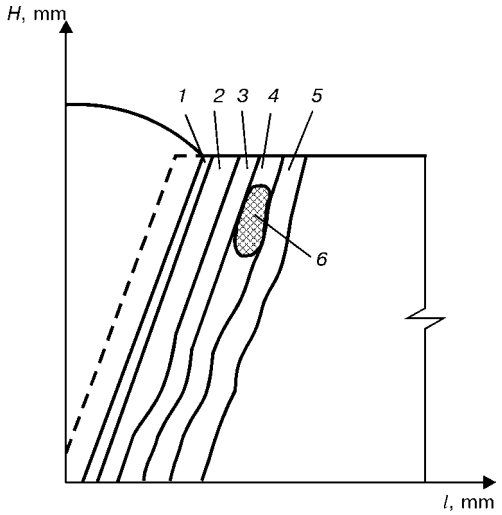

Figure 3. Schematic of regions of a welded joint (welding under standard conditions, geometry — see Figure 1): *1* — fusion; *2* — overheating; *3* — normalising; *4* — incomplete refining; *5* — recrystallisation; *6* — fragment of incomplete refining region where formation of a martensitic structure was revealed (hatched)

with the data of [6], as well as of bainite differing in structure from bainite of the base metal, or sorbite-type eutectoid, which is proved by results of [17]. New products of decomposition of austenite may contain also fragments of martensite with dispersed carbide particles inside the martensite needles, which corresponds to [6].

There is no way of preventing formation of such structures in arc welding. However, modelling of temperature conditions shows that quantitative and qualitative composition of these products in the region studied can be optimised, and formation of fragments

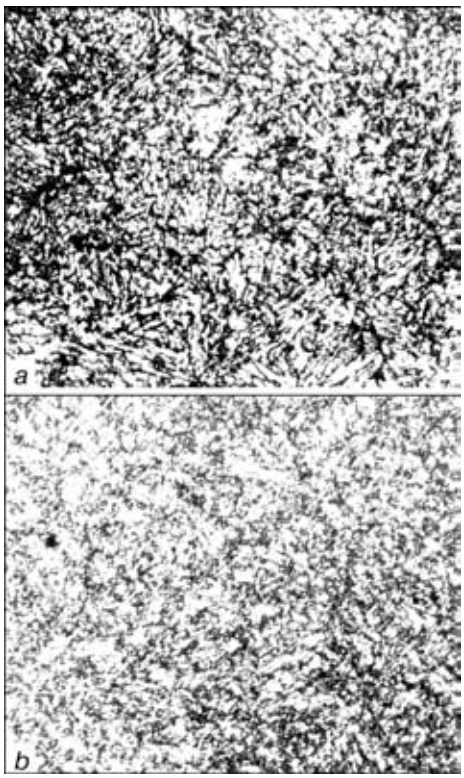

Figure 4. Microstructure of the incomplete refining region (see Figure 1): *a* — welding under standard conditions; *b* — welding under suggested conditions (×400)

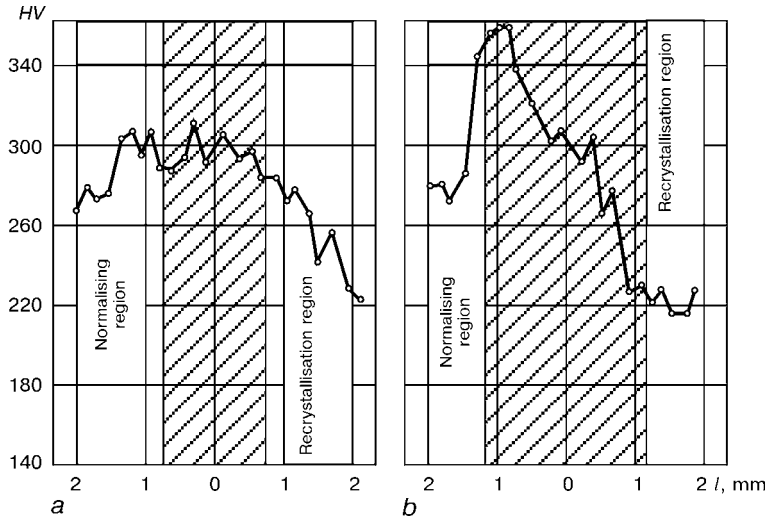

Figure 5. Initial microhardness of welded joints in steel 15Kh1M1F (see Figure 3): *a* — welding under suggested conditions; *b* — welding under standard conditions (incomplete refining region is hatched)

of martensite can be prevented (Figure 4, *a*), or, for example, bainite close in structure to that of the base metal can be produced through appropriate heat input to the base metal.

Modelling shows that formation of fragments of martensite is likely to depend upon the heat input providing an appropriate time of welding heating to a range of A_{c_1}–A_{c_3}, as well as (to a larger degree) upon the cooling rate of about 35 °C/s and higher to a temperature range of 450–250 °C (steel 15Kh1M1F). However, the nature of formation of martensite fragments is not yet clear and requires further studies.

Given that analysis of microstructure of this region is difficult, and based on the experience of its examination, it should be noted that fragments of the martensite structure cannot be revealed to a sufficient degree by using an optical microscope. For this it is necessary to use also the X-ray diffraction method, which allows determination of carbon content of the α-phase from photometry curves. To confirm the data obtained, it is necessary to study also the corresponding replicas.

Martensite is etched out in the form of light spearpoint needles or their twins (see Figure 4, *a*), which agrees with [22]. The presence of martensite fragments is proved also by microhardness measurements (Figure 5). Values of microhardness should be checked using the X-ray diffraction method.

Examination of specimens that fractured shows that carbide reaction $M_3C \rightarrow M_{23}C_6$ and coagulation of carbides, including along the grain boundaries, favouring formation of pores, occur more intensively (under low-temperature creep conditions) on the prior martensite fragments (specimens after heat treatment). However, it is the opinion of the authors of this paper that further studies are required to investigate kinetics of this reaction.

Modelling and subsequent experimental process of automatic welding of these steels in a mixture of shielding gases CO_2 + Ar allowed the expediency of keeping to the upper limit of the welding current (350–380 A) and welding speed (25–30 m/g) to be proved (Figure 6). Studies [6, 17] show that martensite may not be formed in the incomplete refining regions, but they give no explanation how this could be achieved.

Modelling of temperature conditions of arc welding [8, 20] of steel 15Kh1M1F allowed establishing the possibility of an absolute elimination of martensite fragments in the incomplete refining region of welded joints of any thickness, e.g. in automatic welding of samples 50 mm thick of steel 15Kh1M1F. The above samples were welded through the first 30 mm of their thickness at a current of 330 A and welding speed of 25 m/h, and then through the rest of 20 mm — at a current of 370 A and welding speed of 20 m/h. Structure of new portions of austenite decomposition products in the given region consisted primarily of upper bainite and sorbite, and it was close to that of the base metal. The experience shows that temperature conditions for each critical welded joint should be determined individually by the calculations.

Small amounts of carbides $M_{23}C_6$ (about 7 %) were revealed in a carbide component of structure of the given region after welding heating. Small amounts of carbides $M_{23}C_6$ were also detected in other regions

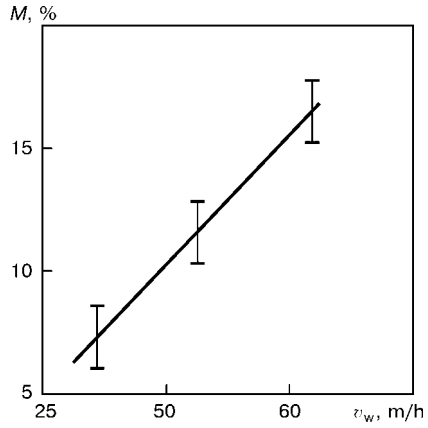

Figure 6. Dependence of the content of martensite *M* in structure of the incomplete refining region upon welding speed v_w (see geometry of specimens in Figure 1)

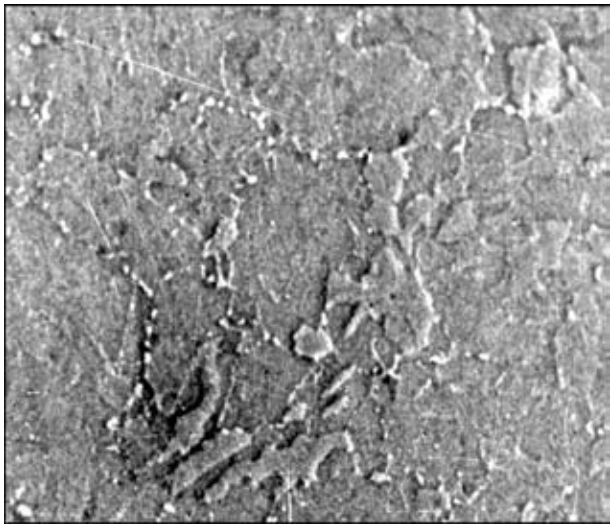

Figure 7. Initial structure of the incomplete refining region (light cementite particles are located mostly along the grain boundaries of tempered bainite; degree of etching of ferrite matrix is different; welding under standard conditions; base metal — steel 15Kh1M1F) (×2500)

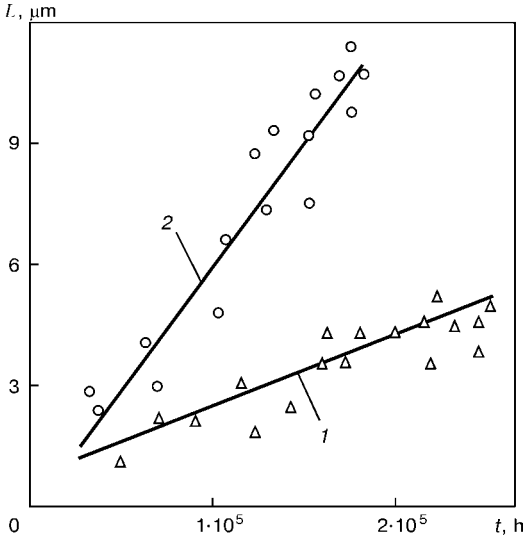

Figure 9. Increase in length of pores, L, under low-temperature creep conditions at T = 570 °C (range of tensile stresses σ = 50–70 MPa): *1* — automatic welding under suggested conditions; *2* — under standard conditions

of the HAZ and in the weld metal after heat treatment of the samples welded under standard and suggested conditions, which finds confirmation in [3]. Unfortunately, tempering after welding (730 °C, 3 h) leads to concentration of carbide precipitates at the grain boundaries (Figure 7), which depends upon the type of new portions of austenite decomposition products. It can be experimentally proved that the intensity of formation of microdamages in this region is determined by the degree of structural heterogeneity under low-temperature creep conditions.

In welding under standard conditions the degree of concentration of carbides $M_{23}C_6$, M_7C_3 and M_3C (fine-dispersed) at the grain boundaries (seeFigure 7) is higher than in a similar structure of the region in welding under the suggested conditions. Initially, a considerable nucleation of individual pores under the creep conditions occurs also at the grain boundaries, where coagulating (at a different intensity) carbides $M_{23}C_6$ and M_7C_3 are located, which agrees with [23].

Figure 8. Metal of the incomplete refining region damaged by creep pores (carbon replica; service life 150,000 h; welding under standard conditions; base metal — steel 15Kh1M1F) (×6000)

The presence of carbides at the grain boundaries leads not only to development of porosity, but also to formation of chains of pores 2–7 μm in size along the grain boundaries (Figure 8). The pore chains in the bulk of grains are smaller and have size of 0.5–2.0 μm, which corresponds to data of [4, 15].

Microdamages in the above welded joints (creep stages I and II) are caused by nucleation and development of pores [16, 21, 23, 24]. Shape of micropores at the initial stage of their development is controlled by decreasing the surface energy, including by difference in the concentration of vacancies over the surface of a pore with a shape close to ellipsoid. It was established that in the process of development of the already formed pores, their increase determined by the intensity of volume diffusion of atoms and the concentration of vacancies depends upon the initial structure (Figure 9), while the shape of the pores differs from ellipsoid.

It can be shown that pores in specimens tested initially nucleate primarily at the grain boundaries normal to the axis of applied tensile stress, i.e. in the regions where also coagulating carbides $M_{23}C_6$ are located. Pores in metal of welded joints operating under the creep conditions initially nucleate in the same manner. It is significant that further on (creep stage II) micropores in structure of the region studied (standard and suggested conditions) are formed also in the bulk of grains (see Figure 8). However, their quantity and degree of development directly depend upon the initial structural heterogeneity of the incomplete refining regions.

Formation of microdamages is favoured also by a probable relative plastic deformation of individual grains of the α-phase, as well as their sub-grains [14], i.e. the probability of increase in the surface of micropores may be realised through the mechanism of interaction of internal slip and slippage along the grain boundaries.

Nucleation and development of porosity in metal of the region considered under conditions of more frequent stops and starts are more intensive, and initially take place primarily along the grain boundaries. However, here carbide phases play an auxiliary role, rather than the central one.

Therefore, the intensity of nucleation and development of porosity in samples welded under the suggested conditions (selected on the basis of data derived by modelling of temperature conditions) decreases approximately by 25–30 %, compared with similar samples welded under the standard conditions. The rate of microdamages of welded joints in steels 15Kh1M1F and 12Kh1MF decreases accordingly.

CONCLUSIONS

1. Intensity of nucleation and development of porosity in metal of the incomplete refining region of welded joints in heat-resistant steels under low-temperature creep conditions was found to depend upon the kind of initial structure of this region.

2. Data of modelling of initial structure of the incomplete refining region served as the basis for the experimental confirmation of the possibility of decreasing its initial structural heterogeneity and, accordingly, decreasing the intensity of formation of microdamages in the region. This will allow performance of welded joints to be improved.

1. Zemzin, V.N. (1972) *Heat resistance of welded joints*. Leningrad: Mashinostroenie.
2. Khromchenko, F.A. (1982) *Reliability of welded joints in tubes, boilers and steam pipelines*. Moscow: Energoizdat.
3. Shron, R.Z., Nebesova, I.F. (1971) Structure, phase composition and long-time strength of chrome-molybdenum weld metal. *Avtomatich. Svarka*, **11**, 9–11.
4. Khromchenko, F.A. (2002) *Service life of steam pipeline welded joints*. Moscow: Mashinostroenie.
5. Dmitrik, V.V., Ilienko, N.A., Kirichenko, E.P. (1991) Improvement of metal mechanical properties of incomplete refining zone. *Svarochn. Proizvodstvo*, **1**, 11–12.
6. Berezina, T.G., Borodina, E.R., Ashikhmina, L.A. et al. (1974) Fine structure of heat-affected zone in welding of 15Kh1M1F steel. *Avtomatich. Svarka*, **12**, 19–22.
7. Miller, K. (1986) *Creep and fracture*. Moscow: Metallurgiya.
8. Dmitrik, V.V. (2000) Simulation of structure of heat-resistant pearlite steel welded joint. *Avtomatich. Svarka*, **4**, 27–30.
9. Kumanin, V.I., Kovalyova, L.A., Alekseev, S.V. (1988) *Metal service life in creep conditions*. Moscow: Metallurgiya.
10. Kasatkin, B.S., Kareta, N.L., Vakhnin, Yu.N. et al. (1958) «White» strip in 15Kh1M1F steel welded joints. *Avtomatich. Svarka*, **12**, 12–16.
11. Diachenko, S.S., German, S.I., Pavlyak, Ya.S. (1960) Investigation of softening zone produced in welding of steels. *Metallovedenie i Term. Obrab. Metallov*, **7**, 24–26.
12. Tsaryuk, A.K. (1999) Peculiarities of phosphorus influence on size of non-metallic inclusions and properties of heat-resistant steel welded joints. *Avtomatich. Svarka*, **4**, 26–30.
13. Gotalsky, Yu.N. (1981) *Welding of dissimilar steels*. Kyiv: Tekhnika.
14. Rozenberg, V.M. (1967) *Creep of metal*. Moscow: Metallurgiya.
15. Khromchenko, F.A., Kalugin, R.N., Lappa, V.A. et al. (1999) Peculiarities of structural changes in welded joints of steel 15Kh1M1F at creep. *Svarochn. Proizvodstvo*, **10**, 12–15.
16. Khromchenko, F.A., Lappa, V.A., Fedina, I.V. et al. (1998) Influence of technological and metallurgical heredity on damage of 15Kh1M1F steel welded joint zones under creep conditions. *Ibid.*, **4**, 18–21.
17. Fomina, O.P., Gavranek, V.V., Diachenko, S.S. et al. (1965) On nature of a white strip in welded joints. *Metallovedenie i Term. Obrab. Metallov*, **1**, 46–47.
18. Fomina, O.P., Gavranek, V.V., Diachenko, S.S. et al. (1965) Simulation of white strip in welded joints. *Svarochn. Proizvodstvo*, **3**, 13–14.
19. Fomina, O.P., Gavranek, V.V., Diachenko, S.S. et al. (1965) Hardness of white strip in welded joints. *Ibid.*, **11**, 5–8.
20. Dmitrik, V.V. (1999) A method of determining the temperature conditions in the molten pool. *Welding Int.*, **2**, 159–161.
21. Dmitrik, V.V. (1999) Stabilisation of conditions of automatic welding of pearlite steels. *Svarochn. Proizvodstvo*, **5**, 11–14.
22. (1972) *Metallography of iron*. Part 2. Structure of steels with microphotograph atlas. Ed. by F.N. Tavadze. Moscow: Metallurgiya.
23. Krutasova, E.I. (1981) *Reliability of metal of power equipment*. Moscow: Energoizdat.
24. Elpanova, N.V., Berezina, T.G. (1989) Influence of structure on kinetics of fracture of 12Kh1M1F steel at creep. *Metallovedenie i Term. Obrab. Metallov*, **7**, 36–39.

STRUCTURE OF BRAZED JOINTS IN HIGH NICKEL ALLOYS PRODUCED BY USING ARC HEATING

V.F. KHORUNOV, S.V. MAKSIMOVA and **I.V. ZVOLINSKY**
E.O. Paton Electric Welding Institute, NASU, Kyiv, Ukraine

Structure, chemical heterogeneity and microhardness of structural components of brazed joints made by using arc heating and adhesion-active brazing filler alloys of the Ni–Cr–Zr system were studied. The use of brazing filler alloys of optimal composition and appropriate techniques was found to provide deposited metal of low hardness and avoidance of cracking of the brazed weld and the HAZ. Application of composite brazing filler alloys was proved to be most promising for repair of blades of unweldable superalloys with a high (over 60 %) content of the γ'-phase.

Keywords: *high nickel alloys, superalloys, γ'-phase, arc heating, brazed joint, deposited metal, brazing filler alloy, composite brazing filler alloy, microstructure, cracks*

Cast heat-resistant Ni-base alloys are used to manufacture blades of gas turbine engines applied in aircraft engineering, ship building and power engineering. The most common method for manufacturing of the blades is investment casting. However, this method leads to formation of different types of defects. Development of a technology for repair of the blades to remove these defects is one of the pressing problems of up-to-date gas turbine manufacturing.

Welding can be used to repair blades from alloys with a comparatively low content of the γ'-phase, which depends mainly upon the weight content of aluminium and titanium [1]. It is believed that alloys with a high total content of these two elements (ZhS6U-VI, ZhS6K, ZhS26, ChS 70, ChS 88, ChS 104VI, IN-738LC, 713C etc.) and a substantial content of the γ'-phase (superalloys) cannot be welded, unless special techniques are employed for welding. Thus, study [2] recommends that preheating to 600 °C (for argon-arc welding) and to 900 °C (for electron beam welding) should be used to make the crack-free welds in welding of alloys with a high content of the γ'-phase. It is the opinion of the authors of this study that in this case it is important to control the cooling cycle during welding. It is also noted that even minor deviations in chemical composition of an alloy may have a substantial effect on its behaviour during welding.

The authors of [1] claim that EBW of alloy IN-738LC can provide crack-free welds if welding is performed with preheating to 1120 °C with or without filler metal. Welded joints in this case have high short-time strength at 850 °C (σ_t = 615–656 MPa, $\sigma_{0.2}$ = 506–544 MPa) and resistance to high-cycle fatigue close to that of the base metal. Distribution of the γ'-phase after comprehensive heat treatment is of a homogeneous character, and particles are 0.4 μm in size.

The authors of [3] claim that susceptibility of alloy 713C to cracking decreases with increase in the welding speed. Apparently, the data of this study are identical to those contained in [1, 2], i.e. they can be reduced to decreasing the cooling rate during welding and decreasing welding stresses. Appreciating the high importance of these data, we should note that results of the above studies were obtained under ideal conditions, which are far from reality, where repair of each type of a defect requires a special approach.

Experimental. The authors of this study offer a different approach to addressing the problem of elimination of cracks in arc heating. This approach consists in decreasing heat input (critical temperature of melting of the base metal is not reached) and providing the possibility of «healing» the cracks formed at the joint boundary. In other words, the authors suggest that tungsten-electrode argon-arc heating should be used and a filler metal should be employed as a brazing filler alloy.

Selection of a brazing filler alloy was based on our experience in using elements of groups IV and V of the periodic table as depressants [4–6]. Brazing filler alloys of the Ni–Cr–Zr system were used in the cast state and in a composite form (mixture of the brazing filler alloy and heat-resistant alloy powders). Alloy with a high (over 60 vol.%) content of the γ'-phase, i.e. ZhS6U-VI, was chosen as the base metal for the studies.

The following experimental procedure was employed. Thermocouple was fixed on the side of the bottom of an artificially induced conical defect to estimate temperature of the weld pool. Arc heating was carried out by two methods: with and without melting of the base metal.

Samples for making microsections were cut normal to the substrate surface. Chemical heterogeneity of the resulting deposited metal was examined using the JEOL scanning electron microscope ISM-840 equipped with the microanalysis system. Examinations were conducted in the secondary electron mode.

Results of metallographic examinations of the samples made by arc heating with melting of the base metal and then adding the Ni–Cr–Zr system filler alloy (in the cast form) showed that microstructure of the deposited metal consisted of primary dendrites

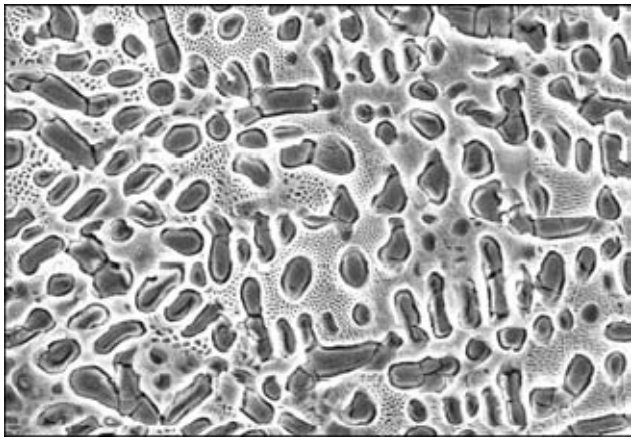

Figure 1. Microstructure of deposited metal produced in arc heating with melting of base metal and using brazing filler alloy of the Ni–Cr–Zr system (×1800)

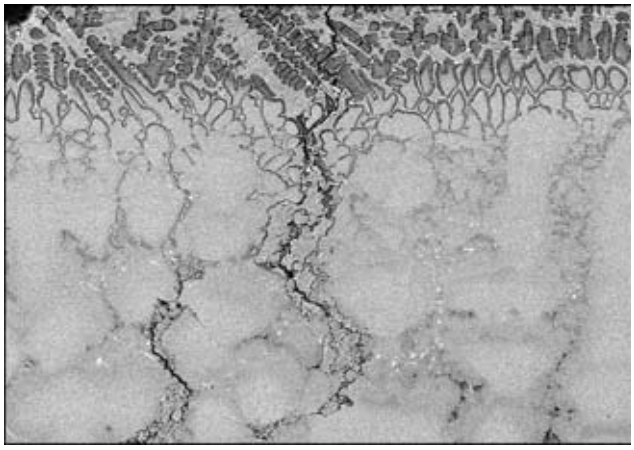

Figure 2. Hot cracks formed in arc heating with melting of base metal (×350)

of a Ni-base solid solution and eutectic component (Figure 1).

As revealed by the examination of chemical heterogeneity, the deposited metal is rich in the base metal elements (Table). Therefore, in the case of melting of the base metal and brazing filler alloy the weld metal is close in chemical composition to the base metal. Formation of isolated hot cracks was seen in the fusion zone. They propagated along the boundaries of grains of the base metal, and in some regions they were partially filled with the brazing filler alloy (Figure 2).

Substantial decrease in thermal effect on the base metal was achieved in the case where the latter was not melted but wetted with the molten brazing filler alloy. Susceptibility to formation of hot cracks in this case decreased, but the most important fact is that they were filled with the brazing filler alloy (Figure 3).

It is apparent that cracks were formed at a temperature above the temperature of solidification of the weld metal, and a brazing filler alloy component characterised by higher flowability penetrated along the boundaries of grains of the base metal. The resulting microstructure of the deposited metal consists of two phases: coarse dendrites of solid solution and eutectic component (Figure 4). Results of examination of chemical heterogeneity of the deposited metal show that mutual diffusion processes between the base metal and brazing filler alloy take place in it. However, these processes are less pronounced (see the Table) than in heating with melting of the base metal.

Further decrease in thermal effect on the fusion zone metal is achieved through using composite filler alloy powders, i.e. mixtures of low-melting point alloy of the Ni–Cr–Zr system and high-melting point high-alloyed heat-resistant alloy ZhS-26U. In this case the filler to base metal ratio is especially important. On the one hand, the higher the weight fraction of the high-melting point component, the higher the level of properties of the deposited metal. On the other hand, weight fraction of the filler alloy should not be too low, as it is necessary to ensure good wetting of the base metal and the possibility of healing the hot cracks if they are formed. The optimal brazing filler alloy to filling agent ratio allows avoidance of cracks and production of the deposited metal with a homogeneous fine-dispersed structure (Figure 5).

Results and discussions. As noted above, high Ni-base alloys with a high content of the γ'-phase are non-weldable. Analysis of the point of the processes that occur in this case shows that, on the one hand, welding leads to a substantial overheating of the HAZ, accompanied by formation of liquid interlayers along the grain boundaries, and a dramatic decrease in metal strength. In this case even a slight effect of welding stresses is enough for a crack to be formed in the base metal. On the other hand, using filler alloys close in chemical composition to the base metal makes it impossible to heal the cracks, as temperature of solidification of the molten pool metal is rather high. In addition, the cracks may be formed in the base metal at some distance from the weld pool. Increase in heat input and decrease in the welding speed, as suggested in [1–3], do decrease welding stresses, but increase the risk of the effect of such a factor as formation of liquid interlayers at the grain boundaries.

Distribution of elements of structural components of deposited metal

Structural components	*Content of elements, wt.%*									
	Ni	*Co*	*Zr*	*Ti*	*Cr*	*Mo*	*W*	*Nb*	*Al*	*Fe*
Arc heating with base metal melting										
Dendrite	57.8	3.4	1.5	0.9	15.1	0.2	16.9	1.2	2.6	0.5
Eutectic	69.3	1.7	19.3	1.0	3.5	–	1.9	1.4	1.9	1.0
Arc heating without base metal melting										
Dendrite	62.4	2.9	2.2	0.2	20.1	0.3	9.2	0.7	1.1	0.9
Eutectic	69.8	1.5	19.9	0.4	4.8	–	0.6	1.6	1.4	–

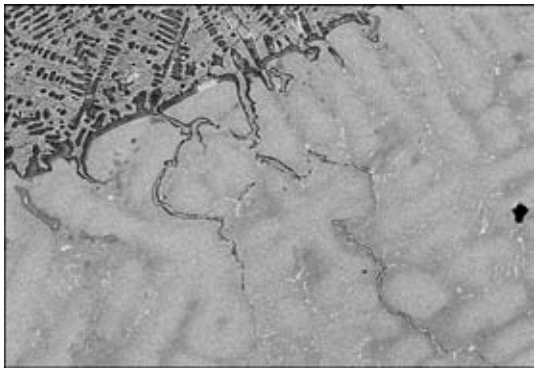

Figure 3. «Healed» cracks at the fusion line formed in arc heating without melting of base metal using brazing filler alloy of the Ni–Cr–Zr system (×300)

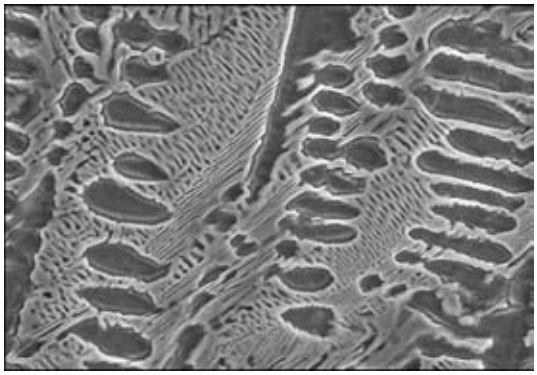

Figure 4. Microstructure of deposited metal produced by arc heating without melting of base metal using brazing filler alloy of the Ni–Cr–Zr system (×1800)

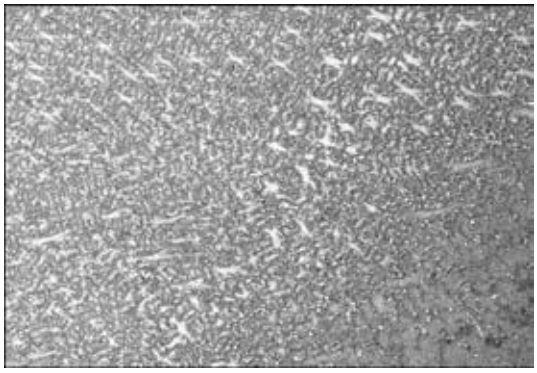

Figure 5. Microstructure of metal at the fusion boundary in sample of heat-resistant alloy ZhS6U-VI produced by using a composite brazing filler alloy (×200)

The approach suggested by the authors of this study proved itself to be very efficient for decreasing hot cracking. Its distinctive feature is that it provides a minimum heat input in arc heating. No liquid interlayers are formed in the HAZ in this case, and wetting of the base metal occurs at temperatures much lower than its melting point. The important role in this case is played by both brazing parameters and peculiarities of brazing filler alloys of new systems, such as the Ni–Cr–Zr system which has a high adhesion activity, increased ductility compared with the Ni–Cr–B–Si system and lower hardness. The latter is well proved by the results of measurement of microhardness of structural components of the deposited metal made by different methods (Figure 6).

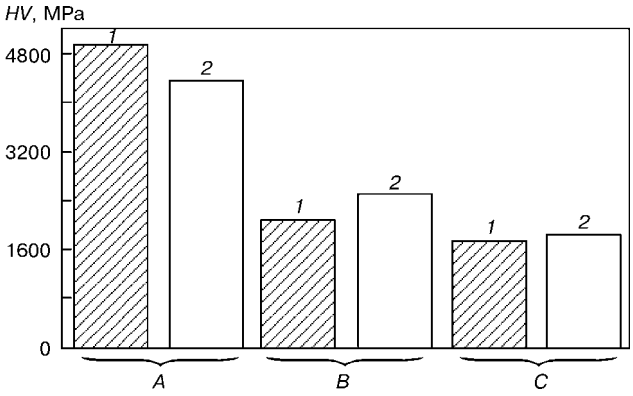

Figure 6. Microstructure of components of deposited metal produced by arc heating with (*1*) and without (*2*) melting of base metal: *A* — base metal; *B* — dendrite; *C* — eutectic

It should be noted that the best results were obtained in the case of using composite brazing filler alloys, rather than the cast ones, as the former allow regulation of not only the deposited metal composition but also the heat input. Moreover, in this case chemical composition of the deposited metal is hardly affected by sizes of defects. Naturally, the ratio of low-melting point to high-melting point components of the composite brazing filler alloy is also important.

Structure of the deposited metal produced by using composite brazing filler alloys consists of uniformly distributed dispersed regions of solid solution and eutectic, which creates favourable conditions for homogenising annealing, resulting from both non-equilibrium structure and comparatively short length of diffusion flows.

CONCLUSIONS

1. Combination of arc heating and adhesion-active brazing filler alloys, such as those of the Ni–Cr–Zr system, used as the filler metal holds high promise for development of a technology for repair of components of hot section of gas turbine engines.

2. The use of composite brazing filler alloys was found to be especially efficient for regulation of chemical composition of the deposited metal and heat input.

3. Using a composite brazing filler alloy and arc heating made it possible to eliminate cracking and produce deposited metal with a homogeneous fine-dispersed structure.

1. Jahnke, B. (1982) High-temperature electron beam welding of nickel-base superalloy IN-738LC. *Welding J.*, Nov., 343–347.
2. Haafkens, M.H., Matthey, J.H.G. (1982) A new approach to the weldability of nickel-base as-cast and powder metallurgy superalloys. *Ibid.*, 25–30.
3. Koren, A., Roman, M., Weisshaus, I. et al. (1968) Improving the weldability of Ni-base superalloys 713C. *Ibid.*, Nov., 348–351.
4. Khorunov, V.F., Ukader, E.M. (1991) Principles for development of eutectic filler metals for heat-resistant nickel alloy brazing. In: *Proc. of Int. Conf. on Joining Welding*, Hague, July 1–2, 1991. Oxford: Pergamon Press.
5. Khorunov, V.F., Ivanchenko, V.G., Kvasnitskij, V.V. (1998) Investigation of Ni–Cr–Zr and Ni–Cr–Hf alloys. In: *Proc. of Int. Conf. on Soldering, Brazing and Diffusion Bonding*, Aachen, May, 1998. Aachen.
6. Khorunov, V., Maksymova, S., Samokhin, S. et al. (2000) Brazing filler alloy containing Zr and Hf as depressants. In: *Proc. of 3rd Int. Conf. on High Temperature Capillarity*, Kurashiki, Nov. 19–22, 2000. Osaka.

CALCULATION OF TEMPERATURE DISTRIBUTION ALONG THE ELECTRODE EXTENSION, TAKING INTO ACCOUNT THE HEAT CONTRIBUTED BY THE DROP

I.V. PENTEGOV and **O.I. PETRIENKO**
E.O. Paton Electric Welding Institute, NASU, Kyiv, Ukraine

A mathematical model has been developed of temperature distribution along the length of electrode extension in consumable electrode CO_2 arc welding, allowing for non-linearity of thermophysical coefficients and impact of heat contributed by the drop, which permits calculation of the temperature gradient and temperature in any point on electrode extension (from the nozzle to the drop). Recommendations are given on selection of electrode extension size.

Keywords: *arc welding, carbon dioxide gas, electrode extension, mathematical model, calculation, temperature, heat conductivity, temperature distribution*

Studying the thermal processes in the section of electrode extension remains to be the most important subject of numerous investigations in the field of welding fabrication [1–10]. However, the conducted analysis of theoretical and practical developments on the issue demonstrated that the processes of temperature distribution along the electrode extension, allowing for thermophysical parameters and heat, contributed by the drop, are insufficiently studied. One of the important and still unsolved problems of the theory of welding processes in consumable electrode welding is solving the equation of heat conductivity for electrode extension in the general form, when the thermophysical coefficients are non-linear functions of temperature.

Electrode extension can be conditionally subdivided into two sections: section of electrode extension adjacent to the nozzle and heated by electric current, where the influence of the heat contributed by the drop, is negligible; and section adjacent to the drop, where heating is due to the impact of electric current and heat supplied through heat conductivity of the drop. Figure 1 shows, how both these sections interface at a certain temperature of the boundary T_1 and electrode extension l_1, corresponding to this temperature. This paper is devoted to determination of these values and issuing recommendations on selection of electrode extension.

The presented mathematical model of temperature distribution along the electrode extension (in consumable electrode CO_2 arc welding, allowing for the non-linearity of thermophysical coefficients and influence of heat conductivity from the drop) is based on solving the Fourier differential equation [11].

Work [12] provided a procedure of calculation of the voltage drop on electrode extension for the first section. Fourier equation has the following form for it:

$$\gamma C_p(T)\, v_f \frac{dT}{dl} - \rho(T) j^2 = 0, \qquad (1)$$

where v_f is the wire feed rate, m/s; γ is the density of metal (steel), kg/m^3; $C_p(T)$ is the specific heat content of steel, J/(kg·K); $\rho(T)j^2$ is the specific thermal power evolved by passing current, W/m^3; $\rho(T)$ is the specific electric resistance of the metal, Ohm·m; $j = 4I/(\pi d^2)$ is the current density, A/m^2.

This equation yielded the dependence of the current electrode extension l on current temperature T of this section of extension and initial temperature T_0 of electrode wire at nozzle outlet:

$$l(T, T_0) = \frac{v_f \gamma}{j^2} \int_{T_0}^{T} \frac{C_p(T)}{\rho(T)}\, dT, \qquad (2)$$

allowing determination of the length of electrode extension to boundary point l_1, if T_1 and T_0 are known

$$l_1(T_1, T_0) = \frac{v_f \gamma}{j^2} \int_{T_0}^{T_1} \frac{C_p(T)}{\rho(T)}\, dT. \qquad (3)$$

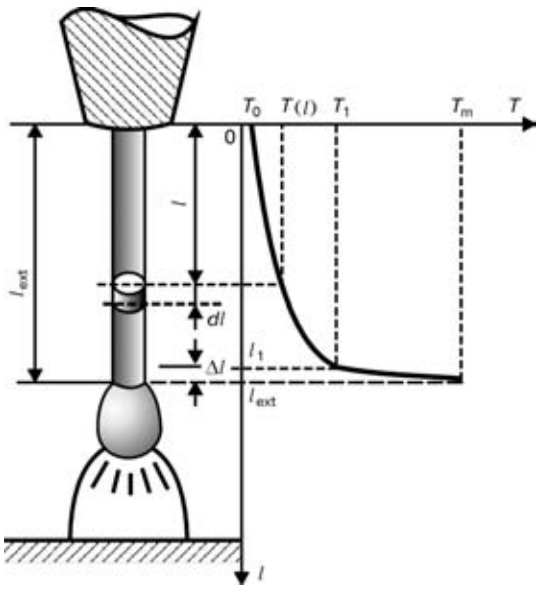

Figure 1. Circuit of distribution of temperature along the length of electrode extension (for designations see the text)

In [12] also a formula has been derived to determine the temperature gradient in the first section of electrode extension (derivative dT/dt):

$$\frac{dT}{dl} = \frac{\rho(T)j^2}{\gamma C_p(T)v_f}. \quad (4)$$

Non-linear approximations of $\rho(T)$ and $C_p(T)$ given in [12], are used in calculations. These formulas, however, are invalid in the second section of electrode extension, which is in the temperature range of T_1 up to wire melting temperature T_m. Therefore, let us consider the section of electrode extension $\Delta l = l_{ext} - l_1$, where the metal heat conductivity has a significant influence on its heating (see Figure 1). Let us assume a system of coordinates, moving together with the wire at a constant wire feed rate for an element of the length of electrode extension dl in the entire section of electrode extension [12]. Temperature of element dl increases during its movement, and the heating process is of a dynamic nature. Let us write Fourier equation for an element of electrode extension in section Δl , allowing for a unidimensional nature of the problem (assuming that radiation and convection losses are negligible [13–15]) in the following form:

$$C_p(T)\frac{dT}{dt} = \lambda(T)\frac{d^2T}{dl^2} + \rho(T)j^2. \quad (5)$$

For a considered system of coordinates the current length of electrode extension $l = v_f t$ [12]. Using this dependence, we will replace variable $dt = dl/v_f$ in equation (5), and will obtain an equation, describing electrode extension in the second section, allowing for heat conductivity and non-linearity of thermophysical parameters:

$$\frac{d^2T}{dl^2} - \gamma v_f \frac{C_p(T)}{\lambda(T)}\frac{dT}{dl} + \frac{\rho(T)}{\lambda(T)}j^2 = 0, \quad (6)$$

where $\lambda(T)$ is the heat conductivity of steel, W/(m·K).

This equation can be solved by numerical methods without simplification, but this no longer permits performance of theoretical generalizations or analysis, which is required to solve the defined problem. In order to derive an analytical solution in the section of electrode extension Δl let us use averaged thermophysical parameters (average values of ratio of specific heat content to heat conductivity and specific electric resistance of electrode material to heat conductivity, respectively) in the integration range and let us introduce the following symbols:

$$a = \frac{\gamma v_f}{T_m - T_1}\int_{T_1}^{T_m}\frac{C_p(T)}{\lambda(T)}dT, \quad b = \frac{j^2}{T_m - T_1}\int_{T_1}^{T_m}\frac{\rho(T)}{\lambda(T)}dT. \quad (7)$$

Calculation of values a and b by these formulas is performed, using non-linear approximations of $\rho(T)$ and $C_p(T)$, given in [12], as well as approximation of the dependence of heat conductivity on temperature:

$$\lambda(T) = \begin{cases} 69.92 - 0.096T & \text{at } T \le 100, \\ 65.73 - 0.049T & \text{at } 100 \le T \le 500, \\ 60.29 - 0.039T & \text{at } 500 \le T \le 700, \\ 56.10 - 0.032T & \text{at } 700 \le T \le 900, \\ 23.027 + 0.005T & \text{at } T \ge 900. \end{cases}$$

Introduction of constants a and b into equation (6) allows transforming it as follows:

$$\frac{d^2T}{dl^2} - a\frac{dT}{dl} + b = 0. \quad (8)$$

In case of replacement of variable $T' = dT/dl$ (new variable is temperature gradient), equation (8) turns into a linear differential equation of the first order:

$$\frac{dT'}{dl} - aT' + b = 0. \quad (9)$$

Integrating this expression in the following limits: temperature gradient from $T'(l_1)$ up to current value of $T'(l)$, electrode extension from l_1 up to current value of l, we obtain an expression to calculate the temperature gradient in any point in the section of electrode extension Δl:

$$\frac{dT}{dl} = T' = \frac{(aT'(l_1) - b)\,e^{a(l - l_1)} + b}{a}, \quad (10)$$

where $T'(l)$ is the temperature gradient in the vicinity of the boundary point from the side of temperature interval Δl.

At transition to variable T and separation of the variables in expression (10), we will take integral

$$\int_{T(l_1)}^{T(l)} dT = \int_{l_1}^{l}\frac{(aT'(l_1) - b)\,e^{a(l - l_1)} + b}{a}dl, \quad (11)$$

then (at $T(l_1) = T_1$) we will write

$$T(l) = T_1 + \left(\frac{T'(l_1)}{a} - \frac{b}{a^2}\right)(e^{a(l - l_1)} - 1) + \frac{b(l - l_1)}{a}. \quad (12)$$

This equation allows calculation of temperature in any point in electrode extension section Δl, if values of T_1, l_1 and $T'(l_1)$ are known. However, if values of T_1 and l_1 as will be shown below, can be selected based on certain grounds, the temperature gradient in the boundary point $T'(l_1)$ can be determined only, when using the boundary conditions on the electrode extension–drop interface. Assuming that at $l = l_{ext}$ value $T(l_{ext})$ is equal to the temperature of melting of electrode wire T_m, and solving at these values equation (12) with respect to $T'(l)$, we find

$$T'(l_1) = \frac{a(T_m - T_1) - b(l_{ext} - l_1)}{e^{a(l_{ext} - l_1)} - 1} + \frac{b}{a}. \quad (13)$$

Substituting expression (13) into formula (12), we obtain the equation for calculation of temperature in electrode extension section $l_1 \le l < l_{ext}$:

$$T(l) = \frac{e^{a(l-l_1)} - 1}{e^{a(l_{ext}-l_1)} - 1}\left(T_m - T_1 - \frac{b(l_{ext} - l_1)}{a}\right) + T_1 + \frac{b(l - l_1)}{a}. \quad (14)$$

Expression (14) provides the condition of the boundary of the considered two sections of electrode extension in terms of temperature in point l_1, but does not provide the boundary by temperature gradient. In the second interval, the averaged thermophysical parameters are used, which are determined from formula (7), and in the first — the precise non-linear dependencies of thermophysical parameters on temperature.

However, there exist conditions, at which it is possible to provide the minimum possible discrepancy of temperature gradients in the boundary point. Determination of these conditions consists in the following. Let us introduce designation $\Delta l = l_{ext} - l_1$ and write $F(T_1, \Delta l)$ as the ratio of temperature gradients in the boundary point by formulas (13) and (4):

$$F(T_1, \Delta l) = \left\{\frac{a(T_m - T_1) - b\Delta l}{e^{a\Delta l} - 1} + \frac{b}{a}\right\} \times \frac{\gamma C_p(T_1) v_f}{\rho(T_1) j^2}. \quad (15)$$

As shown by analysis of the latter expression, this function is always greater than 1 in the temperature range of 600–1044 K. It is obvious that the minimum value of this function closest to 1, corresponds to the best condition of solution co-ordination. Therefore, taking a derivative from this expression by T_1 (considering that values a and b are also function of T_1) and equating it to zero, we obtain the condition for optimum alignment

$$\frac{dF(T_1, \Delta l)}{dT_1} = 0. \quad (16)$$

Solving equation (16) with the specified value of T_1 relative to Δl, we will find interval Δl as a function of v_f and j. The above procedure of finding Δl is easily implemented, using MathCad package (Δl value practically does not depend on T_0 and T_1). Calculation results in Δl interval as a function of v_f and j are given as a family of curves in Figure 2. Values of v_f and j (or current I) for the given electrode wire diameter can be selected by curves given in Figure 3, which are a nomographic generalization of recommendations of KEMPPI Company and a number of publications [1, 6, 16, 17]. In this case, the upper limit of the recommended values corresponds to electrode extension equal to 20 mm, and the lower to 6.4 mm for all the diameters of electrode wire.

Determining Δl and using expression (3), we will find the electrode extension

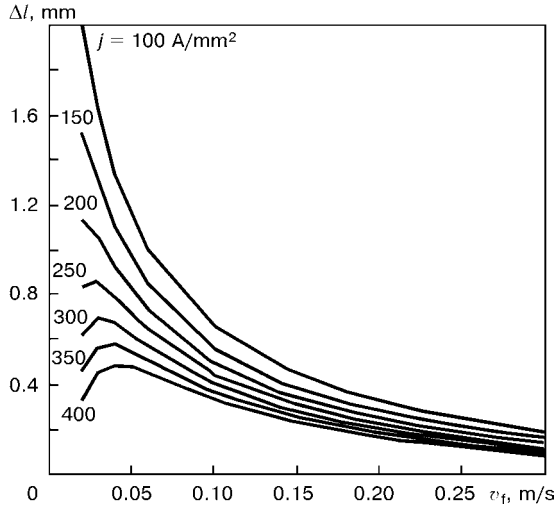

Figure 2. Results of calculations of Δl interval as a function of v_f and j at any values of T_1

$$l_{ext} = l_1(T_1, T_0) + \Delta l. \quad (17)$$

This is the value of l_{ext}, which should be substituted into formula (14) in calculation of temperature distribution along electrode extension in the second interval.

In the first section of the electrode at $0 \le l < l_1$, calculation of temperature distribution along the extension length is conducted by the formula of MathCad package for inverse functions, using expression (2):

$$T(l) = \text{root}\left[\frac{v_f \gamma}{j^2}\int_{T_0}^{T}\frac{C_p(T)}{\rho(T)}\,dT - l, T\right]. \quad (18)$$

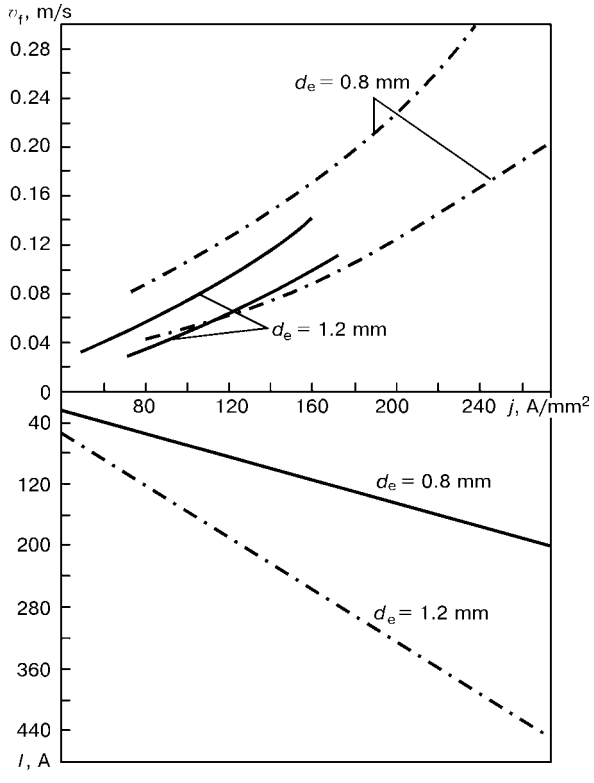

Figure 3. Nomograms for selection of values of v_f and j

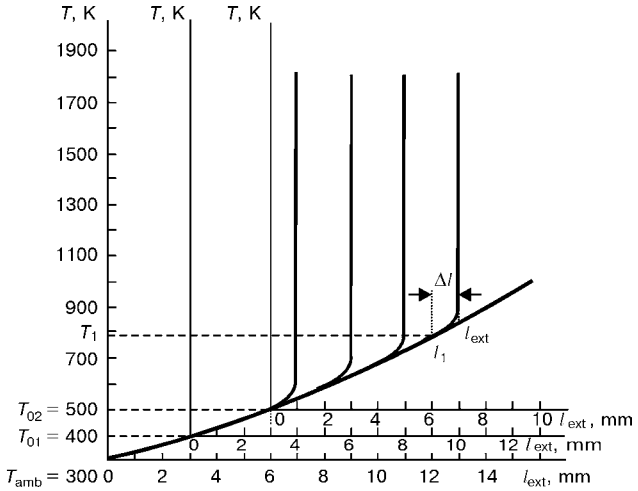

Figure 4. Distribution of temperatures along electrode extension at different specified values of temperature of boundary point T_1 and initial temperatures T_0

In Figure 4 the derived formulas were used to plot a family of curves of temperature distribution along electrode extension at different specified values of temperatures of boundary point T_1 and initial temperatures T_0 for one specific recommended welding mode (d_e = 1 mm, v_f = 0.233 m/s, j = 318 A/mm^2).

Wire temperature T_0 at its exit from the nozzle may be in the range of 150–450 °C [3, 18, 19]. The lower limit corresponds to an unworn copper nozzle, and the upper one to nozzles of different bronzes and cermets at pronounced wear.

If the value of contact voltage drop U_c on the nozzle is known, then wire temperature T_0 can be calculated by the following formula:

$$T_0 = \text{root}\left[\frac{\gamma v_f}{j}\int_{T_{amb}}^{\theta} C_{p\,av}(T)dT - K_U,\ U_c,\ \theta\right], \qquad (19)$$

where T_{amb} is the ambient temperature; $C_{p\,av}$ = = 500 J/(kg·K) is the averaged value of specific heat content of steel in the temperature range of the initial contact heating of the wire; K_U is the coefficient, allowing for the power share consumed in increasing the wire temperature, out of the total power evolved in contact.

Calculation by the formulas of Holm theory [20] for the considered case shows that K_U = 0.512, and it practically does not change with the change of welding mode. Wire temperatures T_0 at nozzle outlet were calculated, proceeding from formula (19) for a number of welding modes tried out in practice (Table). Calculation was performed for nozzle of copper M1 at value U_c = 0.65 V, which corresponds to the case of a new nozzle [21]. The same modes were used to find values of Δl, $l_1 = l_{ext} - \Delta l$ from the above formulas, and temperature in boundary point T_1 was determined from formula (18) at $l = l_1$.

As expressions (2) and (18) depend on wire temperature T_0 when it leaves the nozzle, then in construction of graphic dependencies by these expressions, we obtain a family of curves for different T_0, given in Figure 4. From consideration of the obtained curves it follows that increase of initial temperatures from T_0 up to T_{01} (for instance, at nozzle wear), is equivalent to shifting of the origin of co-ordinates by length

$$l(T_{01}, T_0) = \frac{v_f\gamma}{j^2}\int_{T_0}^{T_{01}} \frac{C_p(T)}{\rho(T)}\,dT. \qquad (20)$$

In this case, if it is necessary to maintain the temperature in boundary point, then the electrode extension should be shortened by this length, or, if we preserve the electrode extension unchanged, the boundary temperature will rise. Calculated values of boundary temperature T_1 from the Table show that T_1 can sometimes be close to a dangerous limit, if an attempt is made to keep the electrode extension unchanged, while changing the welding modes. Shortening of the extension may be recommended to maintain the welding quality with nozzle wear.

There exists a certain flexibility in selection of the temperature of boundary point and electrode extension, but in a rather narrow range. At very short extensions (< 2 mm) there is the risk of the nozzle burning at random oscillations of the welding torch and the process efficiency decreases. At great extensions (and higher temperatures of the boundary), the melting efficiency rises, which is attributable to a

Comparison of calculated curves with experimental data

Experimental data from [6, 17]						*Calculated data*			
d_e, mm	I, A	v_f, m/s	j, A/mm^2	l_{ext}, mm	Δl, mm	l_1, mm	T_0, K (°C)	T_1, K (°C)	l_{ext}, mm (at T_1 = 850 K = const)
0.8	150	0.14	298.4	6.4	0.4	6.0	450 (177)	830 (557)	6.66
		0.168		10	0.364	9.64	421 (148)	944 (671)	8.59
	200	0.2	397.9	6.4	0.2	6.11	493 (220)	1027 (754)	4.66
		0.231		10	0.28	9.72	464 (191)	1343 (1070)	5.84
1.2	150	0.05	132.63	6.4	1.07	5.33	493 (220)	671 (398)	11
		0.06		10	0.96	9.04	457 (184)	707 (434)	14
	200	0.085	212.21	6.4	0.65	5.75	605 (332)	952 (679)	4.87
		0.1		10	0.57	9.43	555 (282)	1048 (773)	6.7

more effective use of the heat to melt electrode metal, but this may give rise to an inadmissible «pulsed» mode of wire heating with a marked deterioration of weld quality [18]. The greater the nozzle wear, the higher the probability of such pulsations, as in a worn nozzle the contact is unstable (alternation of the sliding, spark and arc contacts is possible), which generates heat waves, propagating over the extension and resulting in self-excited oscillations.

With great electrode extensions and high temperatures of boundary point T_1 the process may be stabilized by regulation of the rate of carbon dioxide gas flow, as according to [2] with the increase of the gas flow and decrease of voltage in the nozzle–workpiece section, the drop temperature decreases and the process becomes more stable. For instance, as shown by calculations [2], at currents of about 280 A and extensions of about 25 mm at a large gas flow, temperature T_1 of preheating of 1 mm diameter electrode may reach 1000 °C and more without loss of stability. However, if the gas flow rate is insufficient, then self-excited oscillations may develop in the arc self-regulation system — a periodical change of electrode melting rate and arc length with 5–25 Hz frequency. There exists an optimal range of boundary point temperatures of 400 °C (673 K) $\le T_1 \le$ 800 °C (1073 K), within which no excess consumption of carbon dioxide gas is yet required, and there is no risk of development of self-excited oscillations (with increase of T_1 it is always necessary to increase CO_2 consumption). The lower limit of this range is close to recommendations of [18], which coincide with those for consumable-electrode SAW. At this temperature there is a complete guarantee of the absence of pulsations of the thermal modes. However, at such a temperature of the boundary it is inadmissible to work with worn nozzles, as the required extension length tends to zero, if T_0 is close to 450 °C. Therefore, T_1 in the middle of a range of 500–700 °C (773–973 K) should be selected as recommended temperatures of the boundary point. The Table gives as an example the calculated values of extensions for the considered welding modes, if boundary temperature T_1 is maintained constant and equal to 850 K.

Value l_1 can be calculated not by formula (3), but by approximation

$$l_1 = \frac{v_f}{j^2}\left(T_1^{1/4} - T_0^{1/4}\right)(5\cdot 10^6), \qquad (21)$$

where v_f is measured in m/s; j in A/mm^2; T_1 and T_0 in K; here $l_1(T_0)$ is obtained in mm ($5\cdot 10^9$ is the dimensional coefficient). Error of calculations by this formula in the real range of T_1 variation does not exceed 1 %.

Formula (21) can be converted to the form convenient for determination of the current temperature in the first section of electrode extension adjacent to the nozzle, as a function of the current value of l instead of formula (18):

$$T(l) = \left(\frac{lj^2}{5\cdot 10^6 v_f} + T_0^{1/4}\right)^4. \qquad (22)$$

Determination of the recommended length of electrode extension is reduced to the following. For the values of v_f and j (or current I with subsequent determination of current density j), temperature T_1 selected from curves in Figure 3, recommended for this wire diameter, and known value of T_0, l_1 is found from formula (21) and Δl interval is determined by the curves in Figure 2. After that the length of electrode extension is determined by the following formula:

$$l_{ext} = l_1 + \Delta l. \qquad (23)$$

Results of calculations (see the Table) agree with the data of experiments, given in [6, 16, 17].

Equations, derived during the conducted study for calculation of temperature distribution along the electrode extension, are the basis for further development of a complete mathematical model of power source–welding arc system in consumable electrode CO_2 arc welding.

In conclusion, it should be noted that the developed model allows calculation of the zone, in which electrode heating is determined by heating proper from the passing current, and the length of electrode zone, in which the main thermal processes are determined by heating from the drop.

Expressions were obtained, describing temperature distribution along the solid part of electrode extension with allowance for heat conductivity of the electrode metal, as well as expressions for calculation of the temperature gradient and temperature distribution in the first section of the electrode extension adjacent to the nozzle, and an expression to calculate the temperature gradient and temperature in the second section of electrode extension adjacent to the drop. Temperature distribution along the electrode extension is represented in the form of a function, dependent on welding current, wire feed rate, current density and electrode extension.

Recommendations are given on selection of electrode extension. It is shown that with the change of welding modes it is better to keep constant not the extension, but the temperature of the boundary point between the first and second sections of electrode extension. With increase of the wire temperature, when it leaves the nozzle, electrode extension should be decreased.

It is established that heat conductivity has an essential influence on heating of electrode extension not along its entire length, but only in the section, adjacent to the drop. The derived expression allows determination of the beginning of this section. Solving this problem, taking into account the heat conductiv-

ity, allows calculation of temperature gradient in the section of electrode extension, adjacent to the drop.

The model allows determination of temperature gradient dT/dl on the boundary with the drop at $T = T_m$, which, in its turn, will permit in the future determination of the amount of heat coming from the drop to the electrode, and studying the thermal balance of the drop in greater detail and more accurately than before.

The developed mathematical model of the processes, proceeding in the power source–welding arc system for consumable electrode CO_2 arc welding, will permit development of the data base of various modes of this welding process.

1. Akulov, A.I. (1966) On quantity of heat contributed to the arc by the electrode heated in the extension. *Avtomatich. Svarka*, **5**, 35–38.
2. Antipov, V.V. (1971) *CO_2-welding with thin electrode wire at increased speed of gas flow*. Syn. of Thesis for Cand. of Techn. Sci. Degree. Moscow: N.E. Bauman MVTU.
3. Varukha, E.N. (1997) Allowance for wire preheating in the mathematical model of electrode melting during mechanized welding. In: *Proc. of Russian Sci.-Techn. Conf. on Current Problems of Welding Science and Technology*, Voronezh, 1997. Voronezh: SABA.
4. Dubovetsky, S.V. (1982) *Investigation and development of calculation procedure of CO_2-welding modes for low-carbon and low-alloyed steels*. Syn. of Thesis for Cand. of Techn. Sci. Degree. Kyiv.
5. Marishkin, A.K. (1970) *Investigation of electrode wire heating, melting and evaporation in arc welding*. Syn. of Thesis for Cand. of Techn. Sci. Degree. Chelyabinsk.
6. Panibrattsev, B.K. (1978) Calculation of electrode wire feed rate in CO_2-welding with a short arc. *Svarochn. Proizvodstvo*, **11**, 42–43.
7. Paton, B.E. (1953) *Automatic electric arc welding*. Kyiv: Mashgiz.
8. Rykalin, N.N. (1951) *Calculations of thermal processes in welding*. Moscow: Mashgiz.
9. Quinn, T.P., Madigan, R.B., Siewert, T.A. (1994) An electrode extension model for gas metal arc welding. *Welding J.*, **10**, 241–248.
10. So, G.K., de Boer, F.G. (2001) Analysis of standoff estimation algorithms in GMAW short-circuit transfer mode. *Austral.Welding J.*, **46**, 33–39.
11. Zhukovsky, V.S. (1969) *Principles of heat transfer theory*. Leningrad: Energiya.
12. Pentegov, I.V., Petrienko, O.I. (2002) Method of calculation of voltage drop in electrode stickout length with allowance for non-linearity of thermophysical parameters. *The Paton Welding J.*, **4**, 27–30.
13. Lebedev, A.V. (1978) Influence of heat evolution in electrode extension on arc self-regulation. *Avtomatich. Svarka*, **7**, 10–15.
14. Paton, B.E. (1948) Investigation of electrode heating process in automatic submerged-arc welding. In: *Transact. on Automatic Welding*, 13–28.
15. Paton, B.E., Shejko, P.P. (1965) Metal transfer control in consumable electrode arc welding. *Avtomatich. Svarka*, **5**, 1–7.
16. Potapievsky, A.G. (1974) *Consumable-electrode gas-shielded welding*. Moscow: Mashinostroenie.
17. Chubukov, A.A. (1978) *Study and improvement of reliability of consumable electrode CO_2 arc welding*. Syn. of Thesis for Cand. of Techn. Sci. Degree. Kyiv.
18. Shejnkin, M.Z. (1978) Determination of admissible thin electrode wire extension in CO_2-welding. *Svarochn. Proizvodstvo*, **9**, 24–28.
19. (1987) Untersuchung der Kontaktverhaeltnisse bei der Stromuebertragung auf den Schweissdraht. *Wissenschaftliche Zeitschrift der Technischen Universitaet «Otto von Guericke»*, Magdeburg, 4, 96–102.
20. Holm, R. (1961) *Electric contacts*. Moscow: Inostr. Literatura.
21. Koshkaryov, B.T., Mikhajlov, A.N., Budnik, N.M. (1971) Influence of electrode extension on melting electrode process in CO_2-welding. *Svarochn. Proizvodstvo*, **11**, 30–32.

EXPLOSION CUTTING AND ITS APPLICATION*

V.G. PETUSHKOV, L.A. VOLGIN and **L.D. DOBRUSHIN**
E.O. Paton Electric Welding Institute, NASU, Kyiv, Ukraine

Principles of the technology for explosion cutting of metal structures using elongated cumulative explosive charges (ECEC) developed by the E.O. Paton Electric Welding Institute are considered. Relationships describing the efficiency of ECEC within the framework of the hydrodynamic theory are presented. Examples of successful application of the explosion cutting technology in some industries are given, including under critical conditions where special measures have to be taken to provide protection from the side effects of explosion.

Keywords: *explosive, cumulation, explosion cutting, elongated cumulative explosive charge, main pipeline, emergency situation*

Hydrodynamic cumulation theory, well studied for axisymmetric charges [1], is based on an assumption that collision of a cumulative jet with a barrier results in development of a high pressure, under which the strength of metal can be ignored and the barrier can be regarded as an ideal uncompressible liquid. These conditions are valid if pressure in collision of the jet with the barrier is in excess of $2 \cdot 10^4$ MPa, i.e. if velocity of the cumulative jet is $v_j > 4000$ m/s.

Figure 1 shows schematics of the section of an axisymmetric cumulative charge with a conical metal cavity and the cumulative jet formation. When a plane detonation wave propagates through the charge towards the cavity, elements of liner of the cumulative cavity subjected to compression move inside towards its geometric centre. Their collision causes formation of a high-velocity cumulative jet, resulting from an intensive flow of the internal layers of the metal liner. This jet is followed by a low-velocity pestle of the external layers of the liner that does not participate in penetration through the barrier. At a velocity of the jet equal to $v_j > 4000$ m/s the basic postulates of the cumulation theory can be described using equations of hydrodynamics. Solutions to these equations can be written down as follows:

depth of penetration through the barrier

$$L = l \sqrt{\frac{\rho_j}{\rho_b}}; \qquad (1)$$

velocity of penetration of the jet into the barrier

$$U = v_j \left(\frac{\rho_b}{\rho_j} + 1 \right)^{-0.5}; \qquad (2)$$

velocity of the jet

$$v_j = v_0 \operatorname{ctg} \frac{\alpha}{2}, \qquad (3)$$

where l is the jet length; ρ_j and ρ_b are the jet and barrier densities, respectively; v_0 is the liner reduction velocity; and α is the angle at the liner cone apex.

According to (1), the depth of penetration through the barrier is proportional to the length of the cumulative jet and the square root of the jet to barrier density ratio. It should be noted at this point that the jet extends while moving, and the maximum depth of penetration is provided in a case where the barrier is at a certain (focal) distance from the charge axis. The penetrating ability of the jet depends upon the density of the liner material. Therefore, in practice the preference is given first of all to a liner of the cumulative cavity made from metal, as a rule copper or steel. In addition, to form a high-velocity jet ($v_j \geq$ ≥ 4000 m/s), it is necessary that charges be filled with high explosives, such as hexogen (RDX), octogen or other analogues having a high detonation velocity.

ECEC designed by PWI (Figure 2, *a, b*) is a shaped metal tube filled with explosive. The cumulative cavity of ECEC has a shape of a semi-cylinder. Cylindrical casing of ECEC is made from copper. It

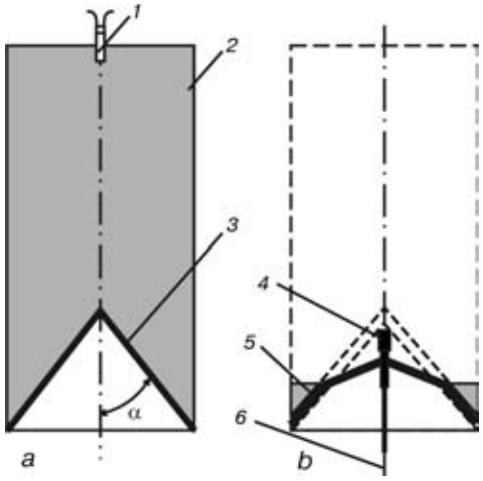

Figure 1. Schematics of section of axisymmetric cumulative explosive charge with a conical metal liner (*a*) and formation of the jet (*b*): *1* — detonator; *2* — explosive; *3* — cumulative cavity; *4* — pestle; *5* — detonation front; *6* — cumulative jet

* The article is based on the paper presented at the International Conference on Cutting Technology, March 5–6, 1997, Hanover.

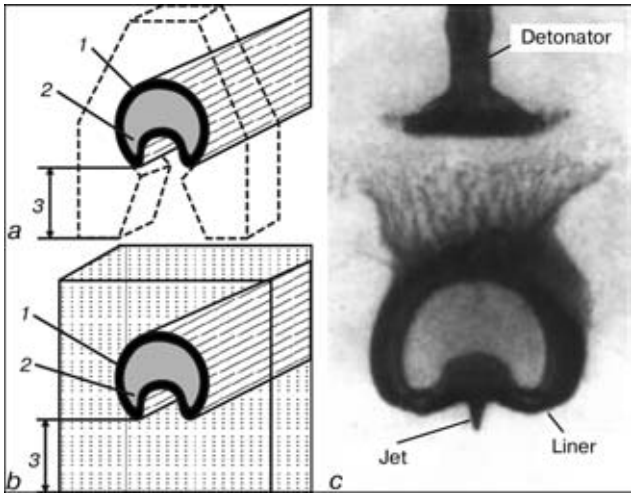

Figure 2. ECEC for ground (*a*) and underwater (*b*) cutting, and pulse X-ray pattern of explosion of ECEC in water (*c*): *1* — explosive; *2* — liner; *3* — focal distance

is charged with RDX compacted during manufacture of the charge to 1.71–1.74 g/cm^3. The detonation velocity of ECEC achieved in this case is up to 8500 m/s.

Results of evaluation of parameters of the ECEC cumulative jet by the pulse radiography (Figure 2, *c*) show that velocity of the leading part of the jet is 2200–3500 m/s, which is a bit lower than that of the cumulative charges with a conical metal cavity. This is attributable to the fact that such factors as strength and compressibility of the jet and barrier materials show up at the above velocities. Equations of hydrodynamics cannot be used in this case.

The following was established as a result of studies for evaluation of optimal parameters and geometric modelling of ECEC [2, 3]:

$$\frac{L}{D} = f\left(\frac{d_c}{D}, \frac{\delta_c}{D}, \frac{F}{D}\right), \qquad (4)$$

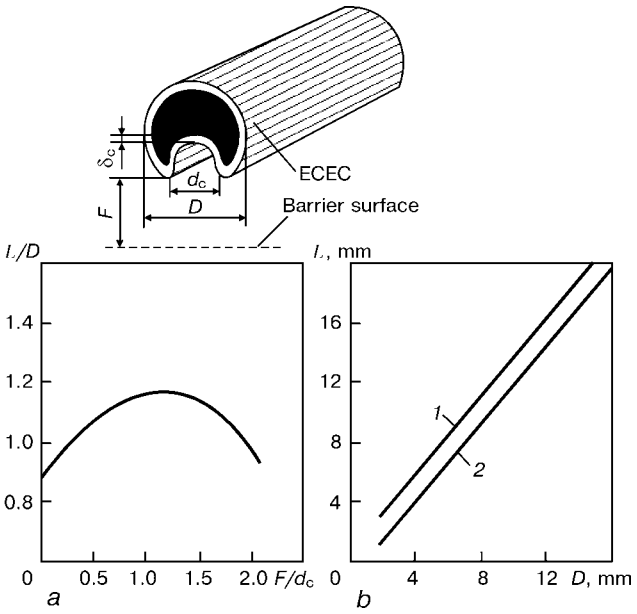

Figure 3. Dependence of the depth of cut upon the focal distance (*a*) and diameter of ECEC (*b*): *1* — low-carbon steel; *2* — stainless steel

where D is the ECEC diameter; d_c and δ_c are the diameter and thickness of the cumulative cavity; and F is the focal distance.

The first two dimensionless parameters in expression (4) characterise ECEC, and the last one characterises its location relative to the barrier.

The following empirical relationships of these parameters were derived on the basis of results of later studies conducted at PWI:

$$\frac{d_c}{D} = 0.42–0.44, \qquad (5)$$

$$\frac{\delta_c}{D} = 0.06–0.07, \qquad (6)$$

$$\frac{F}{D} = 1.0–1.5. \qquad (7)$$

The process of manufacture of ECEC is a sequential drawing of the copper tube preliminarily filled with RDX through the shaping holes of several drawing dies. Drawing of the charge billet is performed to give it the preset size and shape, as well as thickness of the wall of the tube, including the cumulative cavity, and provide the required degree of compacting of the explosive.

Comprehensive studies performed to optimise some technological operations and produce experimental batches of ECEC allowed the development of an optimal flow diagram of the process of manufacture of these charges, ensuring a high degree of safety and quality of the products at minimum costs. The complete set of basic and supporting equipment for mass production of ECEC was built by PWI.

This equipment allows manufacture of ECEC of a straight-line, circular, saddle-shaped or any other configuration with a diameter from 2.5 to 50.0 mm, and, if custom-made, to 80.0 mm. Main types and parameters of standard ECEC for ground and underwater operations are given in the Table, while relationships characterising the degree of penetration of the jet into the barrier are shown in Figure 3.

Oil and oil products play an important role in the fuel and energy system of any country. Transfer and delivery of oil and oil products to customers are done via main pipelines that should be maintained and repaired during service.

In this case, the most important operations are cutting of a linear part of pipelines, cutting out of «repair spools», connection of branch pipes to an active main pipeline without interruption of transfer of a product, as well as others associated with cutting of pipelines. Performing these operations using ECEC has a number of peculiarities and advantages. They include a high cutting speed, high reliability of the process, possibility of a remote control of the process from any distance, and making of holes and slits of any shape and size, depending upon the charge geometry.

Main parameters of ECEC made by PWI

Charge designation	*Content of explosive, g/m*	*Thickness of barrier*	
		ground	*underwater*
UKZ 10	60	10.0	8.5
UKZ 13	90	13.0	11.0
UKZ 14.5	120	14.5	12.5
UKZ 16	160	16.0	13.5
UKZ 19	210	19.0	16.0
UKZ 22	300	22.0	18.5
UKZ 25		Custom-made	
UKZ 50		Same	

Notes. 1. Numbers in designations of ECEC stand for its diameter and guaranteed thickness of the cut barrier under ground conditions. 2. Underwater explosion cutting is performed at a depth of 200 m (diving operators) and 600 m (manipulator).

PWI and VNIISPTneft (Russia) conducted theoretical and experimental studies, the results of which served as the basis for the identification of parameters of ECEC required to ensure an optimal cutting ability of the cumulative jet, and for the development of ingenious and simple designs of devices for explosion cutting of main pipelines.

The ECEC device, the so called external circular cumulative pipe cutter (TrKKN), was developed for transverse cutting of pipelines to cut out the «spool» or a defective region. It consists of two ECEC semi-rings and four adjusting (including two connecting) fixing rods, as well as an electric detonator holder. Fixing rods are made from polyethylene. They provide joining of the semi-rings and their location at an equal focal distance from the pipe surface.

One of the fixing rods has an opening to install the electric detonator that initiates the pipe cutter. At explosion the TrKKN type device is capable of cutting through the steel main pipeline with a wall thickness equal, as a rule, to a diameter of ECEC. The device is intended for cutting main pipelines and other tubular structures with a diameter from 152 to 1420 mm and wall thickness from 10 to 30 mm.

The technology for cutting a «spool» or defective region from a pipeline filled with oil or oil products provides for the use of two pipe cutters. Locations not less than 50 mm wide, where the pipe cutters are installed on a pipeline, are to be thoroughly cleaned on the entire perimeter of a pipe. After installing the pipe cutters, a pit where the «spool» is to be cut out is filled, prior to explosion, with a layer of the air-mechanical foam not less than 1 m thick over the pipe. The use of the foam provides a reliable prevention of fire or blast, when the spool is cut from a damaged pipeline and the space both outside and inside the pipe may have a dangerous concentration of the combustible mixture. Figure 4 shows the moment of outflow of petrol from the defective region of the pipeline immediately after explosion cutting of this region using two pipe cutters (Figure 5) and the air-mechanical foam.

Figure 4. Outflow of petrol from pipeline after explosion cutting using foam protection

Sometimes a pipeline may be in a stressed state induced by compressive stresses. This is the case where the spool may be jammed after the explosion. To make its removal easier (disassemble), three longitudinal ECEC are installed on the pipeline in addition to the two transverse pipe cutters. After the explosion the spool is cut into another three parts which can be readily removed.

If the spool has a large length, it is advisable to cut it out by the method shown in Figure 5. In this case the pipe cutters should be installed in a plane normal to the pipe axis, while another similar pipe cutter should be placed at a small angle to it. It can be easily seen that no jamming of any part of the spool will take place in this case.

The technology was developed to cut out defective gates, valves or other pipe fittings. According to this technology, the pipe cutters are installed on a pipeline on both sides of a gate, and a spiral explosive charge of a standard detonation cord (DC) is located near the above cutters. DC is initiated by the pipe cutters. At explosion the region to be cut is parted and

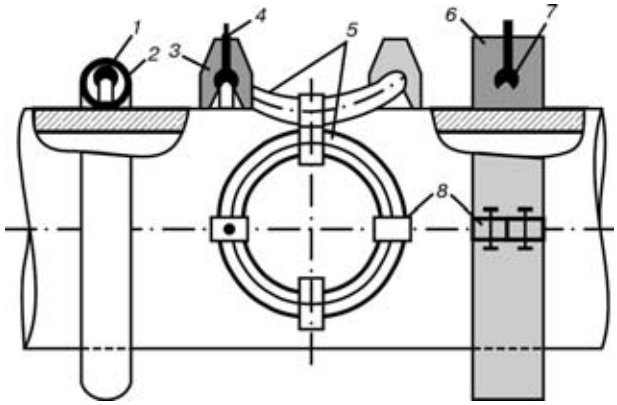

Figure 5. Schematic of the pipe cutting device: *1* — circular ECEC; *2* — protecting metal tube isolating the zone of formation of the cumulative jet; *3* — distance boss; *4* — electric detonator; *5* — saddle-shaped charge; *6* — charge in an all-foam plastic jacket; *7* — ECEC; *8* — connecting piece

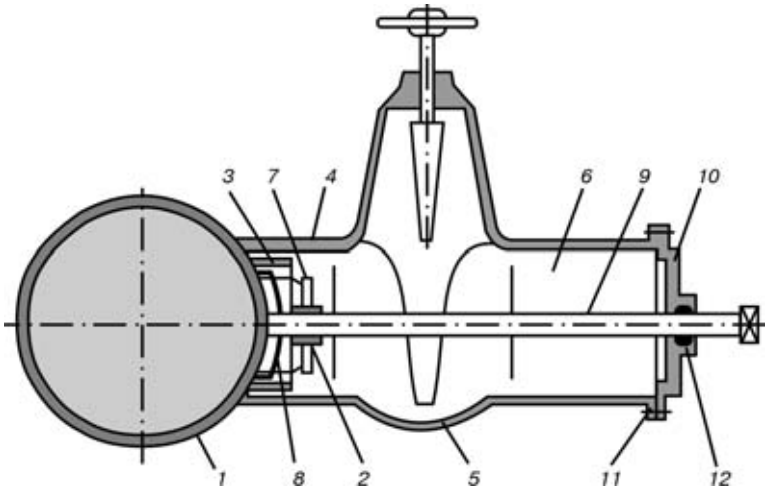

Figure 6. ECEC device for connecting a branch pipe to oil pipeline (see designations in the text)

squeezed, this making it easy to remove from the pipeline.

Investigations were conducted to study the effect of explosion of ECEC on the state of pipeline metal within the cutting zone. It was established that distortion of a pipe was within the tolerable limits and did not exceed 20 % of the pipe wall thickness. Penetration of the cumulative jet into the pipe wall results in sticking of copper to a cut edge, like in the case of cladding of copper to steel by explosion welding. Penetration of the cumulative jet also leads to formation of shock waves in a pipe material near the cutting zone. The shock waves cause structural changes in metal to a depth of 10–15 mm from the external surface of the pipe and increase in its hardness. Size of the hardening zone is smaller than size of the HAZ resulting from subsequent arc welding of a new spool. Nevertheless, the copper-covered part and zone having a changed structure and hardness are as a rule removed from the pipeline by gas cutting prior to installing a new spool.

The use of ECEC and TrKKN developed on its base in main pipelines of Russia and Ukraine during 1973–1990 made it possible to cut more than 3000 repair spools, gates and valves. That provided a substantial improvement in production arrangement, excluded the use of hard manual labour, improved safety conditions, considerably decreased labour consumption and reduced pipeline downtime. Thus, the time of cutting a spool from the 1200 mm diameter pipeline was reduced by a factor of 6 to 8, compared with the previous technology that used gas cutting.

The ECEC device, the design of which is shown in Figure 6, was developed to cut holes in active pipelines for connecting branch pipes to them. Permissible gaps between ECEC and the branch pipe wall, and thickness of the receiving chamber cover were determined in optimisation of the device. Designs of protective screens, reusable pipe unions for fixing the saddle-shaped ECEC and fixtures for complete breaking of a bridge under the ECEC connection in the case of incomplete cutting were developed.

The sequence of mounting of the device on an oil pipeline is as follows. Nut *2* and, aligned with the nut, protective screen *3*, bypass branch pipe *4*, open gate *5* and receiving chamber *6* with a flange are welded to the centre of a hole to be made in pipeline *1*. Pipe union *7* with the saddle-shaped ECEC *8* fixed on brackets and the electric detonator are mounted on the nut using an auxiliary rod. Composite stem *9* is then screwed into the nut by pressing the pipe union with ECEC to the pipeline. Cover *10* is put on the receiving chamber after taking the electric detonator ends out through the sealed outlet. The cover is fixed to the flange using bolts *11*. Sealing between the cover and stem is provided using gland *12*, and that between the cover and flange of the receiving chamber — using a poronite gasket. In detonation of ECEC the screen provides reliable protection of the bypass branch pipe, and the cut out part of the pipeline is forced out together with the stem from the gate to the receiving chamber under the effect of pressure of a liquid oil product. After closing the gate the receiving chamber with all its content is cut out using the circular pipe cutter. The device for removal of the cut out part of the pipe and the receiving chamber can be used many times further on. Because the set of the device is fitted with pipe unions of differing lengths, the device is versatile and can be used for cutting in of any size of branch pipes. The saddle-shaped ECEC is made from one straight-line length of the charge by forming. In some cases the probability exists that a pipe is not completely cut in the location of the ECEC connection. A method was suggested to improve reliability of operation of the saddle-shaped ECEC, consisting in its initiation at a point located at an equal distance from the connection. This is the point where the pressure is increased and an incomplete cut, if any, is broken. If the incomplete cut does take place, a reciprocating motion is imparted to the stem through eyes using levers, this providing complete breaking of the remaining bridge.

The ECEC device, the so called saddle-shaped circular cumulative pipe cutter (TrKKS), was developed to cut holes in pipelines. The device consists of one

saddle-shaped ECEC and four fixing rods, including the electric detonator holder (see Figure 5). TrKKS is intended for cutting holes with a diameter of 80 to 970 mm in main pipelines with a diameter of 219 to 1420 mm and wall thickness of 8 to 22 mm. At explosion the device is capable of cutting a hole in the main pipeline with a wall thickness equal to 0.8 of the ECEC diameter. According to the specifications developed, PWI can manufacture 586 types of TrKKS by orders of customers.

Using ECEC and TrKKS developed on its base in main pipelines of Russia and Ukraine during 1974–1990 allowed connection of 519 branch pipes without interruption of transfer of oil and oil products, which provided a substantial improvement in production arrangement, improved safety conditions and excluded oil pipeline downtime.

Increase in production of oil and gas from offshore fields results in widening of the network of underwater main pipelines. Problems associated with cutting of pipes arise in their maintenance and repair. Stationary platforms, which have to be disassembled after completion of operation of oil and gas fields, increase in number. Problems arise with platforms having foundations up to 15,000–30,000 t in weight, which have to be dismantled in sea down to 100–200 m deep. Costs of their complete dismantling may amount to US$ 100–200 mln, which is 30–50 % of those incurred for their construction and installation. Also, there are traditional operations associated with underwater repair and cutting of hulls of sunk ships, construction of dams etc. Therefore, cutting of metal structures under water is an increasingly wide-spread and topical process.

Explosion cutting using ECEC is advantageous over thermal cutting methods for underwater applications. Its advantages include simplicity of the equipment involved and placement of charges, and possibility of remote control of the process, which reduces the time during which a diver has to stay under water. In addition, the cutting process does not depend upon the depth, and it requires no high-skilled specialists to be performed. There are cases where explosion cutting is indispensable. The examples are operations at facilities with combustible or gaseous explosible mixtures, or operations involving the risk of shear, where parts of structures being cut may fall down.

To provide formation of the high-velocity cumulative jet under water, the cumulative cavity should be protected from ingress of the water. The special ECEC in a foam plastic protective jacket was developed for this purpose. The jacket encloses the ECEC casing and fills in the cumulative cavity. The loss in efficiency of ECEC in this case is no more than 10–15 %. Such charges are capable of working at a depth of down to 50 m. If necessary to work at a depth of 60–70 m, a coating that prevents ingress of water is deposited on the protective jacket. And at a depth of down to 200 m, which is still accessible to a diver, and down to 600 m, where it is necessary to use a manipulator, ECEC is placed in a metal jacket made from an appropriate material.

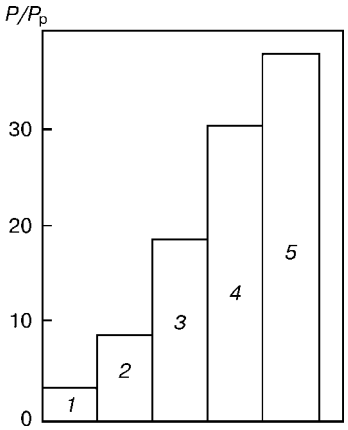

Figure 7. Efficiency of different protective screens by the results of measurement of maximum wave pressure at a distance of 3.5 m from ECEC: *1* — bubble protection; *2–4* — sand, gravel, keramzite and foam plastic screens; *5* — alternating layers of sand and foam plastics

Explosion of the underwater charge results in formation of shock waves, which may cause damage to ichthyofauna of water areas important for economy. The tolerable level of the intensity of shock waves under water should not be higher than 0.6–1.0 MPa. Apparently, commercial application of the underwater explosion cutting technology depends upon the efficiency of means for protection of ichthyofauna from the impact of explosion.

The E.O. Paton Electric Welding Institute and the Institute of Mechanics of the NAS of Ukraine conducted investigations to study the effect of pressure of a shock wave propagating in water in explosion of different types of ECEC, as well as the effect of different types of protective screens on the degree of suppression of the shock waves. Measurements of the shock waves generated by explosion of the ECEC sections with a diameter of 19 mm and length of 250 mm, placed in different protective screens, such as dry sand, foam plastics, keramzite gravel, combined screens consisting of sand layers and foam plastics, as well as screens consisting of air bubbles, were made to evaluate the efficiency of the protection methods and means. Comparative characteristics of the protective screens tested are shown in Figure 7. In this Figure the ratio of maximum values of pressure P in a wave at explosion of the 19 mm diameter ECEC section in water to the peak value of pressure P_p fixed in explosion of the same ECEC using different protective screens is given on the axis of ordinates. As shown by the measurement results, the bubble protection decreases pressure by a factor of 5, the sand screens — 10, keramzite gravel — 20, foam plastics — 30, and alternating layers of sand and foam plastics — 40.

The foam plastic screen is most promising in terms of technological and economic indicators, as it serves as the protective jacket for ECEC and, at the same time, performs the function of a sort of a bubble protection. If necessary, the zone of the safe impact

Figure 8. Appearance of the cut made in a multilayer pipe used in foundation of stationary off-shore platforms

on ichthyofauna can be enlarged by scaring fish from the ECEC explosion zone with a radius of up to 3–5 m using the acoustic methods.

PWI and VNIISPTneft (Russia) developed an underwater circular cumulative pipe cutter (TrKKP), based on the ECEC in a foam plastic jacket, for cutting main pipelines with a diameter of 219–1420 mm and wall thickness of 18-20 mm. The pipe cutter consists of two semi-rings of ECEC in the foam plastic protective jacket with preliminarily placed casings of intermediate charges. In addition, the protective jackets have lugs to which additional weights are connected. They provide fixation of TrKKP to a pipe. Ends of auxiliary DC are put to the casings of the intermediate charges, which are then filled with a fused explosive. The cutter provides cutting of a pipe at the presence of a water layer between it and the pipe equal to not more than 5 mm. After a diver goes out of water, TrKKP is initiated with the electric detonator connected under water to the main DC.

The technology for dismantling of stationary offshore platforms by explosion cutting, providing for protection of ichthyofauna, was developed and successfully tested on the basis of studies conducted by PWI [4]. This technology was applied for the first time in 1978 for cutting of foundation of the drill platform in the Black Sea at a distance of 75 km from the city of Evpatoria. Foundation of the drill platform consisted of three identical blocks, each mounted on nine piles. Each pile was a structure consisting of coaxially located pipes with a diameter of 219–478 mm and wall thickness of 8–11 mm. The space between the pipes was filled with solidified cement. Cutting of the pipes was done at a depth of 33 m in sequence by the following method. First two circumferential transverse cuts were made on an external pipe at a distance of about 700 mm. Then the spool was cut into three equal parts using three longitudinal charges. This caused destruction of the cement layer. Subsequent cutting of smaller diameter pipes was done in a similar way. Circular charges TrKKP 19 and 41 mm in diameter and straight-line ones 19 mm in diameter were employed for dismantling. Appearance of the cut in a multilayer pipe is shown in Figure 8.

96 pipes were cut by explosion in dismantling of the foundation of the drill platform. The total time of underwater explosion operations was 15 days.

In 1985 the explosion technology was applied for dismantling of an exploration platform located in the Azov Sea at a depth of 11 m. In 1986 the similar work was done in dismantling of blocks of stationary platforms in the Black Sea at a depth of 30 and 33 m. In the same year the work was completed on underwater explosion cutting of 30 hydraulic engineering tubular supports located in the Caspian Sea at a depth of 6 m, resulting in dismantling of a region of a scaffold bridge 300 m long. In 1990–1991 pontoons of stationary offshore platforms in the Caspian Sea were successfully trimmed by explosion cutting after they were installed on the shelf.

To maintain their fuel energy balance, many industrialised countries increased construction of nuclear power stations, in addition to growth of production of oil and gas. These stations require maintenance and repair during operation, and subsequently closing and dismantling. Thus, in 1986 in Ukraine, after the disaster at the Chornobyl nuclear power plant, there was the need for emergency repair of the shelter and subsequent dismantling of power unit 4. At present it is necessary to perform sometimes different types of works for dismantling different metal structures in emergency situations. Apparently, allowing for the above advantages of the explosion cutting technology, it presents almost the only solution to the problem for critical conditions. However, a number of specific requirements are imposed on the explosion cutting technology. First of all, these are the preliminary optimisation of the ECEC parameters for a specific metal structure to be cut, remote delivery and installation of ECEC using manipulators (robots), ensuring reliable fixation of ECEC to horizontal and vertical regions of a metal structure with a guaranteed focal distance, remote detonation of ECEC using radio signals, prevention of impact by shock waves on surrounding facilities and probable spread of radioactive dust, as well as fragments of the charge and structure being cut.

Using the available experience and results of special studies, PWI developed two designs of the assembly-transportation device based on TrKKN, intended for cutting tubular metal structures with all the above requirements met. The first design called «tongs» is intended for cutting pipes with a diameter of 89–220 mm, and the second design called «clip» — for cutting pipes with a diameter of 820–1440 mm. If pipes have an intermediate diameter, both first and second devices can be used, depending upon the specific work to be done.

When the «tongs» type device is used (Figure 9), ECEC together with an assembly fixture is fed to the initial position and connected to the manipulator. When doing so, the ECEC semi-rings are in a drawn apart condition. The manipulator moves the device to the site, delivers ECEC to the cutting location, so that the pipe axis and ECEC plane are in a mutually perpendicular position, and then, by translational motion, the manipulator mounts ECEC on the pipe, where it is secured with a special lock and fixing rods having an elastic element on their ends to fix ECEC in any position due to its elastic properties. After the manipulator is moved to a safe place, the detonation of ECEC is provided. Then the place of explosion operations is examined with the help of the manipulator. Depending upon the examination results, the possibility exists of continuing the operations, if necessary. A specific feature of performing field operations in the case of using the «clip» type device is that two manipulators are required to install ECEC, and that the assembly fixture is disconnected from ECEC by making the manipulators move radially from the pipe centre. The rest of the operations are similar to those described above.

Where it is necessary to protect surrounding facilities from a side effect of explosion, this protection is provided by the air-mechanical foam formed by a portable foam generator, which is delivered to the site by the manipulator. A substantial (10 times) suppression of shock waves, decrease in the number of fragments of the ECEC jacket, and an almost absolute elimination of spread of radioactive dust were fixed in this case.

Analogue of the «tongs» type device (Figure 9) was used in 1986 for explosion cutting of fire-fighting pipes 108 mm in diameter on the roof of power unit 3 during liquidation of accident at the Chornobyl nuclear power plant. The level of radiation in that case was 150 R/h.

It should be noted in conclusion that PWI has experience in development and practical application of super-precision linear severing devices based on the use of the explosion energy. The devices are safe for humans and intended for aerospace engineering. They can be used, for example, for making of emergency exits in a pilot's cabin. Similar device was developed for the rocket-space transportation system of the «Energiya–Buran» system. The projected use of the explosion cutting technology is for dismantling of orbital space stations in extra-vehicular activity.

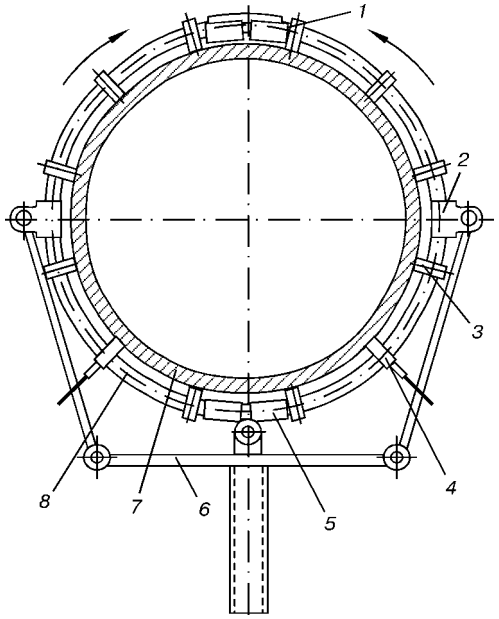

Figure 9. «Tongs» type device based on ECEC for cutting of pipes: *1* — ECEC semi-ring connector; *2* — hinge; *3* — boss for setting the focal distance; *4* — same with a port for electric detonator; *5* — hinged lock; *6* — device alignment and fixation of ECEC semi-rings; *7* — pipe cut; *8* — ECEC semi-ring

1. Lavrentiev, M.A. (1957) Cumulative charge and principles of its action. *Uspekhi Mat. Nauk*, **12**, 41–56.
2. Baum, F.A., Orlenko, P.P., Stanyukovich, K.P. et al. (1975) *Physics of explosion*. Moscow: Nauka.
3. Rainhart, D., Pirson, D. (1966) *Explosion treatment of metals*. Moscow: Mir.
4. Kudinov, V.M., Koroteev, A.Ya., Volgin, L.A. (1987) Experience of application of underwater explosion cutting for dismantling of stationary off-shore platform tubular support. *Avtomatich. Svarka*, **6**, 27–29.

OPTIMIZING OF CONDITION PARAMETERS OF NARROW-GAP ARC WELDING OF QUENCHING STEELS WITHOUT PREHEATING

A.T. NAZARCHUK
E.O. Paton Electric Welding Institute, NASU, Kyiv, Ukraine

Engineering calculation of optimum rate of cooling metal being welded (to provide the technological strength) depending on welding process parameters and section of weld layers, and also with allowance for CCT diagram of overcooled austenite decay is suggested.

Keywords: *arc welding, quenching steels, multilayer welds, welded joints, delayed fracture, cold cracks, portion heat input*

It turns out so, that the arc fusion welding of quenching hull steels is made often using high-alloy austenitic welding consumables to provide the required resistance of joints to cold crack formation [1]. When the low-alloy welding consumables are used it is necessary to use preheating. In some cases the desirable result is attained using the autopreheating.

Drawbacks of these technologies are, firstly, high cost of austenitic materials and lower characteristics of properties of joints as compared with those of parent metal; secondly, the need in auxiliary complex and labour-intensive operation of preheating, which is often not realizable, in particular for large-sized products.

Over the recent years the high-strength austenitic-martensitic consumables are developed for welding quenching steels [2]. In their use, the impossibility of use of post heat treatment, for example, high tempering to relieve the residual stresses, should be noted, except the above-mentioned drawbacks.

Taking into account the above-described situation we think that the possibility of producing metal of high-strength welds, being close to parent metal, is a challenging variant for quenching hard-to-weld steels.

However, to realize this idea the additional investigations directed to attaining the required technological strength of welded joints of quenching steels at a simultaneous increase in strength of the weld metal to the level of the parent metal are necessary. This problem can be solved by combination of different variants of autopreheating and portion-discrete formation of welds [3–5].

In case of autopreheating, for example, using a reciprocating displacements of arc (electrode) [3], its advantages can be realized, if to maximum optimize the rate of cooling metal during fulfillment of each weld layer.

The aim of the present work is to show the feasibility of improving joint metal resistance to cold cracks without preheating in welding quenching steels and to produce weld metal similar to parent metal owing to optimizing metal cooling in fulfillment of each separate layer of the weld.

Taking into account the negative hydrogen effect on technological strength of joints, the measures were taken to limit the content of diffusive-mobile hydrogen in the deposited metal which could not exceed 1.5 cm^3 per 100 g of metal. To determine the hydrogen content, the method of alcohol sample was used.

To optimize the welded joints cooling after fulfillment of each layer with allowance for CCT diagrams of overcooled austenite decay of a definite steel, it is necessary to establish the required rates of cooling metal of weld and HAZ depending on the welding conditions.

To evaluate the thermal condition of elements welded in narrow-gap welding of root welds of thick metal, it is possible to use the calculated scheme of N.N. Rykalin, which takes into account the heat spreading in semifinite body from effect of a spot mobile heat source [6, 7]. In accordance with this scheme the temperature of any spot of the body in quasi-stationary state is determined by the following formula [7]:

$$T_{(R,\ x)} = \frac{q}{2\pi\lambda R}\, e^{-\frac{v}{2a}(x+R)}. \qquad (1)$$

During source displacement in axis x–x, the temperature of spots (where value x is negative) does not depend of speed of its displacement and is equal to temperatures of limiting state of fixed source, i.e. at $R = -x$

$$T_R = \frac{q}{2\pi\lambda R}. \qquad (2)$$

For low-carbon steel $\lambda = 41.8$ W/(m·°C) [7]. Taking into account that $q = I_w U_a \varphi$ (φ — efficiency factor of arc), equality (2) can be written in the form

$$R = \frac{I_w U_a}{2\pi\lambda T_R}\varphi, \qquad (3)$$

where R is the distance in weld axis from arc to point with temperature T_R, m; I_w is the welding current, A; U_a is the arc voltage, V; T_R, °C.

In HAZ (in axis y) the distribution of temperatures depends on welding speed [6, 7]. However, as HAZ in narrow-gap welding is small and located almost at the same distance from the weld axis, i.e. $b/2$ (where b is the gap width), that amounts to 7–9 mm for 14–18 mm gap width, then the calculation can be made with a certain accuracy without taken into account this remark.

Really, as follows from the Table, when plates of 40 and 80 mm thickness and 1200×1600 mm size are welded (weld in the middle along the long side), the calculated estimates of value R for temperatures 220–275 °C are differed from experimental values by 6–15 % that is quite admissible for engineering estimations.

Substituting appropriate values λ to formula (3) and taking into account that in calculations of this kind φ can be accepted equal to 1 (for gas electric welding on open surface $\varphi = 0.8–0.9$), we shall obtain

$$R = \frac{I_w U_a}{2\pi 41.8 T_R}. \quad (4)$$

To optimize the width of groove in narrow-gap welding of quenching steels, the determination of distance from arc to the metal zone with interested to us temperature of autopreheating depending on welding parameter is an important characteristic. This distance can be determined both experimentally and also rather approximately by calculation.

If to make the appropriate measurements or calculations for two temperatures, for example 500 and 300 °C, then it is possible to determine approximately the mean rate of metal cooling in the zone of welding within this range of temperatures. In the given case a traditional analysis of CCT diagrams of decay of the overcooled austenite of steels welded is used for estimation of structures formed in HAZ metal of the welded joints.

Further, we shall do the following. Let us assume that it is necessary to provide the distribution of temperatures T_R in weld axis at the distance R from arc at y and $z = 0$ (Figure 1).

The following equation can be made for narrow-gap welding with allowance for amount of metal deposited for time t:

$$bh_{layer}R\gamma = Pt, \quad (5)$$

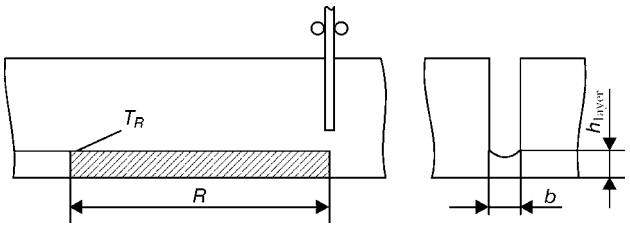

Figure 1. Scheme of calculated determination of groove width depending on amount of deposited metal

where h_{layer} is the layer height; γ is the specific density of the deposited metal (for steel $7.78 \cdot 10^{-3}$ g/mm^3); P is the amount of metal deposited per unity of time for selected parameters of process (g/s). In addition, $t = R/v_w$, where v_w is the welding speed at selected values I_w and U_a.

To transform formula (5) it should be noted that $\psi_{layer} = b/h_{layer}$, hence $h_{layer} = b/\psi_{layer}$. Substituting this expression to formula (5) and, making the appropriate transformations, we shall obtain the calculated width of groove (gap) for selected values of welding current and arc voltage in narrow-gap welding:

$$b = \sqrt{\frac{P\psi_{layer}}{R\gamma}}\, t, \quad (6)$$

where ψ_{layer} is the coefficient of layer shape (ratio of groove width to height of deposited layer); R is determined by calculations by formula (4) or experimentally; t is the time of cooling to temperature T_R, s, at which the quenched structures, prone to cold cracks, are not formed in the joint metal, s.

Parameter $t = t_R$ is selected with allowance for CCT diagrams of decay of overcooled austenite of definite steels welded (Figure 2).

Taking into attention that $R = v_w t$, the final formula of determination of gap width in narrow-gap welding can be reduced to the following form:

$$b = \sqrt{\frac{P\psi_{layer}}{v_w\gamma}}. \quad (7)$$

For the wide range of conditions $P = 6.5–8.5$ kg/h and can be determined by formula $P = pv_f$, where p is the mass of 1 m linear length of wire, kg/m; v_f is the wire feed speed, m/h.

Values of coefficient of layer shape ψ_{layer} should be taken such at which the sufficient resistance of weld metal against hot crack formation is provided. For the narrow-gap welding $\psi_{layer} = 2.5–5.5$.

Optimizing of parameters of process of welding with similar welds of quenching steels

Steel grade	*Sizes of plates welded, mm*	*Welding parameters*		*Temperature of autopreheating T_R, °C*	*R, mm*	
		I_w, A	*U_a, V*		*Experimental*	*Calculated*
14KhN4MDA	1200×1600×540	450–475 / 455	36–38 / 37	220–230 / 225	255	292–301 / 297
30Kh2N2M	120×1600×580	450–500 / 475	38–40 / 39	250–275 / 262.5	265	271–288 / 280

Note. In numerator the range of values is given, while in denominator the mean value is given.

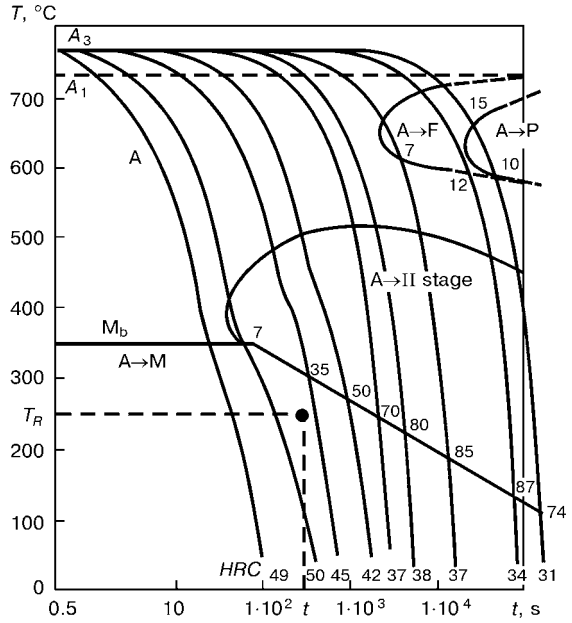

Figure 2. CCT diagram of decay of overcooled austenite in steel of 30Kh2N2M grade

Using CCT diagrams of decay of overcooled austenite for definite steels with allowance for selection of metal structures resistant to cold cracks, it is possible to determine not only T_R, but also the time t to reach this temperature in cooling from the temperature of austenizing. In those cases when there are no appropriate CCT diagrams of decay (for definite steels), constructed in heating up to high temperatures (1300–1350 °C) it is possible to use diagrams for heat treatment approximately (as preliminary) [8].

After selection T_R from formula (4) R is determined at preset I_w and U_a. Welding speed for the selected process parameters is found from ratio $v_w = R/t$. Then, the required gap width is calculated using formula (7), as it is easy to determine P at preset parameters of the process. However, it can be done in another way: to determine required I_w and U_a by presetting P.

After making calculations, including those on determination of gap width b, it is possible to reveal an interesting fact: to provide the calculated width of weld at selected values of welding current and arc voltage in some cases is impossible, as it is necessary to use the transverse oscillations of the electrode. Here, the amplitude A of oscillations is determined approximately on the basis of experimental data:

$$A = \frac{b - (2–5)}{2}.$$

Selection of optimum variant is made by the method of successive approximations. For this purpose, the calculations should be performed for several variants of process parameters (I_w and U_a).

It should be noted that at different conditions the efficiency is adequately determined by P/b ratio and increased with increase in this characteristic. Moreover, the decrease in gap width does not always promote the increase in the process efficiency, as with decrease in gap to provide the quality formation of weld (in particular resistance to hot cracking) it is necessary to decrease the amount of deposited metal per time unity. Cases are possible when at large gaps the higher efficiency of the process can be provided than at small gaps. This is attained by great increase in amount of deposited metal per time unity (for large gaps) and providing the required coefficient of layer shape ψ_{layer} for the narrow-gap welding.

The offered procedure of calculation can be used in welding with a traditional groove preparation. In this case it is rational first of all to determine the area of cross-section of deposited layer S and, taking this into account, to make the usual edge preparation. The cross-section area is determined by formula

$$S = \frac{Pt}{R\gamma}.$$

Taking into account that $R = v_w t$, the formula can be reduced to the form

$$S = \frac{P}{v_w \gamma}.$$

It should be noted here that, in principle, the new approach is suggested to the selection of groove section and amplitude of transverse oscillations of electrode by calculation depending on the process parameters and with allowance for resistance of joints of definite steels welded against cold and hot cracks.

At present the process parameters (taking into account the grade of steels welded) are selected, as a rule, depending on a standardized edge preparation. This approach does not always provide the necessary rate of metal cooling in the lower subcritical interval of temperatures for many hard-to-weld steels, and, consequently, the resistance of metal of their joints against cold cracks.

The developed procedure of selection of conditions was tested in welding plates of 40 and 80 mm thick steels of 14KhN4MDA and 30Kh2N2M grades, respectively. Plates of 600×700 mm size were assembled in the form of a rigid technological sample of type of the Central R&D Institute of Shipbuilding Technologies. Weld was made along the long side of the plate. Welding was performed with wire Sv-07KhGSN3MD. Calculated width of groove at selected parameters of the process, for example for steel of 30Kh2N2M grade, was 21–23 mm. The rest parameters were as follows: I_w = 450–500 A; U_a = 38–40 V; v_w = 8.1 m/h.

CCT diagram of decay of overcooled austenite for steel 30Kh2N2M is given in Figure 2 [5, 8]. Temperature T_R = 230–250 °C. Here, it was necessary to provide $t = t_R$ = 150 and 190 s in accordance with the diagram. The above-mentioned requirement is defined by the formation of metal structures (as a result of austenite decay and developing of processes of self-tempering in welding), resistant against formation of cold cracks. The further calculations were made using the above procedure.

Results of investigations showed that the longitudinal and transverse cold cracks were not revealed in welded joints (Figure 3). This proves a sufficient resistance of joint metal to cold crack formation in welding using the selected technology.

It should be noted that in spite of possibility of producing joints resistant to crack formation with use of preheating (as a result of optimizing cooling during welding a separate layer), it is not always possible to use this method for joining hard-to-weld steels with a high stability of austenite, for example steel 34KhN3M. The thing is that optimizing of rate of cooling joints of these steels in fulfillment only one layer of the weld at optimum conditions can lead to deterioration of mechanical properties of weld metal due to a long duration above A_{c_3}. To eliminate this drawback the offered procedure of calculation should be combined with use of a favourable effect of many-layer nature of welds [5] and their portion-discrete formation [3, 4].

Thus, the optimizing of parameters of welding and autopreheating (length of autopreheating area, temperature) is based on need to provide the temperature of autopreheating of metal in the welding zone at a definite distance from arc, at which it is possible to prevent formation of cold cracks with allowance for a timely repeated thermal effect of arc on this metal. This repeated effect is recommended once or two times per one pass. To realize the process the twin-arc welding and welding with one arc by scheme «two or three layers are made per one pass» are used, that is especially necessary for root welds. When the required temperature of autopreheating is reached, the welding can be performed by scheme «one layer per one pass».

The developed approach of optimizing the groove width (narrow-gap welding) or section of deposited layer (welding with traditional groove) can be used in welding steels not only to provide the required resistance of joints to crack formation, but also for obtaining required mechanical properties of welded joint metal.

CONCLUSIONS

1. Engineering calculation of rate of cooling metal depending on parameters of welding process has been developed with allowance for use of CCT diagrams of decay of overcooled austenite of steel being welded.

2. Feasibility was established to provide the required resistance of joints of hard-to-weld steels of 14KhN4MDA and 30Kh2N2M grades to crack formation by optimizing the rate of cooling metal during welding without preheating.

3. To improve the efficiency of process of welding steels with a high stability of decay of overcooled austenite (without use of preheating) the updating of procedure of calculation as regards to fulfillment of multilayer welds with a portion-discrete formation is required.

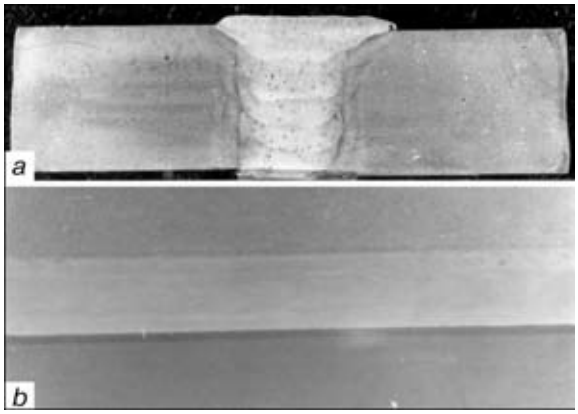

Figure 3. Macrosection of joint of steel 14KhN4MDA made at calculated width of gap: *a* — transverse; *b* — longitudinal

1. (1974) *Technology of fusion electric welding of metals and alloys*. Ed. by B.E. Paton. Moscow: Mashinostroenie.
2. Gotalsky, Yu.N., Snisar, V.V., Kuporev, A.L. et al. *Arc welding method of quenching steels*. USSR athor's cert. 880671. Int. Cl. B 23 K 28/00. Publ. 14.07.81.
3. Nazarchuk, A.T. (1994) Control of weld metal solidification and thermodeformational cycle in automatic arc welding. *Avtomatich. Svarka*, **5/6**, 3–9.
4. Nazarchuk, A.T. (1997) Influence of portion-discrete weld formation on thermal cycle in fusion arc welding. *Ibid.*, **5**, 13–17.
5. Nazarchuk, A.T. (1994) Resistance of joints of quenching steels with multilayer welds to cold cracking. *Ibid.*, **1**, 15–19.
6. Rykalin, N.N. (1951) *Calculation of thermal processes in welding*. Moscow: Mashgiz.
7. Petrov, G.L., Tumarev, A.S. (1967) *Theory of welding processes*. Moscow: Vysshaya Shkola.
8. Popov, A.A., Popova, L.E. (1965) Isothermal and thermokinetic diagrams of decomposition of supercooled austenite. Heat-treater's refer. book. Moscow: Metallurgiya.

EXPERIENCE IN MANUFACTURE OF AIR TANKS OF LOCOMOTIVES AT HC «LUGANSKTEPLOVOZ»

G.G. BASOV, A.N. TKACHENKO and **N.P. EFIMOVA**
Holding Company «Luganskteplovoz», Lugansk, Ukraine

Designs of a specialized welding equipment are presented and technology of manufacture of air tanks of locomotives is given.

Keywords: *design, tank, bottom, shell, volume, air, pressure, technology, condition, welding, welding installation, welding wire, flux, quality*

Indispensable part of the locomotives produced is air tanks of 25–600 l capacity, which are used in brake, automation and fire extinguishing systems [1]. Conditions of their operation are characterized by the presence of a static pressure, acting for short or long time at room and lower temperature, performing here the function of accumulation and conservation of air. In brake systems the tanks of 222, 250, 500, 600 l capacity are used, while in feed systems they are of 120, 222, 250 l capacity and store tanks have 20, 55, compensation tanks 20 and auxiliary tanks 5 and 20 l capacity. For fire extinguishing liquid the 260 l capacity tank is used [2, 3].

Tank (Figure 1) consists of the following design elements: cylindrical shell *4*, made from 5–6 mm thick sheet steel, two convex bottoms *2* of 6–8 mm thickness, pipe connection *1* for connection of air conduit and pipe connection *5* for arrangement of outlet valve. Number and arrangement of pipe connections depends on type of tank installing on the locomotive. The tank has a table indicating name of plant-manufacturer, manufacture number, date of manufacture, allowable pressure and term of inspection [4]. Design of tanks is made in accordance with GOST 14249–73. Shells and bottoms are manufactured from low-carbon steel of grades VSt5sp5 (killed), GOST 380–71, and VSt3sp4 (killed), GOST 380–71 [1].

Below, the technology of manufacture of air tanks on the example of manufacture of main tanks of brake system of locomotives is given, which can be also used for manufacture of gas cylinders.

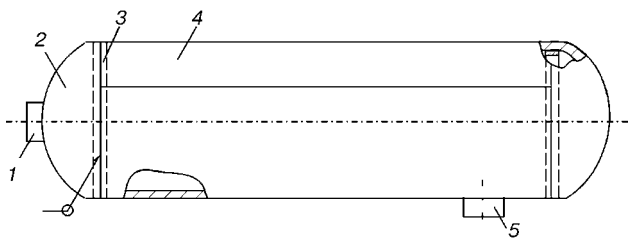

Figure 1. Scheme of tank division into design elements: *1, 5* — pipe connections; *2* — bottom; *3* — backing ring; *4* — shell

Bottoms of above 300 mm diameter are manufactured by a hot stamping, which is made in several stages including stamping from sheet steel, preliminary forming, heating up to 950 °C in furnace, final forming in hot state, straightening and subsequent, mechanical treatment. To manufacture shells from sheet steel, the blanks of a required size are cut, subjected to forming in bending three-roll machines until the necessary diameter, bending preliminary the edges in sheet-bending machines.

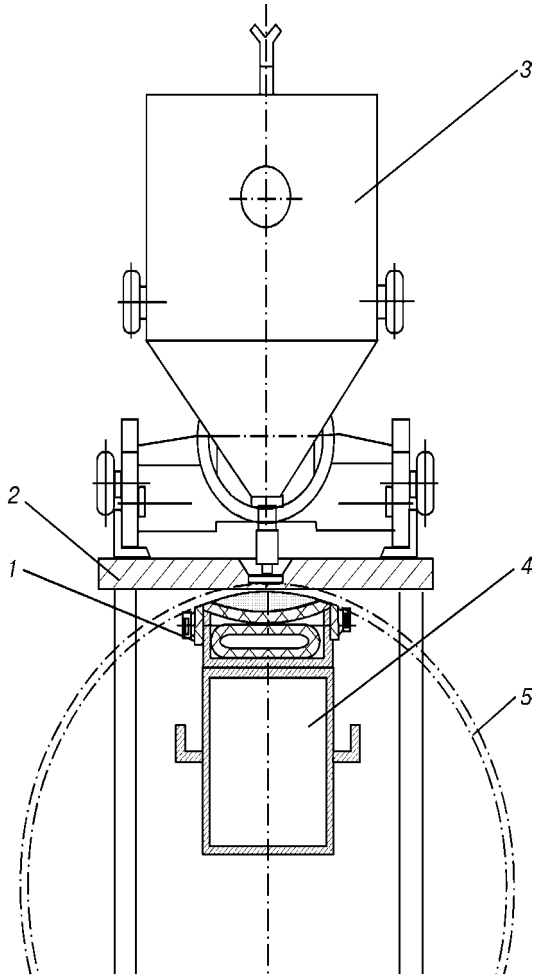

Figure 2. Schematic diagram of installation for automatic submerged arc welding of cylindrical shells on flux cushion: *1* — air hose; *2* — plate with guides; *3* — welding tractor; *4* — pivoted cantilever with flux cushion; *5* — shell

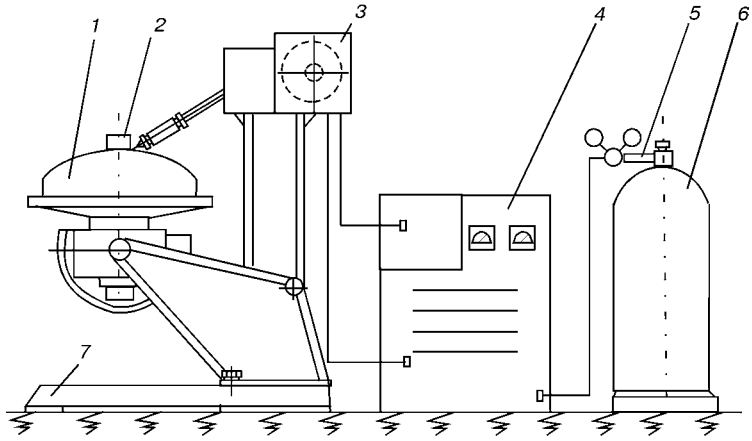

Figure 3. Schematic diagram of installation for welding pipe connection to bottom in shielding gas: *1* — bottom; *2* — pipe connection; *3* — wire feed mechanism; *4* — power source; *5* — gas pipeline; *6* — cylinder with gas; *7* — manipulator

Before welding of longitudinal butt weld the shell is preliminary assembled. For this purpose, its edges are abutted, keeping them in a single plane and providing 1.5 ± 1 mm gap for welding. Two run-out technological tabs are welded-on by the semi-automatic shielded-gas welding around the shell edges.

Welding of longitudinal welds of 300–600 mm diameter shell is made automatically using installation, shown in Figure 2, with a single-sided weld on a flux cushion. Installation consists of a pedestal mounted on a plate, a pivoted cantilever with a flux cushion, two pneumatic cylinders, plate with guides for a welding tractor movement.

As-assembled shell is mounted on a pivot cantilever, moved aside preliminary. Then, the cantilever is returned into operating condition, putting forward the shell butt relative to plate recess. Pneumatic cylinders are switched on for cantilever pressing against the plate, and then the flux is pressed against the butt by pressurizing air supplied to an air hose arranged under the flux. Then, the automatic welding of butt weld is performed by a tractor moving along the plate guides, starting on a run-in tab and finishing on a run-out tab that prevents the formation of craters in the shell weld. Welding is performed with wire Sv-08A of 2 mm diameter using flux AN-348A. An obligatory operation, completing the shell manufacture, is its straightening which is made by the method of rolling in a sheet-bending three-roll machine. Quality of welds is inspected by X-ray method. Condition of fulfillment of a single-sided butt welding of shell longitudinal joint on a flux cushion is as follows [5]: sheet thickness 5 mm, gap width 1.5 ± 1 mm, electrode diameter 2 mm, welding current 425–450 A, arc voltage 32–34 V, welding speed 35 m/h; air pressure in hose — 0.098–1.147 MPa.

Before welding of tank circumferential welds, backing rings (see Figure 1) are placed inside bottoms, which then pressed-in into a shell. To assemble bottoms with a shell, the pipe connections are first welded to them. The welding-on is performed in a shielded-gas automatic installation (Figure 3) consisting of a rotator, on which a bottom and pipe connection, and supports with a fixed welding head are mounted.

Welding of two circumferential welds of the tank are performed simultaneously in a specialized installation (Figure 4).

As-assembled tack-welded tank is transported from a feeder to the a working table, which lifts it for a height of rotation axis with a next clamping of

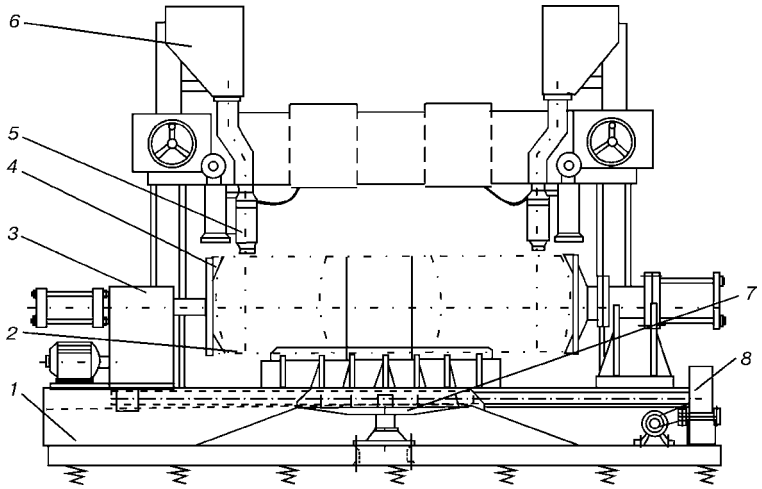

Figure 4. Schematic diagram of a specialized installation for simultaneous submerged arc welding of two circumferential welds: *1* — framework; *2* — tank; *3* — drive of tank rotation; *4* — clamp; *5* — welding head; *6* — hopper bor flux; *7* — lifting table; *8* — drive for tank lifting

workpiece with the help of drives. Then, the nozzles of welding heads are mounted on butts of a shell with bottoms, and simultaneously the drive of tank rotation and welding equipment are switched on. Automatic welding is performed in two passes with welding wire Sv-08A under flux of AN-348A grade at the following conditions: gap width 4–5 mm, wire diameter 2 mm, welding current 375–400 A, arc voltage 28–35 V, welding speed 27–35 m/h, wire feed speed 180–200 m/h. After welding completion, the clamps are moved aside, table is lowered and tank is rolled down on a receiving rack. Circumferential welds are subjected to X-ray control. After approval of quality of assembly and welding, small parts, such as flanges, pipe connections, cramps (for table fastening) are welded on.

Then, the tank is transported to a specialized bench for hydraulic tests, where four tanks are tested simultaneously.

Technical characteristic of a specialized bench

Number of simultaneously tested tanks, pcs	4
Time of testing at highest pressure, min	5
Air pressure, atm	4
Water pressure, atm:	
in tank water filling	2.5
highest in testing	15
lowest in testing	4
Dimensions, mm	4100×3750×1260

Test pressure should not be lower than 1.5 working pressure, that is 12–15 atm (working pressure in brake system of locomotives is 8 atm). Obligatory condition in leakage test is the use of warm (heated) water to prevent the condensate formation on the tank external surface. Defects, revealed by X-ray radiation, are eliminated by the method air-arc gouging and next welding-on by manual arc welding.

Final operations of the manufacture of tanks are preservation and painting. Preservation consists of greasing threaded junctions with anti-corrosion grease, sealing of holes with wooden plugs. The manufactured tanks are transported to the areas of assembly of locomotives.

Implementation of the above-described technology of manufacture of tanks made it possible to avoid completely the use of the manual arc welding that increases the quality of welded joints, improves labour conditions, increases its efficiency and reduces the cost of the air tanks.

1. (1978) *OST 24.140.35–76.* Diesel air vessels. Main sizes and specifications. Moscow: MTiTM, VNITI.
2. (1985) *Diesel TE10M. Operating manual*. Moscow: Transport.
3. Filonov, S.P., Gibalov, A.I., Nikitin, N.A. et al. (1996) *Diesel 2TE116*. Moscow: Transport.
4. Inozemtsev, V.G. (1979) *Railway rolling stock brakes*. Moscow: Transport.
5. (1983) *Welder's reference book*. Ed. by V. Stepanov. Moscow: Mashinostroenie.

MODULAR DESIGN OF THE CONTROL SYSTEM FOR MECHANIZED AND AUTOMATED ARC WELDING

S.I. PRITULA, V.A. LEBEDEV and **V.A. TKACHENKO**
E.O. Paton Electric Welding Institute, NASU, Kyiv, Ukraine

New types of control systems for welding and surfacing equipment are proposed, which are based on the modular design principle. These developments incorporate engineering solutions on adjustable reversible electric drives, using mechanotronic principles of design, and a programmable controller as the higher hierarchic link.

Keywords: *arc welding, surfacing, cutting, cycle, regulation, electric drive, controller, structure, reliability, systems*

Problems, related to the quality of performance of welding and surfacing operations, as well as ensuring reliable operation of mechanized and automated arc welding equipment, still remain to be the main issue in welding fabrication or repair-restoration work. An important condition is the repeatability of the obtained results with a high quality. On the other hand, user of mechanized and automated equipment would like to receive the required types of semi-automatic and automatic machines at a minimum cost and in a short term. This actually means one-day delivery. What should the developer and manufacturer of the required equipment do, when solving the specific problems of welding production?

The purpose of this work consists in providing one of the possible replies to this question. It is obvious that one of the ways to solve the problems, arising in fabrication, repair and restoration of components and parts of various metal structures in view of ever growing requirements to the quality of work performance, in particular, in the case of international co-operation, can be continuous widening of the equipment range. Such a process was possible in former times, and allowed PWI designers gaining priceless experience of development of these types of equipment, which in our opinion is not available in any of the enterprises of research or design-technological profile. It should be noted that in addition to the above diversity, a lot of attention was given to unified engineering solutions [1]. This is impossible now in view of the new economic conditions, when a user is ready to pay only for the final result — a high-effective, cost-effective and technologically attractive equipment.

The wish to take up a suitable place in welding equipment and technology market necessitated development of semi-automatic machines, systems and automatic machines by the modular design principle. Some of these solutions are presented in [2–4], and they can be based on different specific approaches. So, for instance, the semi-automatic machines are designed by the modular principle, using as the basic model the simplest semi-automatic machine as to technical fitting with subsequent enhancement of its functional capabilities. Design of surfacing units by the modular principle is based on the use of individual replaceable components for processing parts of various configuration by surfacing. The method, used in development of automatic welding machines of a modular design, is somewhat similar to the method of development of semi-automatic machines of analogous design, but it features much greater diversity of components and modules. It should be noted that the methodology of designing modular welding units is used to a certain extent in design of automatic welding machines.

Tendencies, related to mechanotronic methods of designing of high-quality highly reliable equipment are becoming more and more clearly traceable in development of semi-automatic and automatic machines of a modular design [5].

Some features of modular design can be seen in the equipment of a number of foreign manufacturers [6]. In this case part of manufacturer tasks are undertaken by the developer of welding equipment. This concerns an abrupt narrowing of the range of types of purchased items, as well as problems, related to layout of the systems, their setting up, testing and subsequent service. This allows the developers and designers finding the most rational and effective technical solutions at minimum cost in production and operation, which will be in demand in specific equipment and technology markets.

In his connection let us consider advanced developments of automated arc welding equipment, based on the modular design principle and use of mechanotronic methodologies. Such developments are based on the mechanotronic module of reversible adjustable DC electric drive, which features a high degree of versatility, i.e. the ability of reliable operation with any electric motors, applied in welding equipment (KPK, KPA, SL, DPU, DP, D25, D90 etc., having different supply voltages, armature winding parameters). Such an ability is provided by readjustable structures of feedbacks [7] in the regulator of rotation frequency of the electric drive shaft and a built-in reverser, operating by the principle of a logic automatic device [8].

The above electric drive fully corresponds to the notion of «mechanotronic component». It should be

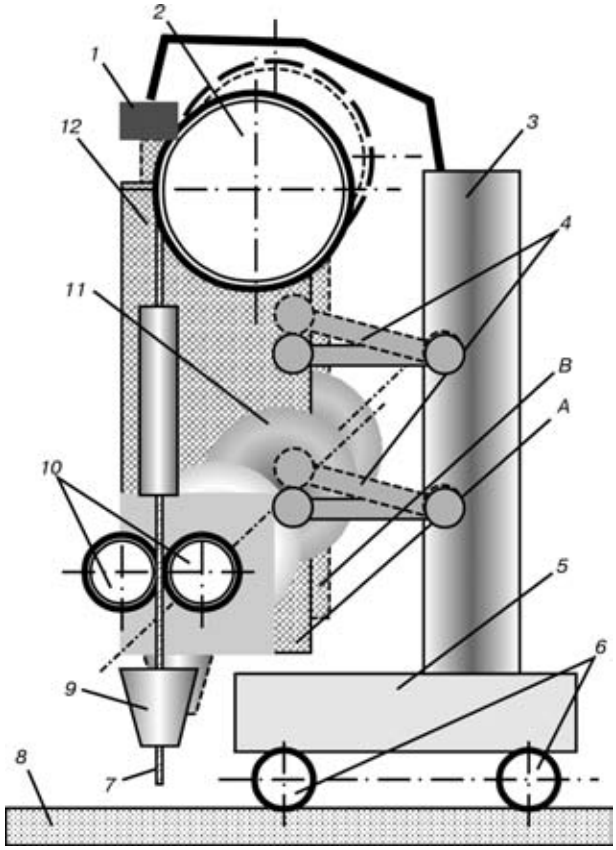

Figure 1. Fragment of a system of arc excitation under the flux: *1* — sensor; *2* — reel with electrode wire; *3* — post; *4* — casing suspension; *5* — carriage; *6* — drive of displacement of the automatic device; *7* — electrode wire; *8* — welded item; *9* — current-conducting tip; *10* — feed and press-down roller; *11* — feed mechanism electric motor; *12* — casing with feed mechanism

noted that the considered electric drive may operate both from resistive and voltage controllers of the frequency of rotation of the drive motor shafts. In addition, an important engineering solution, applied for the electric drive regulator, is the ability to organize feedbacks, both by the parameters of the electric motor proper (analog of measurement of emf-voltage and IR-compensation) and by tachogenerator autput (for electric motors of DPU87–75 type). Use of an electric motor with a tachogenerator significantly widens the range of adjustment of the frequency of its shaft rotation. For instance, for electric motors with tachogenerators the adjustment range is 20–25 times at the rigidity of mechanical characteristics not less than 5 %, and for other electric motors this range is equal to 12–15 times at the same rigidity of mechanical characteristics.

Such electric drives are mounted in all the electromechanical systems of automatic welding machines: mechanisms of electrode wire feed, systems of travel and welding displacement, systems of correction of electrode wire position relative to the butt being welded (following systems). The above electromechanical systems, as well as systems of shielding medium feed (gas, flux) and power supply to the arc are combined by the next device by hierarchy, namely a control device in the form of a purchased programmable controller with a developed program base, which supports entering and processing of both digital and analog signals. The following sensors are connected to controller inputs: automatic machine position; process parameters monitoring; special conditions. We include with the latter the mechanical sensor of arc excitation under a layer of flux for electrode wires of a large diameter (5 mm and more), used to increase process efficiency.

In our opinion, a device for arc excitation under a layer of flux, used in the considered modular automatic machines should be given special attention due to originality of its engineering solution. Figure 1 shows a fragment of the system of arc excitation under a layer of flux, mounted, for instance, in a tractor type automatic machine. The device operates as follows.

When rollers *10* switch on the electrode wire feed the latter moves in the workpiece direction and in case of contact between the wire and workpiece a signal of current flowing in the welding circuit is sent to the control system by the current sensor. When such a signal arrives, reversing of wire feed starts with arc elongation up to the moment of switching on of welding voltage sensor. When these signals coincide, the electric motor of feed mechanism *11* is switched over to working motion and maintaining the arc with simultaneous switching on of the drive of displacement of automatic machine *6* to perform welding. In case, if there are any obstacles to arc excitation, for instance, a piece of flux, which happens quite often, electrode wire runs against the above piece of flux, current sensor does not issue the signal, and the force of the arisen feed resistance is transferred to casing *12*, connected by levels spring-loaded relative to load-carrying post *3* to casing suspension *4* (these may be simply springs). Casing *12* with feed mechanism *1*, reel *2* and current-supplying tip *9* moves from position *A* into position *B* (shifts upwards), triggering off sensor *1*. A signal from sensor *1* triggers off reversal of electrode wire feed, and then by the timer controller signal the wire starts moving again to excitation point. This cycle is repeated until the above combination of signals from the sensors of current and arc voltage appears. The above algorithm of excitation may be changed this way. In case of non-excitation of the arc in this point, a command may be executed for a slight shifting of the automatic machine (1–2 mm) relative to the first point of attempting to excite the arc.

The considered design of the device for arc excitation under a layer of flux fulfills two functions: protects the equipment from breakage, and electrode wire from irreparable bends; signals the condition of arc non-excitation, when the electrode wire has reached a position, where the arc excitation should take place. Programming of electrode wire feed rate, welding speed and open-circuit voltage of welding current source, as well as crater welding up at the moment of welding process completion may be incorporated into the functioning algorithm.

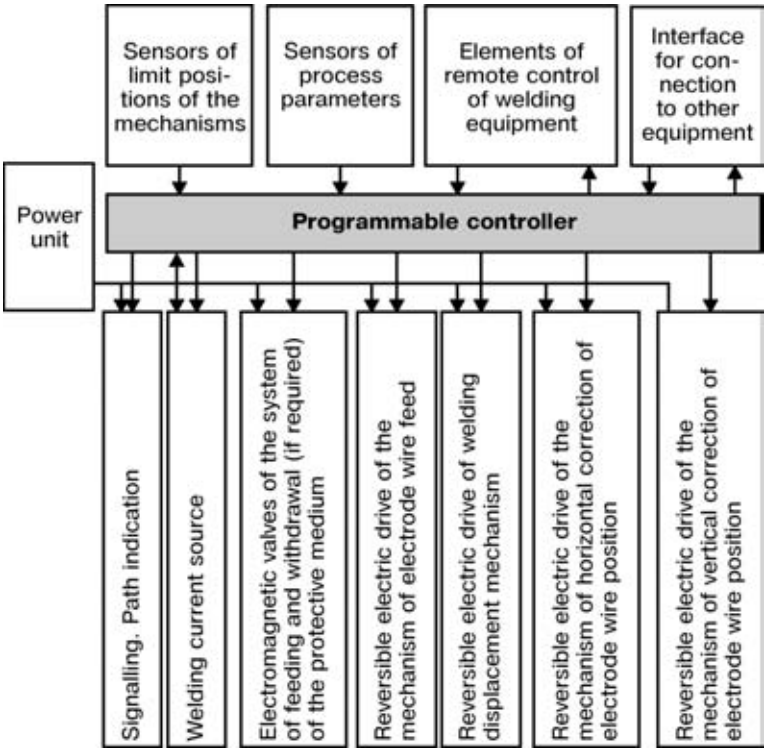

Figure 2. Block-diagram of a new modular system of control of mechanized and automated equipment

It is obvious that the system of devices for arc excitation, when using electrode wires of a greater diameter should be regarded as a system, having a certain methodology of its design and use. Sometimes, in particular for relatively light-weight automatic machines of tractor type, withdrawal of the automatic machine from the workpiece is used as the motion, indicating non-excitation of the arc, instead of an elastic suspension of the electrode wire feed system.

It may be stated that such a system of excitation is quite reliable and not a single malfunction or any weld defects were found in all the cases of its application.

The block-diagram of the new modular control system of mechanized and automated equipment (single-arc variant of the layout) is shown in Figure 2. It is natural that the equipment may be further fitted with other electromechanical systems, for instance, electrode wire oscillator, other sensors, etc. All that will just result in additional mounting of controllable electric drives and establishing new connections. It should be noted that the controller, as a rule, is selected with a deliberately greater number of inputs–outputs than is required in a specific case, and, therefore, some changes in equipment composition do not lead to a cardinal change of the main fitting of the entire system. It is obvious that such a system structurally and functionally is readily adjustable, yet it is practically devoid of all those excess components, which were characteristic of earlier developed equipment of a similar type.

Addition to the control system of an interface for interaction with other equipment allows without any special hardware optimization including into the operating cycle an automatic machine with components, having their own software and hardware, for instance, up-to-date equipment for TV or laser following, as well as peripheral equipment for displacement of the workpiece being welded or surfaced.

Selection of the type or structure of the programmable controller should (if required) take into account the conditions of welding (high level of noise and the associated solutions of the problems of noise protection of electronic devices for control and regulation), as well as the ability to apply various methods to control the welding process, including algorithmized modulation of the modes, control of mass transfer of electrode metal, adaptation to changing parameters of weld metal edge preparation, when using the scanning principle of following with the arc sensor, use of other peripheral devices, for instance for building-in into lines, or controlling auxiliary displacements, etc. It may be further stated that the problems of ensuring noise protection of equipment systems and its reliable functioning are closely connected to layout of all its systems and connection topology. Effective solution of these problems is possible, if developers of this specific kind of equipment have the necessary experience.

It is obvious that the proposed development may be used both in the newly developed structures of mechanized and automated arc welding equipment, and in upgrading of that which the user already has in his facility. Our experience of using the above concept of development of semi-automatic welding machines shows that with availability of a set of mechanical components the working variant of a machine, operating to customer algorithms, may be delivered in 2 to 3 weeks time. It this case a high reliability is guaranteed, which is due to a thorough pre-

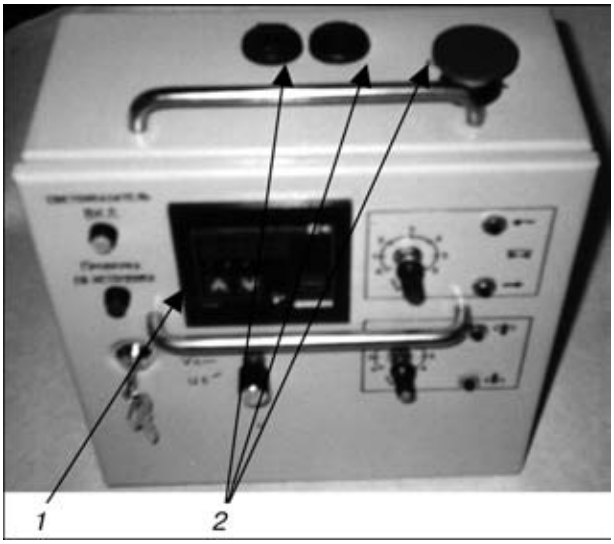

Figure 3. Variant of a new modular system of control of mechanized and automated equipment: *1* — controller; *2* — organs of control of cycle start and stop

liminary retrofitting of all the components and systems, their fast replacement and repairability (if required), as well as guaranteed reliability of batch-produced purchased items.

Variant of development of a new modular system for control of mechanized and automated equipment is shown in Figure 3, and a variant of a single-arc welding machine of tractor type with this control system in Figure 4.

It may be further specified more precisely that in this development it turned out to be sufficient to apply a relatively simple controller of «ZELIO» type, which has simple program tools, which can be serviced by the staff of even small businesses. The welding tractor design incorporates a system of laser lighting, which in the opinion of welding operators, is very useful for current adjustment of the position of electrode wire relative to the butt being welded.

New modular systems of control of mechanized and automated equipment are now installed also in welding and surfacing suspended automatic machines, automatic machines for position butt welding of pipes and other types of welding and surfacing equipment.

CONCLUSIONS

1. Modular principle of design of control systems for mechanized and automated arc welding equipment predetermines the search for such solutions, which would synthesize development of a broad range of semi-automatic and automatic machines for various purposes with a one-type element base, programming of operating cycle and regulation of welding process parameters. Such systems are acquiring more and more of the features of mechanotronic systems.

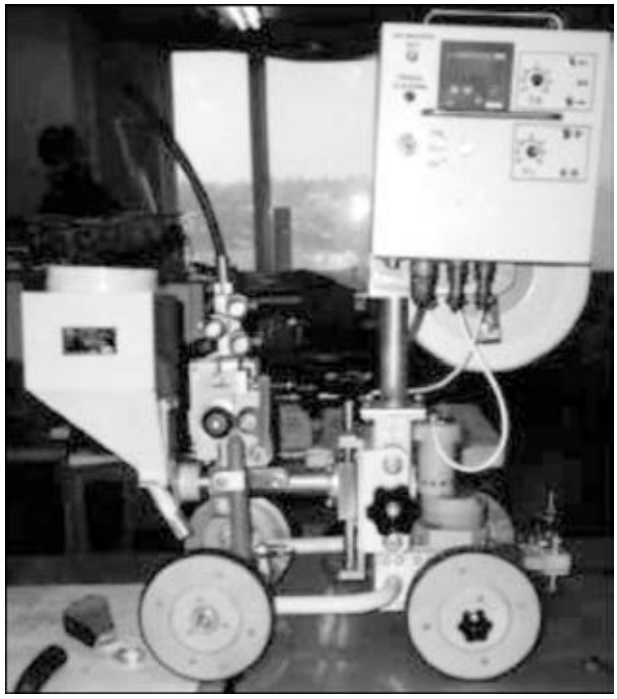

Figure 4. Variant of single-arc automatic welding machine of tractor type with a new modular system of control and system of arc excitation under flux

2. Application of the modular principle of design may be regarded as well-substantiated, if this allows simplifying the package of work on designing such systems, narrowing the element diveristy, simplifying setting up and maintaining the operability, ensuring reliable functioning of the equipment with a high quality of welding, as well as providing maximum fast response of the developers and manufacturers of the above equipment to market demands.

1. Chvertko, A.I. (1988) *Principles of rational design of equipment for automatic and mechanized welding and surfacing*. Kyiv: Naukova Dumka.
2. Lebedev, V.A., Pichak, V.G. (1997) New modular equipment for consumable electrode mechanized arc welding, surfacing and cutting. *Svarochn. Proizvodstvo*, **7**, 32–36.
3. Moshkin, V.F., Lebedev, V.A., Kovalenko, V.F. et al. (1998) Versatile modular surfacing equipment. *Ibid*., **6**, 33–36.
4. Paton, V.E., Moshkin, V.F., Pritula, S.I. et al. (1990) Prospects of development of electric arc welding equipment. In: *Problems of welding and special electrometallurgy*. Kyiv: Naukova Dumka.
5. Poduraev, Yu.V., Kuleshov, V.S. (2000) Principles of construction and current tendencies of megatron system development. *Tekhnologiya Mashinostroeniya*, **3**, 49–53.
6. Paton, B.E., Dudko, D.A., Moshkin, V.F. et al. (1999) Directions of development and improvement of high-efficient systems for mechanized arc welding, surfacing and cutting (Analysis of development of leading manufacturers of welding equipment). *Svarochn. Proizvodstvo*, **11**, 30–35.
7. Lebedev, V.A., Poloskov, S.I., Bratchuk, S.D. (2002) Evaluation of influence of disturbances of electric drive operation on reliability of equipment for mechanized and automatic welding. *Ibid*., **9**, 9–15.
8. Bessky, O.K., Galiguzov, A.A., Korogod, V.I. et al. *Direct current reversible electric drive*. USSR author's cert. 1589361. Int. Cl. H 02 P 5/16. Publ. 30.08.90.

WEAR RESISTANCE OF THERMAL COATINGS PRODUCED FROM COMPOSITE POWDERS «FERROALLOY–B_4C, SiC»

A.P. MURASHOV, E.A. ASTAKHOV, I.A. DEMIANOV and **A.D. KAPULA**
E.O. Paton Electric Welding Institute, NASU, Kyiv, Ukraine

Wear resistance of coatings under gas-abrasive wear conditions was found to depend on the type of hardening phases synthesized during spraying, as well as on the porosity (cohesion strength) of the coating.

Keywords: *wear resistance, gas-abrasive effect, thermal coatings, synthesis, hardening phases, carbides, borides, reduced wear*

To improve the performance of machine components subjected to abrasive wear, the coatings from materials containing carbides of tungsten and titanium or self-fluxing Ni–Cr–B–Si alloys are used [1, 2].

The present work gives the results of testing coatings made from composite powders «ferroalloy–B_4C, SiC» using plasma-arc and detonation methods. Powders were produced by conglomeration using polyvinyl alcohol as a binder, and also partial sintering of samples, compacted from mechanical mixture of powders with a next crushing, milling and selection of powders fractions of not smaller than –100 μm. Plasma-arc spraying was performed at the following condition: current 450 A; voltage 50 V; spraying distance 120 mm; plasma-forming medium-argon-nitrogen gas mixture. In detonation coating the following consumption of gases was established, m^3/h: 0.50–0.55 propane-butane; 1.30 oxygen; 0.65 air. Types of coatings are given in Table 1. Porosity of coatings, determined by metallographic examination, was 5–11 %, moreover, the lower values of porosity were observed in coatings made by the detonation method.

Tests for wear resistance of coatings in the conditions of gas-abrasive wear were carried out using chambers of jet-abrasive treatment. Inside the chamber the gun was fixed so that its axis was under 5° angle with respect to horizontal plane on which 20×15×4 mm size samples were fastened. Thickness of coatings was 0.35–0.40 mm. Distance from sample center to the gun nozzle exit section was 100 mm. As an abrasive material, the powder of electrocorundum of standard grade 14A of 0.5–0.8 mm grains, having 13000–14000 MPa microhardness, was used.

Wear tests were performed in the following sequence. Using a pressure stabilizer the pressure of compressed air, 0.2 MPa, was determined. Samples were blown out with an air-abrasive jet for 10 s. After reference weighing, they were again subjected to treatment for 10 s. All these operations were repeated 4–5 times. At the end of each operation the sample mass loss was evaluated. Rate of wear and reduced mass wear of the coatings were determined from the results of weighing. The latter was recalculated into a linear reduced wear using the values of density of coatings which were determined preliminary by the method of hydrostatic weighing:

$$W_l = W_{mass} / \rho_{coat} S_{coat},$$

where W_l, W_{mass} are the linear and mass reduced wear, respectively; ρ_{coat}, S_{coat} are the density and area of coatings, respectively.

Coatings given in Table 1 were subjected to test for resistance to gas-abrasive wear. Four samples of each type were prepared for tests. Phase composition and maximum microhardness of coatings are given in Table 2, and the results of tests for gas-abrasive wear of sprayed coatings are given in Table 3 and Figure.

Coatings produced from composite powder of FeV–B_4C system containing vanadium borides in their composition were most wear resistant.

Table 1. Coatings used at tests for gas-abrasive wear

No. of experiment	*Method of spraying*	*Type of coating*	*Initial powder, wt.%*	*Method of producing*	*Fraction of powder, μm*
1	Plasma-arc	FeTi–B_4C	15.0 B_4C, rest FeTi	Conglomerate	–80+50
2		FeTi–SiC	22.5 SiC, rest FeTi	Same	–100
3		FeV–B_4C	20.0 B_4C, rest FeV	»	–100
4		FeV–SiC	22.5 SiC, rest FeV	»	–100
5	Detonation	FeV–SiC	22.5 SiC, rest FeV	Conglomerate	–50
6		FeV–SiC	22.5 SiC, rest FeV	Sintered	–63
7		FeV–B_4C	20.0 B_4C, rest FeV	Same	–50

Table 2. Phase composition and microhardness of coatings

No. of experiment	*Type of coating*	*Phase composition*	*Microhardness, MPa*
1	FeTi–B_4C	Fe_3B, Fe_3C, FeTi, Fe_2C, Fe_2Ti, TiB_2, traces B_4C, Fe_2TiO_5 and Fe_3O_4	6660–7660
2	FeTi–SiC	Fe_2Ti, FeSiC, Fe_8Si_2C, Ti_5Si_3, TiO, Fe_2O_3, TiO_2	9000–11000
3	FeV–B_4C	FeV, VB, VC, V_3O_4, V_8O_5, V_2C, σ-VFe, traces Fe_2O_3, Fe_3O_4	16800–18920
4	FeV–SiC	V_4C_3, FeSiC (Fe_8Si_2C), FeV, $VO_{1.27}$, α-SiC, $FeVO_4$	16800–18920
5	FeV–SiC	FeV, $VO_{1.27}$, SiC, V_8C_7	4830–5200
6	FeV–SiC	FeV, $VO_{1.27}$, SiC, V_6Si_5, V_8C_7	4830–5200
7	FeV–B_4C	V_2B_3, FeV, σ-VFe	4700–5200

Table 3. Wear of sprayed coatings at gas-abrasive wear

No. of experiment	*Coating density, t/m^3*	*Time of testing, s*								*Wear intensity*	
		10	*20*	*30*	*40*	*50*	*60*	*70*	*80*	*Mass, g/s*	*Linear, μm/s*
1	5.43	0.0300	0.0600	0.0800	0.1100	0.1300	0.1500	0.1900	0.2000	0.00270	1.650
2	5.32	0.0100	0.0200	0.0220	0.0320	0.0410	0.0600	0.0650	0.0780	0.00090	0.560
3	5.24	0.0050	0.0110	0.0150	0.0190	0.0260	0.0310	0.0370	0.0410	0.00050	0.320
4	5.18	0.0180	0.0350	0.0530	0.0680	0.0860	0.1000	0.1200	0.1380	0.00173	1.110
5	5.26	0.0020	0.0040	0.0060	0.0070	0.0080	0.0110	0.0120	0.0130	0.00018	0.114
6	5.25	0.0040	0.0070	0.0090	0.0130	0.0160	0.0180	0.0210	0.0250	0.00033	0.210
7	5.28	0.0003	0.0007	0.0009	0.0012	0.0014	0.0017	0.0022	0.0024	0.00003	0.020

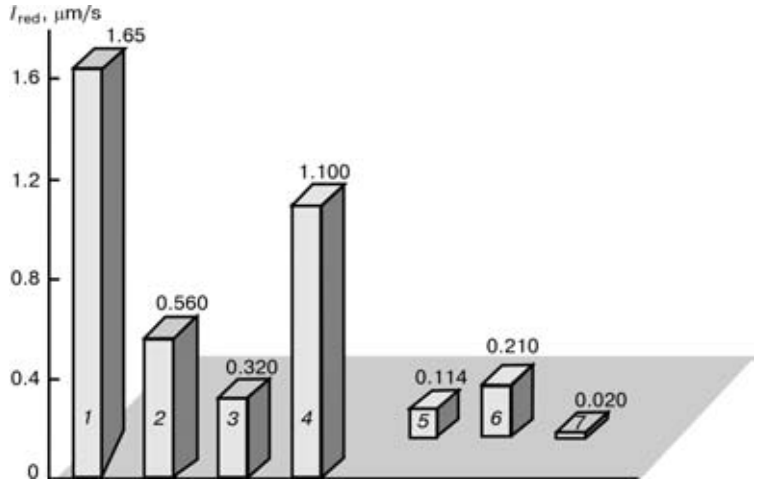

Intensity of wear I_{red} of plasma (1–4) and detonation (5–7) coatings from composite powders of different systems in gas-abrasive weighing: *1* — FeTi–B_4C; *2* — FeTi–SiC; *3* — FeV–B_4C; *4* — FeV–SiC; *5* — FeV–SiC (fraction –50 μm); *6* — FeV–SiC (fraction –63 μm); *7* — FeV–B_4C

Coatings, whose composition after spraying includes titanium carbides and iron carbosilicides, had lower wear resistance and those, produced from powders of larger fractions and characterized by high porosity had the lowest resistance at gas-abrasive wear.

Detonation coatings produced from powder of small fractions (–50 μm) possessed wear resistance, much exceeding the wear resistance of plasma coatings, sprayed from powders of fraction –100 μm. Moreover, the detonation coatings contained a negligible amount of carbide and boride phases, however, they were characterized by the lower porosity.

At similar microhardness of the coating, whose composition included titanium carbide, iron carbosilicides, were inferior by the wear resistance to the coatings containing vanadium borides.

Thus, the wear resistance of thermal coatings in the conditions of gas-abrasive wear at low angles of attack of abrasive is defined by the wear resistance of the hardening phase and matrix. To produce coatings with a high wear resistance in the gas-abrasive conditions of wear, it is rational to use composite powder of FeV–B_4C system, having the 50–80 μm sizes of particles. This will provide the dense coatings with a high cohesion strength.

1. (1973) *High-temperature sprayed coatings*. Ed. by L.K. Druzhinin, V.V. Kudinov. Moscow: Atomizdat.
2. Borisov, Yu.S., Kharlamov, Yu.A., Sidorenko, S.A. et al. (1987) *Thermal sprayed powder coatings*. Kyiv: Naukova Dumka.

CIRCUIT FOR POWERING CONTROL SYSTEMS OF SEMI-AUTOMATIC MACHINES FROM THE WELDING CURRENT SOURCE VOLTAGE

V.A. LEBEDEV
E.O. Paton Electric Welding Institute, NASU, Kyiv, Ukraine

The paper describes the possibility of construction of systems of control and regulation, powered by the welding current source voltage. A simple and effective technical solution is proposed, which allows solving both the problem of protection from high-voltage surges during the welding process, and powering the semi-automatic machine systems during short-circuiting of the arc gap. The above technical solution was implemented in a range of semi-automatic machines of modular design of PSh 107V type and is now used in industry, being independent on welding current source applied in the arc welding process.

Keywords: *mechanized welding, control system, electric drive, welding current source, welding voltage, power, protection, circuit*

In gas-shielded mechanized arc welding the systems of control of the operating cycle of semi-automatic machines and adjustable electric drives can be manufactured with power supply from a welding current source [1]. This simplifies the power and regulating circuits and yields a significant technological effect [2]. Application of such a circuit is justified in case of applying simple parametric regulators of the frequency of rotation of the drive electric motor shaft in the electrode wire feed mechanism (for instance, in A547Um, A825M semi-automatic machines). A grave drawback of such systems is a very narrow range of regulation of the feed rates, limiting their extension to other types of mechanized welding processes (welding of aluminium, surfacing, cutting, pulsed processes, etc.). A large number of developments of systems of control and regulation of the semi-automatic machines were introduced lately, which use microcircuits, transistor electric drives with broad ranges of regulation [3]. It would be useful to provide powering of such devices from a welding current source, which would simplify the power system and solve the problem of having feedbacks by the arc process parameters, which would eliminate any additional electric connections, leading to the semi-automatic machines feed unit.

However, such a design of the electric parts of the semi-automatic machine is difficult, because of the presence of high-voltage components in the spectrum of arc process voltage, which may be the consequence of transient processes in welding with systematic short-circuiting of the arc gap, at arc erring, in welding with power supply from rotating sources of welding current — welding generators (switching over voltages). Figure 1 shows one of the possible characteristic oscillograms of the arc process voltage in CO_2 welding with 1.2 mm electrode wire of Sv-08G2S type. It is seen that the voltage pulses may reach considerable values, which is the source of failure of semiconductor devices in transistor systems.

A technical solution described in [4] was proposed earlier, in order to solve the problem of protection of the systems of control and regulation, when they are powered from the voltage of welding current source changing in a broad range (from open-circuit voltage to welding voltage). A device shown in Figure 2 is proposed for the case with the pulsed components in the voltage spectrum of the arc process.

The circuit includes choke *L1*, connected in series with diode *V1*, which is shunted by resistor *R1*, capacitors *C1, C2* for power accumulation and diode *V2*. Such a protection circuit differs from the filter circuits, which are known and described in technical publications [5]. This is due to the need to simultaneously solve two problems, namely considerable decrease or elimination of the high values of the pulsed component in the spectrum of welding voltage and provision of a continuous power supply to systems, which are powered from a source of welding current.

Before the start of the welding process capacitor *C1* is charged through choke *L1* and diode *V1*, and capacitor *C2* via diode *V2*. Power supply of the semi-automatic machine systems (electric drive, control

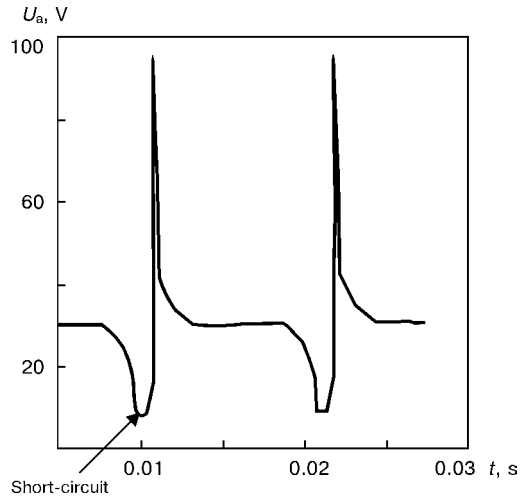

Figure 1. Oscillogram of arc process voltage in CO_2 welding

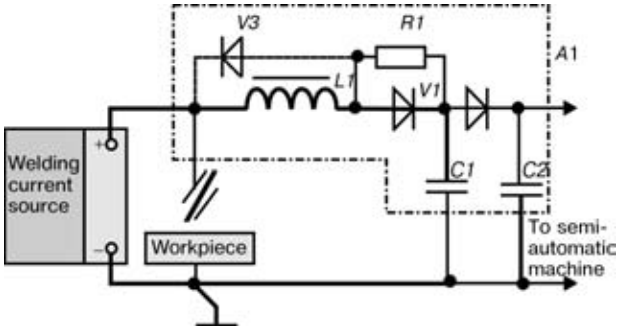

Figure 2. Circuit of protection of the control systems of semi-automatic machines, when they are powered from the welding source voltage

cycle circuits, alarms, etc.) is drawn from capacitor *C2*. During CO_2 welding, when short-circuiting of the arc gap occurs, capacitor *C1* starts discharging through resistor *R1* and choke *L1*. Power is stored in the latter. When the short-circuit disappears (arc excitation) the choke releases its energy to the welding arc. The emf of choke *L1* and high-voltage surges of welding current sources are directed towards each other. A partial suppression of the high-voltage surge occurs. In addition, the choke, having a certain inductance, filters the above surge until its saturation occurs, and the choke inductance is insignificant. During the short-circuit of the arc gap the charge of capacitor *C2* provides power for the systems of the semi-automatic machine.

Calculation of parameters of choke *L1* (inductance, heating), capacitors *C1, C2*, resistor *R1* is conducted by the procedures of [5], and the initial data correspond to the parameters of the short-circuit, i.e. duration of phases of the short-circuiting and arcing known for the arc welding process. The amplitude of the high-voltage surge found for this process by welding voltage oscillograms, should be lowered to the level determined by the capabilities of the used element base. So, for instance, for the transistor electric drive applied in the semi-automatic machines of modular design of PSh 107V type [3] this level should not exceed 60–70 V. In a number of cases, when just the filtering properties of LCR-filter are sufficient for suppression of the high-voltage pulse and the circuit response should be made faster, the choke is shunted by diode *V3* (see Figure 2, dotted line).

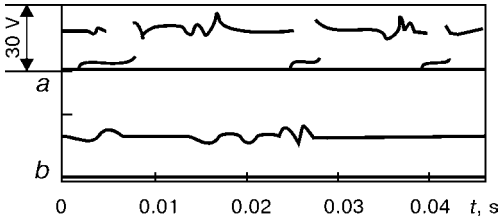

Figure 3. Oscillograms of supply voltage of the semi-automatic machine circuit: *a* — on the arc; *b* — after the protection circuit

The proposed protection circuit is quite simple, and its effectiveness is confirmed by failure-safe operation of semi-automatic machines of P11P107V type, where such circuits are used to solve the problem of ensuring the independence of the semi-automatic machine on the type of the welding current source, used in arc welding.

As an example for protection of the circuit of a semi-automatic machine with power supply to it from arc voltage in CO_2 welding, with short-circuiting of the arc gap with frequency in the range of 50–100 Hz, and inductance of the choke of the welding current source of 0.5 mH, the circuit parameters are as follows: *L1* = 4.5 mH, *C1* = 1000 μF, *C2* = 2000 μF, *R1* = 47 Ohm. Characteristic oscillograms of supply voltage of the circuit of the semi-automatic machine without the protection circuit and with its application are shown in Figure 3. With the same structure of the protection circuit its parameters will vary depending on the kind of welding process and used welding current source (welding circuit parameters, method to produce the welding voltage, presence of high open-circuit voltage, etc.).

Protection circuit may be designed as a separate module with several design variants, and can be batch-produced, also for the needs of upgrading the semi-automatic machine fleet, already in service.

1. Potapievsky, A.G. (1974) *Consumable electrode gas-shielded welding*. Moscow: Mashinostroenie.
2. Lebedev, V.A., Svetnikov, B.G. (1988) Electric drive of semi-automatic welding machine with welding power source. *Avtomatich. Svarka*, **12**, 51–55.
3. Lebedev, V.A., Pichak, V.G. (1998) Semi-automatic welding and surfacing machines of PSh 107 type. *Ibid.*, **7**, 38–42.
4. Lebedev, V.A., Ivanov, G.P., Rozdobudko, G.I. (1980) Stabilisation of the arc voltage supplying the welding machine circuit. *Ibid.*, **9**, 75–76.
5. Veksler, G.C. (1978) *Design of power supply devices*. Kyiv: Technika.

Developed at PWI

ASYNCHRONOUS WELDING GENERATOR

To fulfil welding jobs in the field conditions, the mobile welding units consisting of a welding generator and driven internal combustion engine are widely used. So-called inverted DC generators are widely used for a long time as welding generators. The latter are two-package induction AC machines of increased frequency with a rectifying block and characterized by a relative simplicity and reliability.

However, at present these generators became old-fashioned and do not correspond often to modern technological requirements specified to this equipment. They are not provided with a correction of external static and dynamic characteristics depending on the grade of electrodes and operation conditions used. Smooth adjustment of welding current in inverted generators is limited by a selected rather narrow subrange.

Some advanced technological processes made in the field conditions require the presence of not only welding voltage, but also single- and three-phase mains voltage of 220/380 V and 50 Hz frequency. This made developers and manufacturers of welding units to connect additionally one more machine with a driven engine, i.e. auxiliary AC generator. There is a need often in air-plasma cutting in the field conditions. However, it is impossible to solve all these problems on the base of an inverted welding generator without modification of the latter.

Specialists of PWI have carried out the necessary research works and developed the bases for design of asynchronous welding generators for any currents. The asynchronous generators have some advantages as compared with known inverted welding generators. The main of them are as follows:

- smooth local and remote adjustment of welding current in one range using standard electrical control signal of 0–10 V;
- correction of external static and dynamic characteristics depending on grade of electrodes and operation conditions used;
- presence of single- and three-phase AC mains of 220/380 V voltage and 50 Hz frequency;
- decreased alternating voltage, for example, 24 or 36 V and 50 Hz frequency;
- feasibility of use of the asynchronous welding generator not only for manual arc, but also for other methods of welding, for example, in CO_2, for air-plasma cutting, without high additional material expenses.

Thus, the asynchronous welding generators are superior to traditional inverted generators by a number of technical and technological characteristics. Unique algorithm of welding current control, realized in asynchronous welding generator, provides high quality of welding by any electrode, and opens also wide opportunities for further improvement of welding properties of the asynchronous welding generator and manifestation of its new technological advantages in different types of welding. In addition, the design of developed asynchronous welding generators is provided on base of serial asynchronous electric motors of appropriate power that is a basis of their high reliability, relative simplicity and low cost. Variants of asynchronous welding generators have been developed for different welding currents (from 160 up to 630 A), including two- and four-station types.

Technical characteristic of asynchronous welding generator for 315 A

Rated welding current at 60 % duty cycle, A	315
Rated operating voltage, V	32.6
Range of welding current adjustment, A	40–350
Open-circuit voltage, V	not more than 85
Power of three-phase mains of 380 V and 50 Hz, kV·A	8
Power of single-phase mains of 220 V and 50 Hz, kV·A	3
Mass, kg	not more than 270

For additional information, please, contact: G.N. Moskovich, I.I. Zaruba,
Tel. (38-044) 261-5061, 227-6746.